NFATc1 driven ER-stress responses in the progression of non-alcoholic fatty liver disease

Dissertation

for the award of the degree

“Doctor rerum naturalium” (Dr. rer. nat.)

of the Georg-August-Universität Göttingen

within the doctoral program “Molecular Medicine”

of the Georg-August University School of Science (GAUSS)

Submitted by

Muhammad Umair Latif

from Lahore, Pakistan

Göttingen, 2020

Doctoral Thesis Committee

Prof. Dr. Volker Ellenrieder (1st referee)
Department of Gastroenterology and Gastrointestinal Oncology,
University Medical Center, Göttingen

Prof. Dr. Heidi Hahn (2nd referee)
Institute for Human Genetics
University of Göttingen

Prof. Dr. Hubertus Jarry
Department of Clinical and Experimental Endocrinology,
University Medical Center, Göttingen

Extended examination board

Prof. Dr. Jürgen Wienands
Department of Molecular and Cellular Immunology,
University Medical Center, Göttingen

Prof. Dr. Frauke Alves
Molecular Biology of Neuronal Signals
Max-Planck Institute of Experimental Medicine, Göttingen

Prof. Dr. Michael Zeisberg
Clinic for Nephrology and Rheumatology
University Medical Center, Göttingen

Date of submission of thesis: 08.05.2020

Date of the oral examination: 23.06.2020

DECLARATION

I hereby declare that the thesis entitled “NFATc1 driven ER-stress responses in the progression of non-alcoholic fatty liver disease” has been solely written by myself and with no other sources and aids than quoted.

Muhammad Umair Latif **Göttingen: 08.05.2020**

ACKNOWLEDGEMENTS

All praises to **"ALLAH",** the Almighty, Most Gracious, the Most Merciful, Sustainer of the worlds and His Holy Prophet, **MUHAMMAD (PBUH)**, to whom, I bow my compassionate endowments and who is ever an ember of guidance and knowledge for humanity.

First of all, I have the great pleasure to express my immense gratitude to my mentor, **Prof. Dr. Volker Ellenrieder,** for his excellent and stimulating guidance throughout my doctorate. I have been extremely lucky to have a chance to work with such a motivated and appreciative supervisor. His scientific attitude, vision and leadership are a role model worthy of emulation. I appreciate all his contributions of time and ideas to make my Ph.D. productive and stimulating. He convincingly guided and encouraged me to be professional and do the right thing even when the road got tough. Without his persistent help, the goal of this project would not have been realized.

I feel great pleasure in expressing my heartiest gratitude and deep sense of obligation to my thesis committee members Prof. Dr. Heidi Hahn and Prof. Dr. Hubertus Jarry**,** for their guidance, keen interest, skilled suggestions, and constructive criticism throughout the course of my research work.

I am very thankful to PD. Dr. med. Elisabeth Hessmann and Dr. Shiv Singh for providing their tremendous support during critical phases of my thesis. A very special thanks goes to Dr. Nai-ming Chen, who helped me a lot at the initial phase of my research work. His support is highly appreciated.

I would also like to thank my colleague Geske Schmidt, for analyzing my sequencing results and beside this, being always available for any help required. I am very thankful to Kristina Reutlinger for her immense technical and moral support throughout my project. Besides, I am highly obliged and would like to recognize invaluable assistance from Waltraut Kopp and Sercan Mercan in mouse experiments and stainings. I thank to all other colleagues of the laboratory, especially, Shilpa Patil, Zhe Zhang (Alice), Mengyu Tu, Marie Hasselluhn, Lennart Versemann, Nina Pfeisterer and Friederike Fehlau for their moral and technical support as well as for providing such a friendly and constructive environment.

I offer my heartiest gratitude to my friends, Dr. Aamir Nadeem, Zaheer Abbas, Umer Javed, Dr. Raza-u-Rehman, Dr. Mohsin Shafiq, Dr. Shakil Ahmed, Awais Asim, Abdul-Rehman and Faisal, for being very supportive.

I can never forget the efforts of my father Muhammad Latif Yasin, mother Suraya Latif, my elder brothers Khalid Latif, Sajid Latif and sister Naila Aamir. It may not be enough to contain the words of thanks giving, it may not capture the endearing love that I have for all of them. Their place is a place of love, generosity and benevolence.

I wish to express my deep love and gratitude to my wife Rabia Rajab whose love and support is countless. She helped me to get through this agonizing period in the most positive way. Finally, thanks to my son Alyan Latif for being my stress reliever and making this journey very pleasant for me.

At the end, I am very thankful to HEC, Pakistan and DAAD, Germany for providing me this opportunity.

Muhammad Umair Latif

Dedicated

to

My Parents

Who are always a Pillar of strength to me. Their love for me is so great, I have worked hard to justify it.

Table of Contents

List of Figures

Summary

Non-alcoholic fatty liver disease (NAFLD) mirrors the hepatic manifestation of the metabolic syndrome and is defined by progressive fat accumulation in hepatocytes (steatosis). Uncomplicated NAFLD may progress to a severe form of non-alcoholic steatohepatitis (NASH), characterized by marked organ inflammation and fibrosis. Progression of the disease can lead to distinctive cirrhosis and even the development of hepatocellular carcinoma. Not surprisingly, NAFLD has now emerged as the second most common cause of liver transplantations in the USA and has been predicted to become one of the leading causes of hepatocellular carcinoma in few years (Wong et al., 2015). Unfortunately, however, despite great efforts from multiple research groups, the mechanisms underlying the progression from uncomplicated NAFLD to NASH and beyond, are still largely unknown.

Here, we describe a key role of NFATc1 in NAFLD progression. NFATc1, apart from its well-known function in T-cell activation, has been reported to play a major role in various inflammatory diseases (i.e., skin inflammation) and inflammation-associated tumors as well (i.e., colon cancer, pancreatic cancer). However, its role in inflammation associated liver inflammatory diseases has not been comprehensively studied. This project aimed to characterize the functional implication of NFATc1 and its therapeutic potential in NAFLD development and progression. To address this, we utilized primary hepatocytes, AML12 cells and genetically modified mouse model with hepatocyte-specific genetic alteration in NFATc1.

Initially, we confirmed the robust expression and nuclear localization of NFATc1 in hepatocytes of human NAFLD patients. We also demonstrated fat-induced activation of the transcription factor in hepatocytes and provided experimental evidence that NFATc1 activation is dispensable for the development of steatosis but is strictly required for the progression of the disease. In fact, in-depth biochemical, molecular, and functional analysis revealed that NFATc1 activation promotes inflammation and fibrosis, thus culminating in the development of steatohepatitis. Using transgenic mice with hepatocytes-specific differential expression of NFATc1, we were able to demonstrate that NFATc1 deficiency protects mice from fat-induced inflammation and fibrosis. Mechanistically,

NFATc1 promotes NAFLD through terminal ER stress and subsequent activation of the PERK unfolded protein response pathway in hepatocytes to promote apoptosis and activation of the inflammasome. Lastly, this study highlighted the therapeutic potential of ER stress relief by treatment with TUDCA. In fact, TUDCA application prevented hepatocytes from NFATc1 driven ER stress and UPR pathway activation and hence, resulted in strikingly lower hepatocyte damage (apoptosis and inflammasome activation), inflammation and fibrosis in mouse models of NAFLD.

1.0 Introduction

1.1 NAFLD and NASH

Non-alcoholic fatty liver disease (NAFLD) is one of the most common causes of chronic liver disease and is considered an important component of the metabolic syndrome (Lebeaupin et al., 2018). It is referred to as fatty liver if the fat content exceeds 5% of the total weight and there is no casual alcohol abuse (European Association for the Study of the Liver (EASL), European Association for the Study of Diabetes (EASD) and European Association for the Study of Obesity (EASO), 2016). NAFLD stems from the accumulation of free fatty acids (FFA´s) in hepatocytes, which mainly originate from food sources or are formed under cellular stress conditions in hepatocytes as result of de novo lipogenesis. Under physiological conditions, FAA´s undergo β-oxidation following their export via very-low-density lipoproteins (VLDL). However, due to the consumption of high fat/high caloric diet and lack of physical activity, excessive fat is taken up by hepatocytes. Under stress conditions, hepatocytes store these FFA´s and build up fat vacuoles that eventually cause ballooning of hepatocytes, a process called steatosis. NAFLD may progress from steatosis (fatty liver) to non-alcoholic steatohepatitis (NASH). NASH is defined as fatty liver (steatosis) with inflammation that initiates the synthesis of extracellular matrix (fibrosis). It is considered a more severe and progressive form of the disease that can further develop into advanced fibrosis, cirrhosis and liver cancer (Anstee et al., 2013; Garcia et al., 2019; Kim et al., 2018). Importantly, due to lack of proper diagnostic markers and absence of proven treatment options, NAFLD/NASH is arising as a serious health issue around the globe. Apart from liver injury, recent studies have established NAFLD as a risk factor for cardiovascular diseases (Byrne et al., 2015).

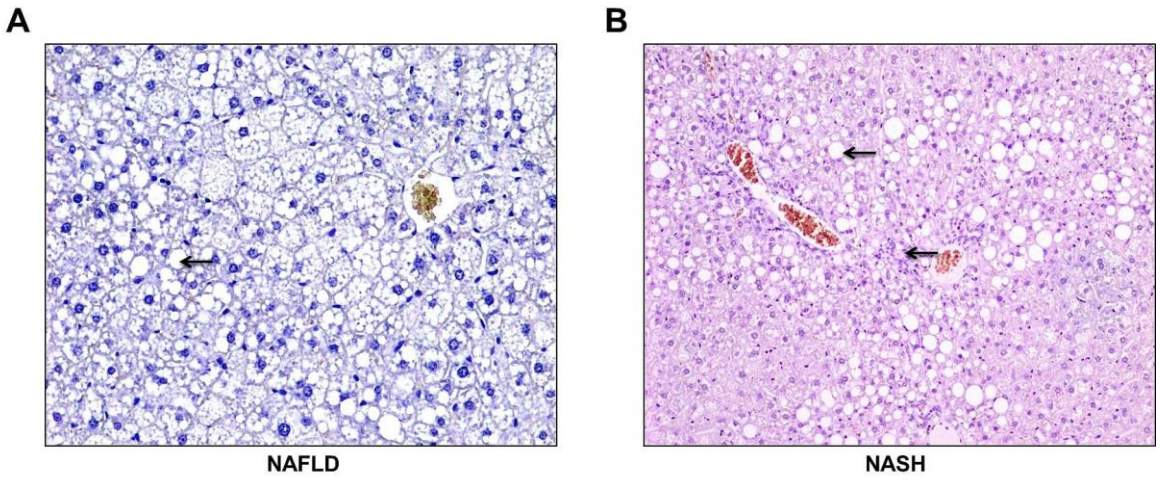

Figure 1: Steatosis and Steatohepatitis

(A) Fat accumulation in the cytoplasm of hepatocytes causing steatosis or NAFLD. **(B)** Steatosis along with progressive inflammation in the liver mirrors non-alcoholic steatohepatitis (NASH).

1.2 Epidemiology of NAFLD

The far-reaching lifestyle changes in industrialized countries have led to a massive increase in metabolic disorders and chronic diseases such as NAFLD and type 2 diabetes (T2DM). The worldwide prevalence of NAFLD is 25.2%, with the prevalence in the Middle East and South America being even higher at 31.8 % and 30.4% respectively. In Asia, Europe and North America, the average prevalence is 24-27%. Men are more often (19% to 31%) affected than women (16% to 16%) or children (3% to 11%) (Wong et al., 2015). Interestingly, the rate of NAFLD associated hepatitis (NASH) has also doubled in the last 10 years (Younossi et al., 2018; Younossi et al., 2016). In total, about 10-15% of all NAFLD patients experience progression to NASH and about 25% of these patients develop signs of fibrosis, cirrhosis and eventually hepatocellular carcinoma (HCC). Thus, the NAFLD-NASH sequence represents an important risk factor for the development of liver cancer, particularly in western countries. (Kim & Lee, 2018b; Schuppan et al., 2013; Younossi et al., 2011). In fact, about 75% of chronic liver diseases and around 14% of all HCC cases evolve in the course of NAFLD/NASH (Younossi et al., 2015).

1.3 Pathogenesis of NAFLD

Multiple environmental, genetic and metabolic factors contribute to the development and progression of NAFLD. For instance, changes in lifestyle, lack of physical activity, intake of high caloric and high-fat diet along with glucose and cholesterol, are some of the major environmental factors that lead to obesity and insulin resistance, which in turn, increase hepatic FFA´s influx. Until now the underlying mechanism responsible for NAFLD progression towards NASH are not fully understood. However, recent experimental evidence propose a "**two-hits model**" (Giorgio et al., 2013; Lebeaupin et al., 2018), in which the first hit is mediated by the accumulation of FFA´s in the form of triglycerides [Fig 1A]. FFA´s coming from adipose tissues are major sources of fat taken up by the liver and makeup to 60% of hepatic fat accumulation (Steneberg et al., 2015; Van Herck et al., 2019). These fatty acids undergo esterification into triglycerides or β-oxidation before cellular export can occur. Impaired hepatic β-oxidation leads to a decrease in fatty acid export and consequent accumulation hepatocytes (Postic et al., 2008; Steneberg et al., 2015). Besides these factors, multiple genetic factors, particularly variations in the expression of fatty acid metabolizing genes i.e. FADS (fatty acid desaturase), PNPLA3 (patatin-like phospholipase domain-containing protein 3) etc. also contribute in enhanced fatty acid accumulation in hepatocytes (Romeo et al., 2008; Wang et al., 2015). The continued influx of FFA´s culminates in oxidative and endoplasmic reticulum stress in hepatocytes, and this event defines the second hit that causes disease progression through inflammasome activation (NLRP3), cytokines/chemokines release (IL1, IL6, CxCl10, CxCl11 etc.), and induction of programmed cell death (Cleaved caspase 1,3,7 etc.) (Berlanga et al., 2014; Dowman et al., 2010; Kim et al., 2018a). The cytokines/chemokines and DAMPs (damage-endogenous-associated molecular patterns) secreted from damaged hepatocytes as well as the apoptotic bodies activate hepatic macrophages, which in turn secrete pro-inflammatory cytokines (IL1, IL6, TNFα etc.). Together, these processes result in progressive activation of hepatic stellate cells and infiltration of immune cells to form a highly

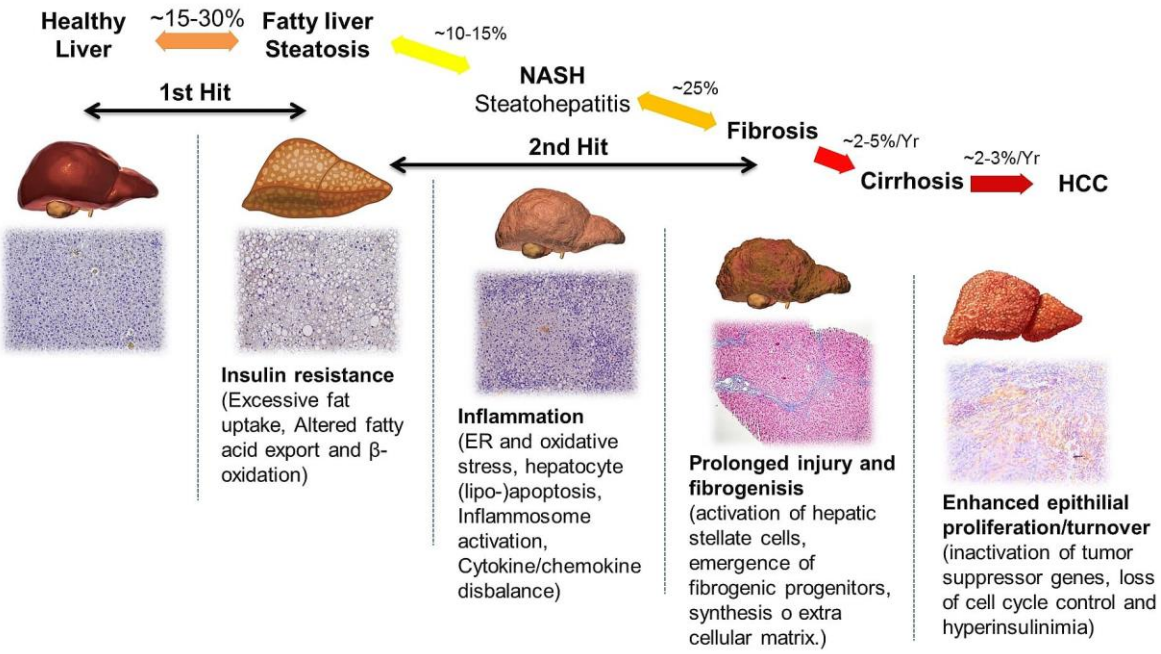

Figure 2: The NAFLD progression model

Displaying the development of NAFLD (1st hit) and its progression to NASH (2nd hit) fibrosis, cirrhosis and hepatocellular carcinoma (HCC). The underlying cellular pathomechanisms are also shown.

inflammatory and fibrotic environment [Fig 1B-Fig 2] (Berlanga et al., 2014; Capece et al., 2013; Cha et al., 2018; Haukeland et al., 2006; Sircana et al., 2019).

1.3.1 Fatty acid accumulation induces ER stress

Hepatocytes are rich in endoplasmic reticulum where protein synthesis, folding, lipid biogenesis and calcium homeostasis is controlled. It has been shown that FFA's accumulation in hepatocytes can cause defects in protein folding in the endoplasmic reticulum, thus leading to ER stress and activation of critical downstream signaling pathways to restore ER homeostasis. Chronic ER stress can lead to sustained activation of the so-called unfolded protein response (UPR) that eventually causes severe cell defects and set stage for the development of liver diseases, e.g. NAFLD progression from steatosis to NASH and beyond (de Freitas Carvalho et al., 2019; Lee et al., 2017; Lind et al., 2017; Zhang et al., 2014). Endoplasmic reticulum utilizes three distinct stress sensing mechanisms: protein kinase RNA-like endoplasmic reticulum kinase (PERK), activating

transcription factor 6 (ATF6) and inositol-requiring enzyme 1 (IRE1) (Lebeaupin et al., 2016; Lee et al., 2017). These stress sensors are transmembrane proteins, which under normal physiological conditions resides in the ER lumen and are bound to the Glucose-Regulated Protein 78 (GRP78, BiP). Under stress conditions, transmembrane sensors dissociate from GRP78 and activate the unfolded protein response (UPR) pathway (Groenendyk et al., 2014; Lebeaupin et al., 2018; Lind et al., 2017; Zhang et al., 2014).

1.3.1.1 Inositol requiring enzyme 1 (IRE1)

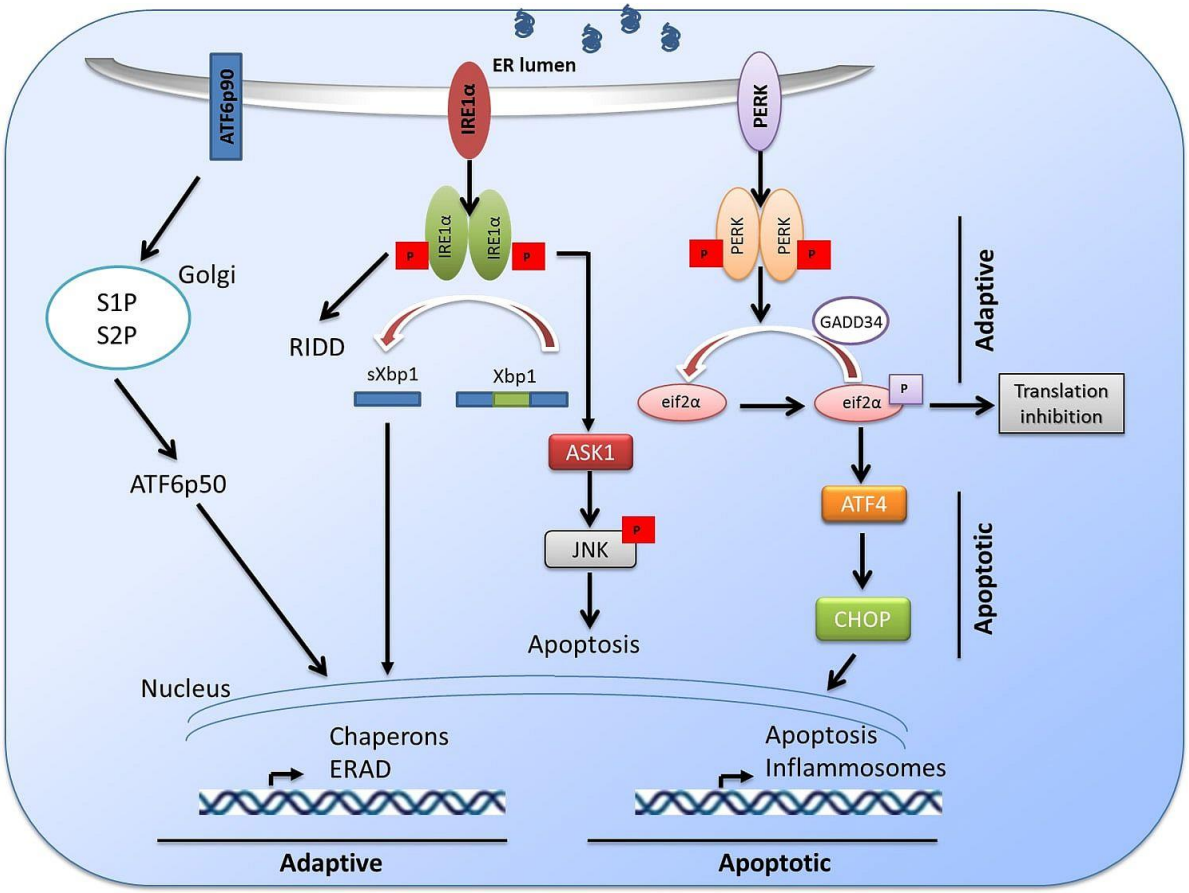

Figure 3: Unfolded protein response (UPR) pathway in ER stress signaling

Schematic diagram of the unfolded protein response (UPR). Modified from (Lebeaupin et al., 2018).

The Inositol Requiring Enzyme 1 **(**IRE1) signaling cascade is the most conserved among the three ER stress signaling components of the UPR. IRE1 is a transmembrane protein with two homologs, IRE1α and β (Liu et al., 2015; Maiers

et al., 2019). Under stress conditions, IRE1α auto-phosphorylates with its kinase activity domain and turn on its endoribonuclease activity domain which splices 26 nucleotides of the X-box binding protein 1 (XBP1) (Oikawa et al., 2009). Spliced XBP1 (XBP1s) translocates into the nucleus to control gene transcription of chaperones and other factors involved in ER-associated degradation (ERAD) to facilitate proper folding and degradation of misfolded proteins accumulated in the ER (Liu et al., 2015; Maiers & Malhi, 2019; Tirosh et al., 2006; Zhang et al., 2014). IRE1α also recruits tumor-necrosis factor (TNF) receptor-associated factor 2 (TRAF2), thus activating apoptosis-signal-regulating kinase 1 (ASK1). ASK1, in turn, drives c-Jun N-terminal kinase (JNK) activity for subsequent activation of pro-apoptotic proteins (Bim) while inhibiting anti-apoptotic proteins (Bcl2) (Hu et al., 2006; Urano et al., 2000). IRE1α also mediates the process of IRE1α-dependent decay of mRNA (RIDD) to limit and negatively regulate genes translation or transcription. Together, the IRE1α mediated signaling cascade is the adaptive mechanism of UPR to restore the ER homeostasis and resolve the stress conditions (Hollien et al., 2009; Hollien et al., 2006; Liu et al., 2015; Maiers & Malhi, 2019).

1.3.1.2 Activating transcription factor 6 (ATF6)

ATF6 with its two isoforms, ATF6α and ATF6β, is a transmembrane ER-resident protein with a cytosolic transcription factor domain (Adachi et al., 2008; Wu et al., 2007). During ER stress conditions, ATF6 translocate into the Golgi apparatus (Nadanaka et al., 2004; Shen et al., 2002). Here, S1P and S2P proteases cleave full length ATF6 (ATF6p90) into its active form ATF6α (ATF6p50) that migrates into the nucleus and regulates expression of different genes involved in protein folding and ERAD i.e. BiP and other chaperons (Lebeaupin et al., 2018; Yamamoto et al., 2007). ATF6α has also been reported to activate XBP1 transcription.

1.3.1.3 The Protein kinase RNA-like ER kinase (PERK)

Prolonged disturbance of ER homeostasis induces dimerization and activation of PERK, a transmembrane ER stress sensor protein (Romine et al., 2019; Wang et al., 2018). Upon activation, PERK phosphorylates the eukaryotic initiation

factor (eif) at its alpha subunit, which subsequently attenuates translation in general but fosters selective mRNA translation of the Activating Transcription Factor 4 (ATF4). ATF4, in turn, promotes transcription of several stress-responsive genes involved in pro-survival and pro-apoptotic signaling i.e. the CCAAT enhancer-binding protein (C/EBP) homologous protein (CHOP) (Lebeaupin et al., 2018; Romine & Wiseman, 2019). CHOP is a central mediator of the UPR that – depending on the stimulus and duration of the UPR response – can induce pro-survival, pro-apoptotic and pro-inflammatory signals as well. Under transient ER stress conditions, CHOP inhibits the PERK downstream signaling cascade through induction of the DNA damage-inducible 34 (GADD34) gene that de-phosphorylates eif2α and thus terminates ATF4 activation. However, prolonged ER stress leads to sustained activation of UPR responses (called terminal UPR) including CHOP mediated activation of the NLRP3 inflammasome and pro-apoptotic proteins (PUMA, Caspase 1) (Lebeaupin et al., 2016; Liu et al., 2019; Willy et al., 2015).

1.3.2 ER stress-induced hepatocyte inflammasomes activation

Inflammasome activation is a central process of the innate immune system and responsible for the inflammatory response upon tissue injury. This occurs mainly via activation of caspase-1, IL-1β and IL-18 (Guo et al., 2015). Several components are involved in activation of the inflammasome, particularly the nucleotide-binding oligomerization domain (NOD) leucine-rich repeat containing receptors (NLR) containing pyrin domain 3 (NLRP3) protein, which upon stimulation activates caspase-1 by cleavage. Cleaved caspase-1, in turn, activates IL-1β and IL18 (pro-inflammatory cytokines) and other pro-inflammatory cytokines and promotes cell death (pyroptosis) (Guo et al., 2015; Wree et al., 2014). Recent studies identified an important role of the NLRP3 inflammasomes in fat-induced inflammation and the progression of NAFLD. Accordingly, high levels of NLRP3 inflammasome markers (NLRP3, Caspase-1, Caspase-11, IL1β and IL18) have been reported in liver biopsies from NAFLD patients with steatohepatitis (NASH) (Csak et al., 2011; Wree et al., 2014).

1.3.3 Hepatocyte death

Fatty acid-induced liver cells death is a critical feature of NAFLD progression. Recent studies have reported increased hepatocyte apoptosis in NAFLD patients with progressive disease (Adams et al., 2005; Feldstein et al., 2003). Apoptosis can be induced by multiple factors i.e. cellular stress, generation of reactive oxygen species and DNA damage etc. However, these factors mediate apoptosis either via the extrinsic or intrinsic pathways. The extrinsic pathway involves death receptor signaling and subsequent activation of a cascade of caspases (caspase 1, 3, 7, 8) to induce apoptosis (Alkhouri et al., 2011; Arrese et al., 2016). The intrinsic pathway involves signaling from intracellular organelles (mitochondria, endoplasmic reticulum etc.) in response to stress stimuli (oxidative stress) and release of additional proteins (cytochrome C, CHOP etc.) that in turn trigger caspases (Alkhouri et al., 2011; Elmore, 2007; Syn et al., 2009). In response to fatty acid-mediated oxidative stress, prolonged ER stress can cause hepatocyte apoptosis. Inositol requiring enzyme 1 (IRE1) and Protein kinase RNA-like ER kinase (PERK) branches of ER stress can induce apoptotic signaling pathways in hepatocytes (Lebeaupin et al., 2016; Wang et al., 2018; Zhang et al., 2014). In detail, activated IRE1α induces apoptosis via activation of pro-apoptotic proteins (Bax and Bim) through TRAF2 mediated activation of apoptosis-signal-regulating kinase 1 (ASK1) followed by activation of c-Jun N-terminal kinase (JNK) (Hu et al., 2006; Urano et al., 2000). PERK signaling activates the CCAAT enhancer-binding protein (C/EBP) homologous protein (CHOP), which is a major regulator of ER stress-induced apoptotic factors such as PUMA and Casapse1.

1.3.4 Inflammation and fibrosis

Persistent fat-induced hepatocyte damage has recently been shown as one of the key mechanisms in NAFLD progression (Ibrahim et al., 2018; Zámbó et al., 2013). Consistently, fatty acid accumulation in hepatocytes generates prolonged ER-stress, which may then trigger cell death (pyroptosis). Damaged hepatocytes release stress signals (Danger associated molecular patterns (DAMPs)) to initiate inflammatory responses (Chen et al., 2018)and progressive fibrosis. Danger associated molecular patterns (DAMPs) released from affected hepatocytes activate the innate immune system via Kupffer cells (KC) activation

and this gives rise to hepatic inflammation in the liver (Luedde et al., 2014; Seki et al., 2015). In fact, activated Kupffer cells release pro-inflammatory cytokines, chemokines (tumor necrosis factor-alpha (TNFα), tumor growth factor-*β* (TGF-*β*), Interleukin-6 (IL-6)) and chemotactic agents (C-C motif ligand 2 and 5 (CCL2 and CCL5) to foster organ inflammation immune cells recruitment (e.g. monocytes, macrophages etc.) as well as activation of hepatic stellate cells (HSCs). Activated HSCs are a major source of extracellular matrix protein secretion and hence, play a key role in organ fibrosis (Arrese et al., 2016; Van Herck et al., 2019; Vonghia et al., 2013).

Hepatocyte ER stress can induce liver inflammation through inflammasome-dependent and independent mechanisms. For instance, CHOP induction in response to prolonged ER stress can activate caspase 1 (casp1) and this event results in activation of premature IL-1β (a pro-inflammatory cytokine). CHOP also mediates hepatocyte NLRP3 inflammasome activation. Inflammasomes play a vital role in inducing inflammation via release of pro-inflammatory cytokines (IL-1β, IL1α and IL-33 etc.) (Chen et al., 2018). Upon activation by inflammasomes, IL-1β induces IL-6 and TNFα production which, which stimulate activation of macrophages and stellate cells to cause inflammation and fibrosis (Negrin et al., 2014). Mice with either IL-1α or IL-1β knock-down show significantly reduced steatosis and inflammation after exposure to high-fat diet (Kamari et al., 2011). Blocking of ER stress-induced NLRP3 inflammasomes or its components protects against hepatocytes pyroptosis and liver inflammation. Previous studies have suggested NLRP3 inflammasomes as potential therapeutic target for NAFLD and its progression to NASH (Han et al., 2018; Wree et al., 2014).

1.4 Nuclear factor of activated T-cells (NFAT)

NFAT (Nuclear factor of activated T cells) transcription factors were first discovered and extensively studied in T-lymphocytes, where they play essential roles during the process of activation. The NFAT family comprises four calcium-regulated members (NFATc1-NFATc4), which reside in the cytosol in an inactive and hyperphosphorylated form. Upon cytokine stimulation and calcium driven activation of the calcineurin phosphatase, NFAT becomes activated through

dephosphorylation of numerous well-defined serine residues, thus allowing nuclear translocation and subsequent DNA binding at GGAAA consensus sequences of their target gene promoters. Of note, NFAT proteins bind DNA with only low affinity and therefore need to interact with other transcription factor(s) to control target gene expression (Pan et al., 2013). The selection of partnering transcription factors and other chromatin regulating proteins, e.g., HDAC proteins, not only define NFAT-DNA binding capacities but also determine NFAT substrate specificity and hence, control the functional consequences of NFAT transcription. Increased expression and activation levels of NFAT members, specifically of NFATc1, have been reported in patients with livers diseases including progressive NFALD (Mancini et al., 2009; Shaw et al., 1988).

Upon activation, NFATc1 controls hallmarks of tumorigenesis (e.g. loss of contact-mediated growth inhibition, acquisition of growth autonomy and protection from apoptosis) through its ability to regulate gene transcription NFATc1 is overexpressed and transcriptionally active in multiple epithelial cancers (e.g. hepatic cancer, colon cancer, pancreatic cancer) and particularly in tumors embedded in an inflammatory environment (Daniel et al., 2014; Mancini & Toker, 2009). Moreover, NFATc1 is ectopically induced and highly active in most human pancreatic cancer, where its

expression correlates with peritumoral inflammation, de-differentiation and a particular aggressive and highly metastatic phenotype (Buchholz et al., 2006; Chen et al., 2015). Our laboratory has previously shown that NFATc1 forms complexes with different transcriptional regulators, e.g. STAT3, myc, c-Jun and

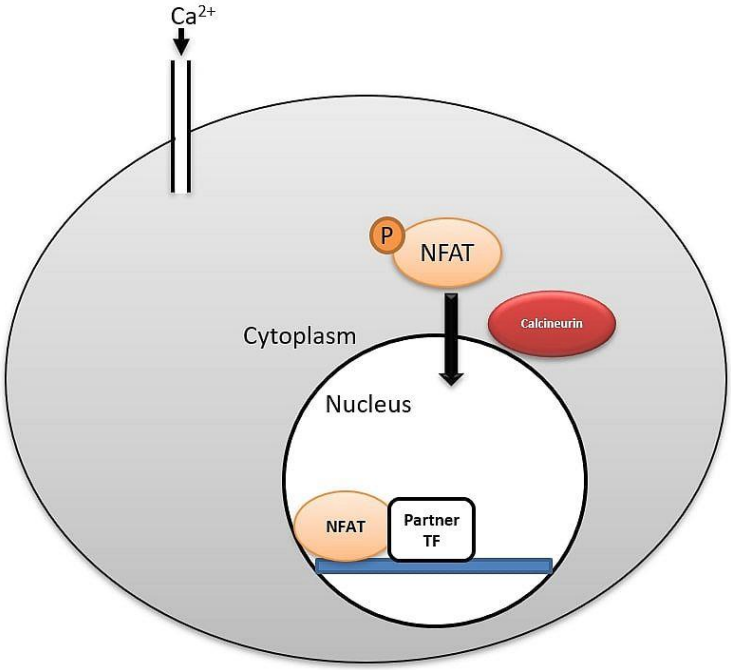

Figure 4: Regulation of Nuclear factor of activated T-cells (NFAT)

NFAT is a family of transcription factors comprising four calcium-regulated members NFAT1 (NFATc2), NFAT2 (NFATc1), NFAT3 (NFATc4) and NFAT4 (NFATc3). NFAT proteins reside in the cytosol in a hyperphosphorylated state. Calcium influx activates calcineurin via calmodulin to dephosphorylates cytoplasmic NFAT at serine residues. Upon activation, NFAT shuttles into the nucleus and regulates gene transcription in concert with other partner transcription factors. (Modified from (Fernandez-Zapico et al., 2010).

Sox2 to govern

extracellular signals and control cell-type and cell-activation dependent gene signatures and functions in Kras-driven pancreatic cancer (Baumgart et al., 2014; Singh et al., 2015).

1.4.1 NFATc1 in the development and progression of hepatic diseases

In the past, the role of NFATc1 in liver disease has not been thoroughly investigated. In fact, only a few scientific studies have examined NFATc1 expression and function in the liver. These studies, however, unequivocally showed high levels of NFATc1 in patients with NAFLD and hepatic tumor cells as well, where it controls proliferation and survival. Immunostaining in hepatic tumor cells showed nuclear translocation of NFATc1 and overexpression of its activator calcineurin (Wang et al., 2012; Zhu et al., 2016). Unfortunately, so far, no data are available on the role of NFAT signaling in NAFLD development and progression, although NFAT is well-known for its capacity to promote cytokine release and inflammation in many epithelial cells under stress conditions. In addition, most recently, NFATc1 has been identified as a novel ER stress-induced transcription factors involved in UPR signaling (Jiang et al., 2016).

1.5 Objectives

NFATc1 regulation and function been studied extensively in human inflammatory diseases and in the development of various solid tumors e.g., skin inflammation, pancreatic cancer etc.(Alrefai et al., 2016; Chen et al., 2015; Köenig et al., 2010). In the liver NFATc1 expression was found to be upregulated in NAFLD patients and in HCC samples as well, although its precise role in NAFLD development and progression has not been addressed so far (Zhu et al., 2016).

This project was aimed to explore the impact and the underlying mechanisms of the NFATc1 transcription factor in NAFLD progression to NASH and subsequent liver fibrosis. Specifically, we hypothesize that NFATc1 drives NAFLD disease progression in response to prolonged ER stress through regulation of cell damage/death and activation of the inflammasome.

We will address the following aims:

(i) To characterize the expression and functional role of NFATc1 in fat-induced NAFLD progression.

(ii) To determine NFATc1-mediated signaling mechanisms and gene signatures in fat-induced NAFLD progression

(iii) To analyze the role of NFATc1 signaling in fat-induced ER stress and activation of unfolded protein responses (UPR)

(iv) To validate the therapeutic potential of ER stress relief on fat-induced and NFATc1 driven NAFLD progression

2.0 Materials

2.1 Antibodies

Antibodies used in this study for western blot (WB), Immunohistochemistry (IHC) and immunofluorescence (IF) are listed in the following tables along with their origin, dilutions and applications:

***Table 1: List of Antibodies*:**

All the antibodies used along with their specie, application, concentration and company are listed below.

Primary Antibody	Origin	Dilution (WB)	Dilution (IHC/IF)	Company
β-Actin HRP	--	1:40000	--	Sigma-A3854
CD45	Rat	--	1:50	BD-550539
HA-tag	Rabbit	1:1000	1:100	Cell signaling-3724
Eif2α	Rabbit	1:1000	--	Cell signaling-9722
p-eif2α	Rabbit	1:1000	--	Cell signaling-9721
CHOP	Mouse	1:100	--	Cell signaling-2895
Cleaved caspase 3	Rabbit	1:1000	1:200	Cell signaling-9661
Cleaved Caspase 1	Rabbit	1:1000	--	Cell signaling-67314
Cleaved IL1β	Rabbit	1:1000	--	Cell signaling-52718
Ddit3/CHOP	Rabbit	--	1:100	Abcam ab179823
NFATc1	Mouse	1:500	--	Santa Cruz sc-7294

NFATc1	Rabbit	--	1:100	Abcam ab25916
NLRP3	Mouse	1:1000	1:100	Adipogen AG-203-0014-C101
P53	Mouse	1:1000	--	Cell signaling-2524
pP53 (s15)	Rabbit	1:1000	--	Cell signaling-9284

***Table 2: List of secondary antibodies*:**

Secondary antibodies used in this study with their origin, application and concentrations are listed below.

Secondary antibody	Origin	Dilution (WB)	Dilution (IHC/IF)	Company
Anti-mouse IgG, HRP-linked	rabbit	1:10000	--	Cell signaling-7074
Anti-rabbit IgG, HRP-linked	mouse	1:10000	--	Cell signaling-7076
Goat anti-mouse IgG H+L (cy3)	Goat	--	1:500	Dianova 115-165-003
Goat anti-rabbit IgG - H&L (cy3)	Goat	--	1:500	Abcam ab6939

2.2 Primers

All the primers used for RT-PCR and genotyping are listed below.

***Table 3: Primers used for Real-time PCR*:**

Primers were diluted to 10µM concentration in Aqua dest.

Gene		**Sequence**
Atf3	Forward	5′-GGAGTGCCTGCAGAAAGAGT-3′

	Reverse	5′-CCATTCTGAGCCCGGACAAT-3′
Atf4	Forward	5′-TGGCACAGTCAAGGCTGAGA-3′
	Reverse	5′-CTTCTGAGTGGCAGTGATGG-3′
Bak1	Forward	5'-ATATTAACCGGCGCTACGAC-3'
	Reverse	5'-AGGCGATCTTGGTGAAGAGT-3'
Ccl1	Forward	5′-GGATGTTGACAGCAAGAGCA-3′
	Reverse	5′-TAGTTGAGGCGCAGCTTTCT-3′
Ccrl2	Forward	5'-TGTGTTTCCTGCTTCCCCTG-3'
	Reverse	5'-CGAGGAGTGGAGTCCGACAA-3'
Cebpb	Forward	5'-CAAGAAGACGGTGGACAAGCT-3'
	Reverse	5'-GTCAGCTCCAGCACCTTGTG-3'
Caspase-2	Forward	5'-GAATGAACCTTATCGGGCATAACT-3'
	Reverse	5'-GATGACGGGTGATAGTGTGAGACA-3'
Caspase-3	Forward	5′-AGGGGTCATTTATGGGACA-3′
	Reverse	5′-TACACGGGATCTGTTTCTTTG-3 ′
Caspase4	Forward	5’-GGCAGGACAAATGCTTCTTC-3’
	Reverse	5’-TGCGGTTGTTTCTCTCCTTT-3’
Caspase7	Forward	5′-CAGACCGCTCCTCTATCATCT-3
	Reverse	5′-CATCGGTCTCCCCTAAAATG-3′
Chop	Forward	5′-AAGATGAGCGGGTGGCAGCG-3′
	Reverse	5′-GCACGTGGACCAGGTTCTGCT-3′
Cxcl2	Forward	5′-GAAGTCATAGCCACTCTCAAGG-3′
	Reverse	5′-TTCCGTTGAGGGACAGCA-3′
Cxcl 9	Forward	5′-CGGACTTCACTCCAACACAG-3′
	Reverse	5′-TAGGGTTCCTCGAACTCCAC-3′
Cxcl 10	Forward	5′-TGCCATTCTGATTTGCTGCC-3′
	Reverse	5′-TGCAGGTACAGCGTACAGTT-3′
Cxcl 11	Forward	5’-GGCTGCTGAGATGAACAGGAA-3’
	Reverse	5’-AAAGACAGCGCCCCTGTTT-3’
Cxcl 13	Forward	5′-CAGGCCACGGTATTCTGGA-3′
	Reverse	5′-CAGGGGGCGTAACTTGAATC-3′
Gapdh	Forward	5′-ATGACTCTACCCACGGCAAG-3′
	Reverse	5′-CTGGAAGATGGTGATGGGTT-3′
Il-1β	Forward	5′-TGGACCTTCCAGGATGAGGACA-3′
	Reverse	5′-GTTCATCTCGGAGCCTGTAGTG-3′

Il-6	Forward	5′CATGTTCTCTGGGAAATCGTGG 3’
	Reverse	5′GTACTCCAGGTAGCTATGGTAC 3’
Il-18	Forward	5′-CAGGCCTGACATCTTCTGCAA-3′
	Reverse	5′-CTGACATGGCAGCCATTGT-3′

Table 4: Primers used for genotyping

Target	**Direction**	**Sequence**
Cre	Forward	5′-ACCAGCCAGCTATCAACTCG-3′
	Reverse	5′-TTACATTGGTCCAGCCACC-3′
NFATc1 (Knock-out)	INT2S-5	5′-AAGGAATTACTGGGAAGCCTGGCA3′
	INT3S-2	5′-AGGGACTATCATTTGGCAGGGACA-3′
	INT3AS-2	5′-ACAGGAAACAGCTCTGTTCCACAC-3′
c.n. NFATc1 (Knock-in)	Forward	5′-CATGTCTGGGAGATGGAAGC-3′
	Reverse	5′-TCTCGAGCTACTTGTCATCG-3′
Rosa26	Forward	5′-GGCGGATCACAAGCAATAAT-3′
	Reverse	5′-GAGTCTTCTGGGCAGGCTTA-3′

2.3 Nucleic Acids

Table 5: List of small interfering RNA´s (siRNA) Used

Nucleic acids used for gene silencing and overexpression are listed below:

siRNA	**Supplier**	**Catalog No.**
NFATc1	Thermofisher Scientific	AM16708

Table 6: List of constructs and their vectors used for overexpression

Construct	**Insert**	**Mutation**	**Source**	**Vector**	**Resistance**	**Tag**

MSCV-caNFATc1	mut. caNFATc1	Ser to Ala Mut. In conserved residues of SRD + all SP repeat motif	Human	MSCV - GFP	Ampicillin	HA (N-Term) Flag (C-T.)

2.4 Chemicals

Chemicals used are listed with their respective companies:

***Table 7: List of Chemicals*:**

All the chemicals used in the present work and their respective companies, are listed below.

CHEMICAL	**COMPANY**
Albumin standard	Thermo Scientific, Waltham, USA
Acetic acid	Sigma-Aldrich, St. Louis, USA
Acrylamide (30%/0,8%)	Carl Roth GmbH Co. KG, Karlsruhe, Germany
Agarose	Biozym Scientific GmbH, Oldendorf, Germany
Aqua	B.Braun, Melsungen, Germany
Bovine serum albumin (BSA)	Serva, Germany
β-Mercaptoethanol	Merck, Darmstadt, Germany
Boric acid	Merck, Darmstadt, Germany
Bromophenol blue	Sigma-Aldrich, St. Louis, USA
Calcium chloride	Applichem, Darmstadt, Germany

Citric acid monohydrate	Carl Roth GmbH Co. KG, Karlsruhe, Germany
Collagenase	Roche, Basel, Switzerland
cOmplete™	Roche, Basel, Switzerland
Dexamethasone	Sigma-Aldrich, St. Louis, USA
DTT	Sigma-Aldrich, St. Louis, USA
ECL Plus	PerkinElmer, Inc., Waltham, USA
EDTA	Acros organics, Belgium
EGTA	Sigma-Aldrich, St. Louis, USA
Ethanol	ChemSolute®, Th.Geyer ingredients GmbH & Co.KG, Höxter, Germany
Eosin	Sigma-Aldrich, St. Louis, USA
Fatal bovine serum (FBS)	Biowest S181B-500
Formaldehyde (4%)	Merck, Darmstadt, Germany
Fructose	Carl Roth GmbH Co. KG, Karlsruhe, Germany
HEPES	Carl Roth GmbH Co. KG, Karlsruhe, Germany
Glycerol	Carl Roth GmbH Co. KG, Karlsruhe, Germany
Glucose	Merck, Darmstadt, Germany
Haematoxylin	Sigma-Aldrich, St. Louis, USA
Hydrochloric acid	Carl Roth GmbH Co. KG, Karlsruhe, Germany
Hydrogen peroxide	Carl Roth GmbH Co. KG, Karlsruhe, Germany

Insulin-Transferrin-Selenium-Ethanolamine (ITS -X) (100X)	Life technologies, Carlsbad, CA 51500-056
Isoflurane	AbbVie Deutschland GmbH & Co. KG, Ludwigshafen, Germany
Magnesium chloride	Applichem, Darmstadt, Germany
Methanol	Carl Roth GmbH Co. KG, Karlsruhe, Germany
Non-fat milk powder	Carl Roth GmbH Co. KG, Karlsruhe, Germany
Normal Goat serum	Abcam ab7481
Natriumfluorid (NaF)	Sigma-Aldrich, St. Louis, USA
Orthovanadat (NaO)	Sigma-Aldrich, St. Louis, USA
Penicillin/Streptomycin (P/S)	Sigma-Aldrich, St. Louis, USA
PBS (Dulbecco's)	Biochrom, Berlin, Germany
PMSF	Sigma-Aldrich, St. Louis, USA
Potassium chloride (KCl)	Merck, Darmstadt, Germany
Potassium dihydrogen phosphate (KH_2PO_4)	Merck, Darmstadt, Germany
Protein assay die reagent concentrate (Brad ford reagent)	Bio-rad Hercules USA 5000006
Sodium phosphate dibasic (Na_2HPO_4 x 2 H_2O)	Carl Roth GmbH Co. KG, Karlsruhe, Germany
Roticlear	Carl Roth GmbH Co. KG, Karlsruhe, Germany
Rotimount	Carl Roth GmbH Co. KG, Karlsruhe, Germany
Saline (0,9% NaCl)	B.Braun, Melsungen, Germany

Sodium chloride	Merck, Darmstadt, Germany
Sodium citrate	Sigma-Aldrich, St. Louis, USA
Sodium dodecyl sulphate	Carl Roth GmbH Co. KG, Karlsruhe, Germany
Sodium hydroxide	Acros organics, Geel, Belgium
Sodium Orthovanadate	Sigma-Aldrich, St. Louis, USA
Sodium pyrophosphate	Sigma-Aldrich, St. Louis, USA
Sodium pyruvate	Gibco® Thermo Scientific, Waltham, USA
Sodium Palmitate	Sigma-Aldrich, St. Louis, USA
Trypsin	Gibco® Thermo scientific, Waltham, USA, 15400-54
TUDCA	Sigma-Aldrich, St. Louis, USA
Thioacetamide	Sigma-Aldrich, St. Louis, USA
Tris-HCl	Carl Roth GmbH Co. KG, Karlsruhe, Germany
Tris-base	Carl Roth GmbH Co. KG, Karlsruhe, Germany
Triton X-100	Sigma-Aldrich, St. Louis, USA
Trizol	Invitrogen by Thermo scientific, Carlsbad, CA
Tween-20	Sigma-Aldrich, St. Louis, USA
Water Per Oxide, 30%	Carl Roth GmbH Co. KG, Karlsruhe, Germany

2.5 Kits and Reagents

***Table 8: List of kits and reagents*.**

All the kits were used according to the manufacturer's instructions.

KITS/REAGENTS	COMPANY
Agarose A Beads	Merck Millipore, Billerica, USA
Agarose G Beads	Merck Millipore, Billerica, USA
iScript cDNA Synthesis Kit	Bio Rad Laboratories, Hercules, USA
iTag Universal SYBR Green Supermix	Bio Rad Laboratories, Hercules, USA
DAB ImmPACT	Biozol, Vector Laboratories, Eching, Germany
MycoAlert Mycoplasma Detection Kit	Lonza Group, Basel, Switzerland
Trans-Blot Turbo RTA Midi Nitrocellulose Transfer Kit	Bio Rad Laboratories, Hercules, USA
Cytokine proteome profiling kit	R&D systems, Boston, USA
Peroxidase Rabbit IgG Vectastain ABC Kit	Biozol, Vector Laboratories, Eching, Germany
Peroxidase Mouse IgG Vectastain ABC Kit	Biozol, Vector Laboratories, Eching, Germany
Proteome Profiler Human Cytokine Array Kit	R&D systems, Boston, USA

2.6 Buffers

2.6.1 Western blot buffers

Table 9: Composition of the ready gel stock solutions.

All the buffers used in western blot and their compositions are listed in the tables below:

Solution	Components	Concentration
Stacking gel Stock solution	Tris base	0.5M
pH 6.8	SDS	0.4%(v/v)
Separating gel Stock Solution	Tris base	1.5M
pH 8.8	SDS	0.4%(v/v)

Table 10: Composition of "ready to use" separating gel solutions

Solution	**Components**	**Amount**
Separating gel 10% "ready-to-use" (20 gels)	Separating gel stock solution	25 ml
	Ampuwa (H_2O)	36.7 ml
	Acrylamide (30%/0.8%)	33.3 ml
	Glycerin	5 ml
Separating gel 15% "ready-to-use" (20 gels)	Separating gel stock solution	20 ml
	Ampuwa (H_2O)	20 ml
	Acrylamide (30%/0.8%)	50 ml
	Glycerin	5 ml
Ready-to-use stacking gel solution	Separating gel stock	25 ml
	Ampuwa (H2O)	59 ml
	Acrylamid (30%/0,8%)	16 ml

Table 11: Composition of laemmli and running buffer

Solution	Component	**Concentration**
Laemmli buffer	Tris pH6,8	225 mM
	DTT	100 mM
	Bromophenol blue	0.02% (v/v)
	Glycerol	50% (v/v)
	SDS	5% (v/v)
Running Buffer (1x)	Tris-Base	250mM
	Glycerin	1.92M
	SDS	1% (v/v)

Table 12: Tris buffer saline (1L) pH 7.4 (TBS)

Component	**Concentration (w/v)**
Tris-Base	6.05 %
NaCl	8.73 %

Table 13: Composition of whole cell lysate (WCL) buffer

Buffer	**Component**	**Concentration**
Whole cell lysate buffer	HEPES pH 7,5 – 7,9	50mM
	NaCl	150nM
	EGTA	1mM
	Glycerin	10% (v/v)
	Triton X-100	1% (v/v)

	NaF	100 mM
	$Na_4P_2O_7$ x 10 H_2O	10 mM
	cOomplete™ (Roche)	1x (following manufactures protocol)
	1mM Orthovanadat	1mM

2.6.2 Immunohistochemistry/immunofluorescence buffers

Following tables contain all the buffers used in IHC or IF and their components.

Table 14: Buffer used in IHC/IF and their composition

Buffer	**Component**	**Concentration (w/v)**
Phosphate buffer Saline	NaCl	40%
(5L) pH 7.2-7.4	KCl	1%
	KH_2PO_4 (Potassium dihydrogen phosphate)	1%
	Na_2HPO_4 x 2 H_2O (Sodium phosphate dibasic)	3.%g
Citrate buffer (pH=6.0)	Citric acid monohydrate	2.1%
	Aqua dest	1L
TE buffer 10x (pH=9.0)	Tris-Base	12.1%
	EDTA	3.7%
	Aqua dest	1L

2.7 Cell Culture

All the cell lines, primary cells and mediums used are listed in tables below.

Table 15: Cell lines and primary cells used

Cell line	Company
AML12 cells	ATCC CRL-2254
Primary hepatocytes	Isolated from NFATc1^{WT}, NFATc1$^{+/-}$, and NFATc1$^{-/-}$ mouse

Table 16: Mediums used to maintain cells

Medium	Company	Catalogue No.
DMEM/F-12 1:1	Thermo fisher scientific	Gibco-11320074
Williams Medium E (1x)	Thermo fisher scientific	Gibco-22551-022

2.7.1 Primary cells isolation

Buffers:

Following buffers were used for isolation of mouse primary hepatocytes:

Table 17: Composition of Buffers for primary hepatocytes isolation

Buffer	Component	Concentrations
HANKS buffer (1L) pH=7.4	NaCl	8% (w/v)
	KCl	0.4%(w/v)
	Na_2HPO_4 * $2H_2O$	0.06%(w/v)
	KH_2PO_4	0.06(w/v)
Composition of HANKS buffer I	HANKS buffer pH07.4	200ml
	0.5 M EGTA	800µl

	10% (v/v) Glucose	2ml
Composition of HANKS buffer II	HANKS buffer pH 7.4	100ml
	10%(v/v) Glucose	1ml
	5mMol/L $CaCl_2$	1ml
	Collagenase	0.3 mg/ml

2.7.2 Mediums:

Following mediums were prepared and used in hepatocytes cultures:

Table 18: Mediums used for primary hepatocytes cultivation

Medium	Ingredient	Concentration
Attachment Medium	William's Medium E	
	FCS	10% (v/v)
	Dexamethasone	100nM
	Glutamine	2mM
	Penicillin/streptomycin	1% (v/v)
Pre-starvation medium	William's Medium E	
	Dexamethasone	100nM
	Glutamine	2mM
	Penicillin/streptomycin	1% (v/v)
Starvation Medium	William's Medium E	
	Glutamine	2mM
	Penicillin/streptomycin	1% (v/v)

2.8 Equipment's

The equipment used in this study is listed below:

Table19: List of equipment

Equipment	Company
Agarose gel electrophoresis chamber-Model 40-0911	Peqlab Biotechnologie GmbH, Erlangen, Germany
Arium®pro ultrapure water system	Sartorius, Göttingen, Germany
Aspirator with trap flask	Grant Instruments Ltd, Cambs, England
Autoclave	TecnomaraIntegraBiosciences, Deutschland GmbH
Class II safety cabinet (S2020 -1.2)	Thermo Fisher scientific, Waltham, USA
Cold plate (Histocore Arcadia c)	Leica Biosystem, Wetzlar, Germany
Dri-Block Heater DB2A	Techne, Staffordshire, UK
Flex cycler block	Analytikjena, Germany
Fluorescence Microscope System	Leica Camera, Wetzlar, Germany
Heating plate	Leica Biosystem, Wetzlar, Germany
HERAcell 240i CO_2 incubator	Thermo Scientific, Waltham, USA
Ice flaker (AF80)	Scotsman, Edinburgh, UK
INTAS- ECL Chemostar imager	INTAS Science Imaging Instruments GmbH, Göttingen, Germany
Inverted microscope (CKX53SF)	Olympus, Tokyo, Japan
Light microscope "BX43"	Olympus, Tokyo, Japan
Magnetic stirrer (RH B S000)	IKA®Laboratory equipment, Germany
Microplate Luminometer "LUMO"	Autobiolabtec Instruments Co.,Ltd, Zhengzhou, China

Microplate reader "PHOmo"	Autobiolabtec Instruments Co.,Ltd, Zhengzhou, China
Microwave (NN-E209W)	Panasonic; Japan
Microtome (Leica RM2265)	Leica Biosystems, Wetzlar, Germany
Mini-PROTEAN Tetra Cell	Bio Rad Laboratories, Hercules, USA
MSA Minishaker	IKA, Staufen, Germany
Multifuge X1 Centrifuge Series	Thermo Scientific, Waltham, USA
Multipette plus	Eppendorf, Hamburg, Germany
NanoPhotometer P-330	Intas Science Imaging Instruments, Goettingen, Germany
Neubauer chamber	Assistant, Sondheim/Rhön, Germany
Paraffin Tissue embedder (EG1150H)	Leica Biosystems, Wetzlar, Germany
pH meter (FiveEasy™ Plus FEP20)	Mettler-Toledo AG, Schwerzenbach, Switzerland
PerfectSpin 24R Refrigerated Microcentrifuge	Peqlab, Erlangen, Germany
Pipetboy acu 2	INTEGRA Biosciences, Biebertal, Germany
PowerPac Basic Power Supply	Bio Rad Laboratories, Hercules, USA
Precision balance PCB	Kern & Sohn, Balingen, Germany
PSU-20i Orbital Shaking Platform	Grant Instruments, Shepreth, UK
Refrigerator 4°C (Comfort)	Liebherr, Bulle, Swtzerland
Safe 2020 Class II Biological Safety Cabinets	Thermo Fisher Scientific, Waltham, USA

Sequenza™ slide rack (cadenza system)	TED PELLA, INC, Redding, CA
Shandon coverplate™ (cadenza system)	Thermo Scientific, Waltham, USA
Sprout Minicentrifuge	Biozym Scientific, Hessich Oldendorf, Germany
StepOnePlus Real-Time PCR System	Thermo Fisher Scientific, Waltham, USA
Thermomixer 5436	Eppendorf, Hamburg, Germany
Tissue dehydration machine (automated)	Leica Biosystems, Wetzlar, Germany
Trans-Blot Turbo Transfer System	Bio Rad Laboratories, Hercules, USA
TX-400 4 x 400mL Swinging Bucket Rotor	Thermo Fisher Scientific, Waltham, USA
Universal Oven UN55	Memmert, Schwabach, Germany
VacuuHandControl VHC^{pro}	Vacuumbrand, Wertheim, Germany
Vacuum pump: BVC Control	Vacuumbrand, Wertheim, Germany
Vortex	Heidolph Instruments GmbH & Co. KG, Schwabach, Germany
Water bath (WNB14)	MemmertGmbH+Co. KG, Schwabach, Germany
Weighing balance	Sartorius AG, Göttingen, Germany
-20°C freezer	Liebherr, Bulle, Swtzerland
-80°C Ultra low temperature freezer (MDF-U54V)	Sanyo electric Co.,Ltd Japan

2.9 Consumables

Table 20: List of consumables

Materials	Company
Centrifuge tube 15 and 50 ml	Sarstedt, Nümbrecht, Germany
Cell strainer-100µm	Falcon, Durham, USA
Cell scrapper	Sarstedt, Nümbrecht, Germany
Cello meter counting chamber	Nexcelom Bioscience, Lawrence, MA
Cryo pure vial	Sarstedt, Nümbrecht, Germany
Combitips advanced (Multipipette tips)	Starlab International GmbH, Hamburg, Germany
Filter paper (western blot)	Bio Rad Laboratories, Hercules, USA
Graduated sterile pipettes (2,10,25 and 50ml)	Greiner bio-one, Frickenhausen, Germany
Glass coverslips (24×32, 24×60)	Menzel Gläser®, Menzel GmbH+Co KG, Braunschweig, Germany
Micropipette filter tips	Starlab International GmbH, Hamburg, Germany
Micropipette tips	Starlab International GmbH, Hamburg, Germany
Microtome blade (S35)	Feather safety Razer Co. Ltd, Japan
Microtube (1.5 and 2ml)	Feather safety Razer Co. Ltd, Osaka, Japan
Injection needle (Sterile)	Sarstedt, Nümbrecht, Germany
Nitrocellulose membrane	B.Braun, Melsungen, Germany
Parafilm	GE Healthcare lifesciences, Marlborough, USA
PCR tubes	Pechiney plastic packaging, Chicago, USA
Scalpel	Sarstedt, Nümbrecht, Germany

Serological pipette (2ml)	Feather safety Razer Co. Ltd, Osaka, Japan
Sponge Pad for XCell IITM Blotting	Greiner bio-one, Frickenhausen, Germany
Superfrost glass slides (Histology)	Thermo Scientific, Waltham, USA
Syringe (1ml)	BD Plastic, Madrid, Spain
Syringe (5,10,20ml)	B.Braun, Melsungen, Germany
Sterile syringe Filter (0.2µm)	Labsolute, Th.Geyer ingredients GmbH & Co.KG, Höxter, Germany
Tissue culture multiwell plates	Greiner bio-one, Frickenhausen, Germany
Tissue culture flasks	Greiner bio-one, Frickenhausen, Germany
Tissue culture dishes (2cm, 10cm)	Sarstedt, Nümbrecht, Germany
Tissue cassette	Sanowa, Leimen, Germany

3.0 Methods

3.1 Mouse models

In order to investigate the hepatocyte-specific role of NFATc1 in NAFLD development and its progression to NASH, we employed a hepatocyte-specific Nfatc1 knock-in and knock-out approach using the Cre/loxP system. For the generation of Alb-Cre;NFATc1$^{fl/fl}$ mice, mice with heterozygous expression of cre-recombinase under albumin promoter (Alb-cre$^{+/-}$, kindly provided by Dr. Ihtzaz Malik) were crossed with NFATc1$^{fl/fl}$ mice, which bear loxP flanks adjacent to the regulatory domain (exon 3) of Nfatc1 (Aliprantis et al., 2008), to generate NFATc1$^{fl/fl}$; Alb-cre$^{+/-}$ mice with homozygous loss of NFATc1 (hereafter referred to as NFATc1$^{-/-}$). The *c.n.Nfatc1* knockin strain (C57BL/6 background) was generated as described previously (Baumgart et al., 2014). In detail, an N-terminal HA-tagged constitutively active version of NFATc1 containing serine to alanine substitutions in the conserved serine-rich domain was cloned into the ROSA26 promoter locus (Artemis Pharmaceuticals). To obtain Alb-Cre; ROSA26-LSL.c.a.NFATc1 (NFATc1$^{+/-}$) mice, Alb-cre$^{+/-}$ strains were crossed with c.a.NFATc1 mice. Mice harboring heterozygous cre-recombinase under albumin promoter (Alb-Cre$^{+/-}$) with wildtype NFATc1 expression were used as control (referred to as NFAT^{WT}). Mice containing Alb-cre were kept in heterozygous background to avoid cre-induced toxicity (Gkretsi et al., 2008). Breeding of mice was performed in the Central Animal Facility of the UMG.

All mice were kept under controlled atmosphere in 12 hours light and dark cycles and genotyped at the age of 3-4 weeks. At the age of 8 weeks, mice were subjected to treatments as indicated below.

3.1.1 Western diet (WD) and components

Western Diet (WD) for mice consists of solid commercially available western diet (ssniff Spezialdiäten GmbH, E15721-347) and enriched drinking water, containing 45% (w/v) glucose (Merck) and 55% (w/v) fructose (Carl Roth GmbH). 8 weeks old mice (male and female) with specific genotypes were either fed for 4, 12 and 20 weeks, with normal diet (ND) and water or with western diet. Each group included 5 animals each time point. Food and water were provided *adlibitum* to both groups.

3.1.2 Thioacetamide (TAA) treatment

To induce liver fibrosis, TAA (Sigma-Aldrich) was injected (25 mg/kg) intraperitoneal (i.p.) in 8 weeks old mice were (n = 5 for each time point). The TAA treatment was performed for 4, 12 and 20 weeks, 3 times/per week, respectively. The control group was injected with vehicle (0.9% NaCl, Merck). During treatment, mice were provided with food and water *ad libitum*.

3.1.3 Tauroursodeoxycholic acid (TUDCA)

The endoplasmic reticulum (ER) stress inhibitor, TUDCA (Merck Millipore, dissolved in PBS) was injected i.p. along with Western Diet (WD). 8 weeks old mice were fed with WD for 20 weeks. In the course of continued WD treatment mice were injected 3 times per week of either TUDCA (500 mg/kg of body weight) or vehicle (PBS).

During treatment, the body weight of each mouse was recorded once a week. At the final time point, mice were anesthetized and sacrificed, followed by harvesting of liver, spleen and blood for molecular, histological and serological analysis.

All the mouse experiments were approved by LAVES and carried out according to the regulations of the Federation of European Laboratory Animal Science Associations (FELASA).

3.2 Cell culture

3.2.1 Alpha mouse liver-12 (AML12) cells

The AML12 cell line (obtained from ATCC CRL-2254) is derived from mouse hepatocytes and exhibit normal hepatocytes features. These cells are widely used as primary hepatocytes replacement for *in vitro* studies involving hepatocyte metabolism, stress signaling and cell damage analysis. AML12 cells were cultured in Dulbecco's Modified Eagle Medium (DMEM)/Nutrient Mixture F-12 (1:1) supplemented with 10% FBS (Biowest S181B-500), 40ng/ml dexamethasone and 5ml/500ml of Insulin-Transferrin-Selenium-Ethanolamine (100X) (Life Technologies 51500-056). Cells were maintained in the incubator at 37°C with 5% CO_2. The medium was exchanged 2 times per week after washing with sterile PBS. At 90% confluency, cells were sub cultivated after washing with PBS, by trypsinization (Gibco, 15400-54 1:10 in PBS). Cultivation medium was added to stop trypsinization and cell were seeded according to target experiment.

3.2.2 Primary hepatocytes

Primary hepatocytes were isolated from 8 weeks old *NFATc1*^{WT}, *NFATc1*$^{+/-}$ and *NFATc1*$^{-/-}$ mice. Hepatocyte isolation was performed using a modified double perfusion method as described (Severgnini et al., 2012). The mouse was anesthetized under 4% isoflurane, followed by cervical dislocation and dissection of the abdominal cavity. The liver was perfused from portal vein using peristaltic perfusion pump, with pre-warmed HANKS buffer-I, at a slow flow rate until the buffer reaches the liver. A small cut was made at visceral vena cava, followed by increasing the speed of perfusion to 8 ml/min for 2-3 minutes to remove blood from the liver. Perfusion tube was switched from HANKS buffer-I to pre-warmed HANKS buffer-II at same speed for 8 minutes or until the liver is swollen. The Liver was harvested and kept in the attachment medium. Next steps were performed in sterile conditions under the safety cabinet. The liver along with the attachment medium was transferred to a petri dish and hepatocytes were released from liver sacs. Rest of the tissue debris was discarded, and the liver suspension was collected after filtering through a 70µm cell strainer. Additionally, 15 ml of attachment medium was used to wash the petri dish and added to the

suspension through the cell strainer. Followed by centrifugation of the combined suspensions at 500rpm for 3 minutes at room temperature (RT) (deceleration was set at 2). After removing the supernatant, the pellet was re-suspended in 15ml attachment medium by pipetting gently up and down. The cell suspension was centrifuged again at the same conditions. This step was repeated 3 times followed by cell pellet re-suspension in 10ml of attachment medium. Cells were counted manually, and viability was assessed using trypan blue staining. 1 million cells/well were seeded in 6 well plates according to the required experiment and incubated at 37°C with 5% CO_2. Six hours later plates were washed with sterile PBS two times. Subsequently, the pre-starvation medium was added, and cells were incubated overnight. Next day, plates were washed 2x with PBS and cells were provided starvation medium including treatment.

3.2.3 Sodium palmitate

Sodium palmitate (Sigma, City, Germany) was used for *in vitro* studies of cells. 2mM stock solution of palmitate in conjugation with BSA (1:6) was prepared in 150mM NaCl. BSA was first dissolved in 150mM NaCl, by heating at 37°C for a working concentration of 0.34mM. Half of the BSA was diluted in 150mM NaCl 1:1 for a final concentration of 0.17mM. BSA solution was sterile filtered, aliquoted and stored at -20°C to be used as a vehicle. At the same time, 61.2 mg of sodium palmitate was dissolved in 50ml of 150mM NaCl, by heating up to 70°C. This solution becomes milky at 60°C and gets clear when the temperature reaches 70°C. Once the palmitate solution becomes clear, transfer 44ml of sodium palmitate solution into the remaining half of the BSA solution at 37°C while stirring, for 1 hour. The pH of the solution was adjusted to 7.4 and the final volume of 100ml filled up with 150mM NaCl, to reach a final concentration of 2mM. The Sodium palmitate/BSA solution was filtered, aliquoted in glass vials and stored at -20°C.

3.2.4 Tauroursodeoxycholic Acid (TUDCA)

TUDCA (Millipore, 580549), a bile acid used as endoplasmic reticulum (ER) stress inhibitor, was used in cell culture to treat AML12 and primary hepatocytes. TUDCA was dissolved in H_2O for a concentration of 20mM. Subsequently, it was filtered and stored at 4 °C for further experiments.

3.2.5 Transfection

To study the role of NFATc1 in fat-induced cell damage, AML12 cells were transfected either with siRNA for *NFATc1* (Invitrogen,288360) or with constitutively active NFATc1 construct (Table 5). Cells were seeded in 6 well plates and allowed to grow until 60% of confluency. siRNA or c.a. NFATc1 construct was prepared in serum-free media with Lipofectamine 2000. Transfection control was given only Lipofectamine 2000 in serum-free media. Mix was then incubated for 10 to 15 minutes at room temperature followed by its delivery to cells. Upon adding transfection medium, cells were provided with serum-containing media in equal volume and incubated for 24 hours 37°C with 5% CO_2.

3.2.6 Cellular Treatments

Fatty acid-induced NFATc1 expression, activation and downstream signalling were analysed in AML12 cells and primary mouse hepatocytes isolated from 8 weeks old mice. Cells were seeded in 6 well plates and allowed to attach overnight before treatment. **I)** For confirmatory analysis of fat-induced NFATc1 activation, AML12 cells and primary hepatocytes from *NFATc1*^{WT} mice were exposed to either vehicle (BSA) or 100µM and 200µM palmitate (Sigma) for 12hours. **II)** For analysis of NFATc1-mediated downstream signaling, AML12 cells were first subjected to 24 hours of transfection with siRNA for *NFATc1* (table 4). After 12 hours of transfection, cells were exposed to 200µM palmitate either alone or in combination with *NFATc1* knock-down. Control cells were exposed to vehicle (Lipofectamine 2000 with BSA). In contrast, primary hepatocytes isolated from *NFATc1*^{WT}, *NFATC1*$^{+/-}$ and *NFATc1*$^{-/-}$ mice were exposed directly to 100µM

and 200µM palmitate. BSA was added in controls as vehicle. **III)** To analyze the effect of ER stress inhibition on cell damage, AML12 cells were treated with 200µM palmitate alone or in combination with 500µM TUDCA (Millipore) dissolved in water. Controls were treated with the corresponding vehicle. In additional experiments, AML12 cells were transfected with constitutively active NFATc1 construct (Table 5) for 24 hours either alone or exposed to 500µM TUDCA after 12 hours of transfection. Control cells were treated with vehicle (lipofectamine and water). Cells after each treatment were harvested for protein and RNA isolation followed by molecular analysis of respective markers i.e. NFATc1, ER stress and apoptosis markers etc.

3.3 Molecular Methods

3.3.1 Genotyping

DNA for genotyping was isolated from tail biopsies of 3 to 4 weeks old mice. Biopsies were subjected to tissue lysis by incubating in 75µl of alkaline lysis buffer (0.2mM EDTA,25mM NaOH), for 30 minutes at 95°C. Next, 75µl of neutralization buffer (40mM Tris-HCl) was added and lysates were stored at -20°C.

Isolated DNA samples were amplified by Polymerase chain reaction (PCR). PCR reaction mix (table 22) was prepared by mixing DNA with PCR mix (, KAPA2G Fast HotStart genotyping mix with dye, Nippon genetics KK5621) and genotype-specific primers (table 4). PCR was carried out in T100 thermal cycler (Bio-Rad 186-1096) using the protocol described in table 23. Amplified fragments were separated by gel electrophoresis (PerfectBlue horizontal Maxi gel systems, Peqlab 700-540) and visualized using ultraviolet trans-illuminator (Bio-Rad Chemidoc XRS+).

Table 19: Reaction mix for genotyping PCR

Genotype	Ingredients	Volume (1x)
NFATc1 k.o.(NFATc1$^{-/-}$)	Master mix	6.25µl
	INT2s-5	0.5µl

	INT3s-2	0.5µl
	INT3As-2	1µl
	H_2O	3.25µl
	DNA	2µl
c.n.NFATc1(NFATc1$^{+/-}$) **and** ***Albumin-cre (NFATc1^{WT})***	Master mix	6.25µl
	Primer Forward	0.5µl
	Primer reverse	0.5µl
	H_2O	4.25µl

Table 20: PCR program. Following PCR programs were used for genotyping of NFATc1$^{-/-}$, NFATc1$^{+/+}$ and NFATc1^{WT} mice.

Genotype	**Temperature**	**Time**	
NFATc1 k.o.(NFATc1$^{-/-}$)	94°C	2 min	
	94°C 66°C 72°C	30 sec 30 sec 1 min	35 cycles
	72°C	5 min	
c.n.NFATc1(NFATc1$^{+/-}$)	95°C	5 min	
	95°C 60°C 72°C	30 sec 30 sec 1 min	35 cycles
	72°C	10 min	
Albumin-cre (NFATc1^{WT})	95°C	2 min	

	95°C 60°C 72°C	30 sec 30 sec 1 min	29 cycles
	72°C	5 min	

3.3.2 Protein isolation and estimation

AML12 cells and primary hepatocytes seeded in 6 well plates were harvested after each experiment for protein isolation. The medium was discarded, and cells were washed twice with ice-cold PBS. Next, WCL buffer (Table 13) was added in each well (30µl to 50µl depending on cell density) followed by scraping of cells and collection of lysates in microcentrifuge tubes. For preparing protein lysates obtained from mouse tissue, small slices of liver were taken from frozen tissues and homogenized in 500µl – 700µl of WCL buffer. Cell lysates and tissue homogenates were incubated on ice for 20 minutes and centrifuged at 13500 rpm, 4°C for 20 minutes. The supernatant was transferred to new tubes and stores at -20°C.

The protein concentration of samples was determined by Bradford assay (Bio-Rad), following manufacturer's instructions. 1µl of each sample was measured in technical duplicates. Known concentrations of BSA dissolved in WCL buffer (Table 13), were used as standards. The absorbance of the samples was measured in microplate reader PHOMO (Autobiolabtec Instruments Co., Ltd) at 595 nm. A standard curve was calculated based on absorbance values of standards and further used to estimate µg/µl protein concentration in samples.

3.3.3 Western blot

Protein lysates were separated based on their size, using sodium dodecyl sulphate-polyacrylamide gel electrophoresis (SDS-PAGE). Samples were prepared by adjusting lysates, prepared in WCL buffer, to equal protein

concentration (1µg/µl) and mixed with 5x laemmli buffer containing 5% (v/v) β-mercaptoethanol. Subsequently, samples were subjected to heating at 95°C for 5 mintues followed by a short spin and cooling on ice.

Gels were prepared (Table 8 & 9) according to the target protein sizes i.e., 15% gels were used for protein with low molecular weights (< 50 kDa) while, 10% gels for high molecular weight proteins (<50kDa up to 180kDa). 20µg – 30µg of prepared samples and 5µl of Pre-stained Protein ladder (Thermo Fischer Scientific, 26617) were loaded in gels followed by electrophoresis in 1x running buffer (Table 11).

In the Next step, protein separation gels were subjected to immunoblotting on nitrocellulose membrane. Immunoblotting was performed in a semi-dry blotting system (Trans-Blot Turbo^{TM} transfer system (Bio-Rad 1704150)) using Trans-Blot Turbo RTA Midi Nitrocellulose Transfer Kit (Bio-Rad 1704271) following the manufacturer's instructions. 10% gels were blotted for 22 minutes, and 15% gels were blotted for 10 minutes at 1.0 ampere and 25 volts. Afterward, blotting membranes were washed for 3 minutes with 1x TBS containing 0.1% tween20 (TBS-T) and blocked for 1 hour at RT in blocking solution (5% milk in TBS-T). Membranes were then incubated with primary antibodies (Table 1) diluted in the blocking solution, overnight at 4°C. On the second day, primary antibodies were removed, membranes were washed 3x for 10 minutes each with 1x TBS-T and incubated with respective secondary antibodies (Table 2) diluted in blocking solution for 1 hour at RT. After removing secondary antibodies, membranes were washed again 3 times for 10 minutes each with 1x TBS-T. Antibody binding was detected by using enhanced chemiluminescence solution (ECL or ECL plus, PerkinElmer NEL10500EA) on membranes for one minute. Membranes were processed for imaging in Intas ECL chemocam Imager (Intas Science Imaging Instruments) using chemostar software (Intas Science Imaging instruments).

3.3.4 RNA isolation

Cells treated in 6-well plates were washed 2x with ice-cold PBS. After aspirating PBS completely, 800µl of TRIzol (Ambion, 15596018) was added in each well and incubated at RT for 2-3 minutes. Cells were scraped and collected in 1.5ml

tubes for further processing or stored at -80°C for later use. 200µl chloroform was added in each tube and vortexed vigorously followed by 5 minutes incubation at RT. Samples were subjected to phase separation by centrifugation at 13500 rpm for 15 minutes at 4°C. The upper aqueous phase was collected in fresh tubes and isopropanol was added in a 1:1 ratio. Samples were mixed thoroughly by inverting tubes followed by 10 minutes of incubation at RT and centrifugation at 13500 rpm for 30 minutes at 4°C. The supernatant was removed, and the pellet was washed 2 times by resuspending in 1ml of 75% ethanol and centrifugation at 13500 rpm for 5 minutes at 4°C. At the end, ethanol was aspirated completely, and tubes were incubated for 20 minutes at RT with open lids, to evaporate remaining ethanol. Pellet was resuspended in 30µl RNase-free aqua, incubated for 5 minutes at RT and stored at -80°C.

3.3.5 cDNA and qRT-PCR

Gene expression at mRNA level was analysed by quantitative real-time polymerase chain reaction (qRT-PCR). Complementary deoxyribonucleic acid (cDNA) was first synthesized from RNA using iScript ™ cDNA synthesis Kit (Bio-Rad 1708890) following prescribed protocol by the manufacturer. RT-PCR sample mix (table 21) was prepared by mixing cDNA with SYBR green (iTaq ™ Universal SYBR® Green supermix Bio-Rad 172-5121) and gene-specific murine primers (for genes and their primers see table 3) in 96-well plate (Applied Biosystems by Thermo Fischer Scientific, MicroAmp Fast 96-Well Reaction Plate 4346907) sealed with an adhesive film (Applied Biosystems by Thermo Fischer Scientific, MicroAmp Optical Adhesive Film 4311971) afterward. Each sample was run in technical triplicates. qRT-PCR was performed in StepOne Real-Time PCR system (Applied Biosystems) using standard conditions. Data was analysed in Microsoft Excel by normalizing the expression of each gene to the expression of housekeeping gene *Gapdh* based on cycle threshold (CT) values.

Table 21: Composition of 1x reaction mix.

Ingredients	**Volume**

SYBR Green	5µl
Primer Forward	0.05µl
Primer Reverse	0.05µl
H_2O	3.9µl
Sample	1µl

3.3.6 Whole-cell transcriptome sequencing and analysis

Total RNA was isolated from AML12 cells after the required treatment, as described previously. Before making RNA libraries for RNA sequencing, purity and integrity of RNA samples were validated by gel electrophoresis using 1% agarose gel containing Midori Green Advance (Biozym 617004). RNA bands were visualized using Bio-Rad Gel documentation system. TruSeq RNA Library Prep Kits (RS-122-2001 and RS-122-2002) from Illumina were used to prepare libraries following instructions from the manufacturer. Briefly, mRNA was purified using magnetic beads attached with oligo-dT. Purified mRNA fragmented cDNA was synthesized. Endpoint repair was performed to convert overhangs (generated due to fragmentation) into blunt ends followed by adenylation of 3´ ends to prevent ligation of fragments with each other and to attach with an adapter at corresponding ‘T’ nucleotide on the adapter. Indexing adapters were ligated with ds cDNA. These adapters enable cDNA to hybridize on the flow cell. DNA fragments containing adapters at both ends were enriched and amplified by PCR. cDNA concentration was measured by Qubit (Thermo Scientific Q32854). Fragment sizes and purity were analyzed with high sensitivity DNA analysis kit (Agilent 5067-4626) using Agilent Bioanalyzer 2100. Following library preparation and quality assurance, libraries were pooled, and sequencing was performed by NGS Integrative Genomics Core Unit, University Medical Center Göttingen, Germany.

Obtained FastQ files were analyzed by using usegalaxy.eu (Afgan et al., 2018). Fastq files were analyzed for quality control followed by mapping with murine transcriptome (mm9) using TopHat tool (version 2.1.1) (Kim et al., 2013) with very sensitive bowtie2 settings. HTSeq (version 0.9.1; -f bam -r pos -s reverse -

a 10 -t exon -m union) was used to count the number of aligned reads (Anders et al., 2015). Principal component analysis (PCA) was performed to analyze the difference between groups and similarities between replicates of each group. DESeq2 (Love et al., 2014) was utilized to measure PCA. Cuffnorm (version 2.2.1.2) tool was used to normalize the expression levels and fragment counts and differential expression (DE) was analyzed using Cuffdiff (version 2.2.1.5) (Trapnell et al., 2010). Fragments per kilobase million (FPKM) threshold was set to greater than 5. Heat maps were generated in GraphPad prism 7.0 based on z-scores of each replicate.

NFATc1-dependent differentially expressed genes with log2fold values >= 0.05 were used in the reactome (https://reactome.org/) pathway database, to identify the upregulated and downregulated pathways. The most relevant pathway and candidate genes involved in these pathways were selected and validated for their NFATc1-dependent RNA and protein expression using qRT-PCR and WB.

3.4 Histology

3.4.1 Tissue collection and processing

Upon completion of treatment time points, mice were anesthetized by CO_2 and sacrificed by cervical dislocation. The Liver, spleen, and pancreas tissues were harvested and fixed in 4% formaldehyde (PFA) in PBS, overnight at RT. The rest of the tissues were frozen in liquid nitrogen for later RNA and protein isolation and stored at -80°C. After fixation, tissues were dehydrated with increasing concentrations of ethanol from 70%-99%, in automated tissue dehydration machine (Leica Biosystems TP1020). Dehydrated tissues were embedded in paraffin blocks using paraffin tissue embedder (Leica Biosystems EG1150H). Paraffin blocks were cooled down at HistoCore Arcadia C cooling plate (Leica, 14600005015) and stored at 4°C before sectioning. 4µm thick sections of paraffin blocks were sliced with a microtome (Leica RM2265) and flattened on the water in a water bath at 37°C and fixed on SUPERFROST® glass slides (Thermo Scientific) by incubating overnight at 37°C.

3.4.2 Hematoxylin and Eosin staining (H&E)

Slides with tissue sections were deparaffinized in Roticlear (Carl Roth A538) two times for 10 minutes each, followed by rehydration steps of ethanol serial dilutions (100%, 95%, 80% and 50%) for 3 minutes each. Slides were washed 3 times in tap water and incubated in hematoxylin (Sigma 51275) for 5 minutes followed by washing under running tap water for 5 minutes. Slides were counterstained with eosin (Sigma-Aldrich HT110232) for 30 seconds and washed 3 times in tap water. Tissue sections were dehydrated again by incubating in increasing concentrations of ethanol (70%, 80%, 96% and 99%) 3 minutes each. In the following step, slides were incubated in Roticlear 4 times for 5 minutes each. Coverslips were mounted on tissue sections using Rotimount (Carl Roth HP68.2) and observed under the microscope after drying.

3.4.3 Immunostaining

For immunohistochemistry (IHC), sections after deparaffinizing and rehydration were subjected to antigen retrieval by boiling in citrate buffer pH=6.0 (Table 14) for 25 minutes. Next, slides were cooled for 30 minutes at the bench top and washed 3 times with tap water followed by incubation in 3% H_2O_2 (in H_2O) for 10 minutes. H_2O_2 blocks endogenous peroxidase activity. Slides were washed again 3 times with tap water, aligned in the Cadenza slide holder system (Sequenza™ Slide Rack) and washed with 1x PBS containing 0.1% Tween-20 or Triton X-100 (PBS-T). Slides were then blocked with 10% (w/v) BSA in PBS-T for 1 hour at RT, to reduce unspecific binding. Primary antibodies were diluted in respective dilutions, in PBS-T with 1% (w/v) BSA. 200µl of the primary antibody was added to each slide and incubated overnight at 4°C. Next day, slides were washed 3x with PBS-T and incubated for 1 hour at RT with respective biotinylated secondary antibody (provided in Biozol, ABC Vectastain ABC kit PK4001 and PK4002) diluted (1:200) in PBS-T with 1% (w/v) BSA. Following secondary antibody, slides were washed again 3 times with PBS-T and incubated for 1 hour at RT with streptavidin-biotin complex prepared by mixing solution A (avidin) and solution B (biotin) (provided in Vectastain ABC kit), 10µl each in 1ml of TBS-T. Next, slides were removed from the cadenza system and incubated with 3,3'-Diaminobenzidine (DAB) substrate (Vector DAB ImmPACT SK-4105) until brown

color started to develop. Slides were counterstained with hematoxylin before dehydration and coverslips were mounted.

3.4.4 Immunofluorescence (IF)

For IF, 45000 cells per well were seeded in 24 well plates containing the coverslips in each well. Cells were allowed to attach overnight or until 50%-60% confluency, followed by the treatment according to the respective experiment. Next, the medium was removed, cells were washed twice with 1x PBS and fixed in 4% PFA (Merk Millipore) in PBS. Cells were washed twice with PB buffer (Table 14) and permeabilized by incubation with phosphate buffer supplemented with 0.4% (v/v) Triton X-100 and 10% (v/v) normal goat serum (NGS) for 1.5 hours at 4°C. Primary antibodies (Table 1) diluted in PB buffer containing 0.4% Triton X-100 and 2% NGS, were added and kept at 4°C overnight. Following day, cells were washed 3 times with PB buffer for 5 minutes each and incubated with secondary antibodies (Table 2) diluted in PB buffer with 0.4% Triton X-100 and 2% NGS for 1 hour at 4°C. Next, cells were washed 3 times with PB buffer, prior and after 1-minute incubation with 4’,6-diamidino-2-phenylindole (DAPI) (Sigma Aldrich D9542) in 1:2000 dilution in water, followed by mounting of the coverslips on slides.

3.4.5 Picrosirius red staining

To analyze fibrosis in the liver tissues of mice, collagen staining was performed using picrosirius red staining kit (Polysciences, Inc) according to the manufacturer’s instructions. Picrosirius red stains the total collagen (red color) present in the tissue. Briefly, slides with fixed tissue sections were deparaffinized and rehydrated, like described before, prior to 6 minutes incubation in Weigert's hematoxylin solution. After 5 minutes of washing under tap water, slides were incubated in solution A (phosphomolybdic acid) for 2 minutes. Slides were then washed with distilled water and incubated in solution B (picrosirius red F3BA stain) for 1 hour followed by treatment with solution C (0.1N HCl) for 2 minutes

and 45 seconds incubation in 70% ethanol. In the end, slides were dehydrated, and coverslips were mounted.

3.5 Statistical analysis

Statistical analysis was perfomed by Graphpad Prism 7.0 using unpaired t-test, one-way ANOVA and two-way ANOVA, respectively (described in each figure legend). Statistical significance was always mentioned as * = $p < 0.05$, ** = $p < 0.005$, *** = $p < 0.0005$, **** = $p < 0.0001$. Error bars indicate means with standard deviation.

4.0 Results

This project studied hepatocyte-specific activation of NFATc1 and its role in the development and progression of NAFLD. We followed the idea that NFATc1 activation can drive steatosis induced inflammation and fibrosis and thus contributes to disease progression. To test this hypothesis, we generated different *in-vitro* and *in-vivo* models and performed in-depth biochemical, functional and transcriptional analysis.

4.1 NFATc1 expression/activation in NAFLD/NASH

NFATc1 has been identified as a master regulator in multiple inflammatory and inflammation-driven diseases, e.g. pancreatitis induced pancreatic cancer, colon cancer and in skin cancer as well (Baumgart et al., 2014; Buchholz et al., 2006; Chen et al., 2015; Daniel et al., 2014; Mancini & Toker, 2009; Singh et al., 2015). By contrast, only little is currently known about the role of NFATc1 in the development and progression of liver diseases, although previous studies suggested increased NFATc1 expression in NAFLD and in hepatic tumor cells (Wang et al., 2012; Zhu et al., 2016).

Accordingly, immunohistochemical analysis conducted in human NAFLD samples revealed robust expression and nuclear localization of NFATc1 in steatotic hepatocytes [Fig 5A]. To investigate fat-induced NFATc1 expression at both mRNA and protein levels, we treated primary mouse hepatocytes and AML12 liver cells with palmitate for a period of 12 hours. Fig 5B-5E illustrates our findings and demonstrates significant upregulation of NFATc1 mRNA and protein levels in both cell systems. Immunofluorescence analysis in AML12 cells also confirmed increased nuclear localization of the factor following palmitate treatment as compared to untreated controls [Fig 5F-5G].

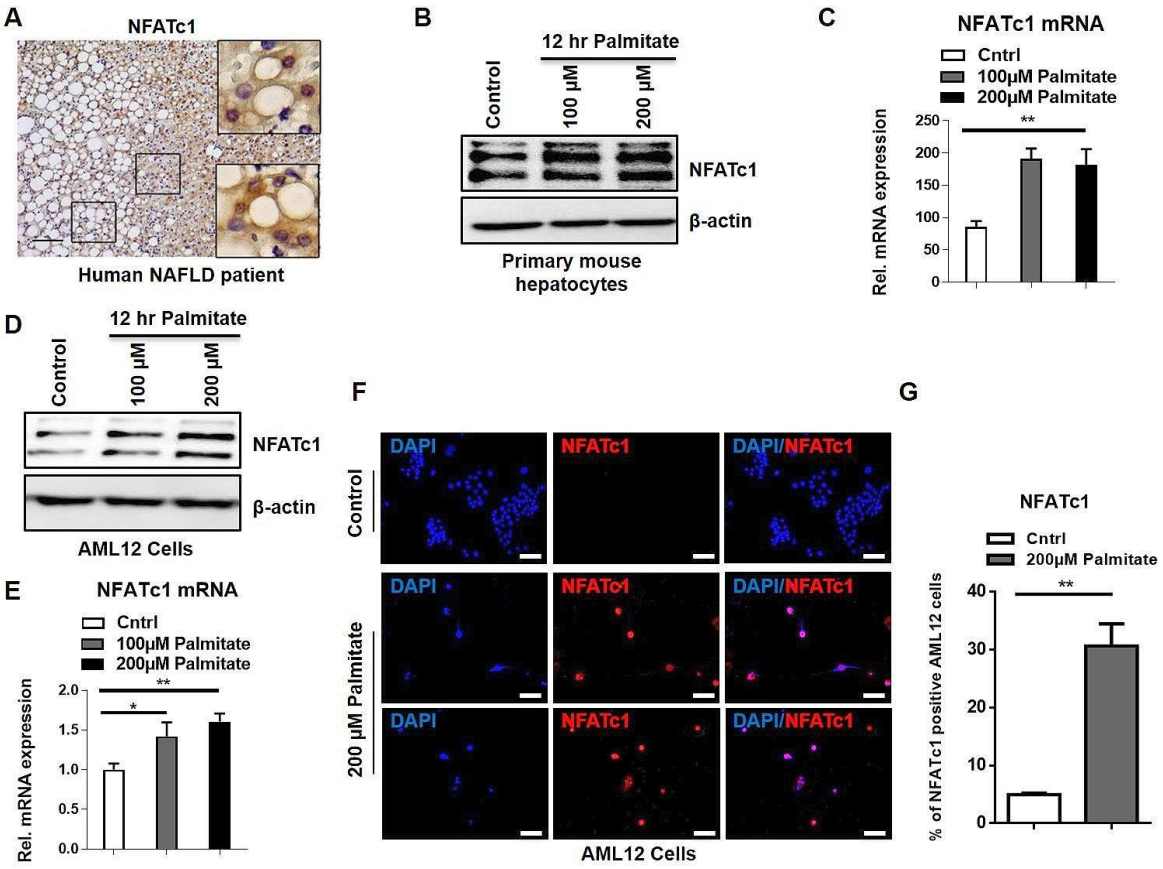

Figure 5: Fat accumulation induces NFATc1 expression and activation in hepatocytes

(A) Representative image of NFATc1 nuclear staining in NAFLD patient biopsies by IHC (n=3). Western blot and qRT PCR analysis of *Nfatc1* expression following 12hours palmitate treatment for two respective concentrations in primary hepatocytes **(B, C)** and in AML12 cells **(D, E)**. For qRT-PCR mRNA expression was normalized to Gapdh. **(F)** AML12 cells treated with 200µM palmitate were stained for NFATc1 via IF. **(G)** Quantitative analysis of NFATc1 IF in AML12 cells was done by using image j and data represents percentage of NFATc1 positive cells following palmitate treatment (n=3). Statistical analysis in **C and E** was performed by Dunnett's multiple comparison test using ordinary one-way ANOVA and in section G using unpaired t test with Welch's correction. Scale bar in section A = 50µm and in section F =100µm. (* = $p < 0.05$, ** = $p < 0.005$.)

Next, we analyzed the levels of NFATc1 expression and nuclear localization in-vivo using a well-established NAFLD mouse model, in which feeding with a high-fat diet (referred to as "western diet") causes progressive fat accumulation in hepatocytes (Machado et al., 2015). In detail, 8 weeks old C57Bl/6J mice (alb-

cre, see section 3.1) with endogenous expression of wild-type NFATc1 (NFATc1^{WT}) were either fed with normal diet or western diet, respectively [Fig 6A] for up to 20 weeks.

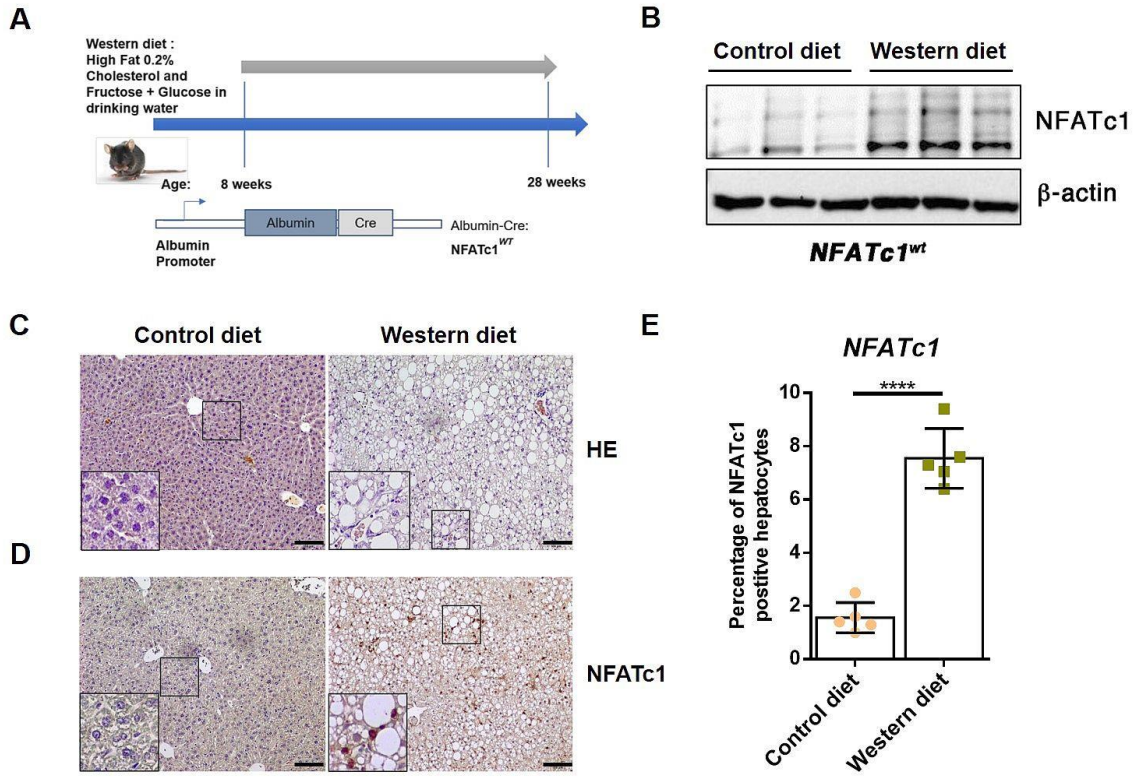

Figure 6: Western diet-induced steatosis and NFATc1 activation in mice

(A) Genetic mouse model with wild-type NFATc1 expression and western diet treatment scheme. **(B)** WB analysis of NFATc1 expression in liver tissue lysates. Mice were treated for 20 weeks with control or western diet, as indicated. **(C-D)** H&E staining and NFATc1 IHC (D) in liver tissue sections from 20 weeks treated mice (n=5). **(E)** Quantitative analysis of NFATc1 IHC. 10 random images from each individual mouse were analyzed using image j. Statistical analysis was performed using parametric un-paired t-test with Welch's correction. Scale bar in section **C-D** = 100µm and scale bar for zoom-in images= 200µm. (**** = p< 0.0001).

Liver tissue lysates were prepared from control and western diet treated mice. Our analysis revealed a significant upregulation of NFATc1 protein expression in liver tissue lysates from western diet treated mice, while expression remained unchanged in untreated mice [Fig 6B]. In addition, H&E staining of liver tissue

sections confirmed the development of hepatic steatosis (NAFLD) after western diet treatment. By contrast, control mice did not display any features of liver damage or steatosis [Fig 6C]. Moreover, NFATc1 was highly induced in the nucleus of ballooned hepatocytes containing fat vacuoles [Fig 6D]. Cellular quantification confirmed a highly significant increase of nuclear NFATc1 localization in hepatocytes of western diet treated mice in comparison to control [Fig 6E].

4.2 Genetically modified mouse models and characterization

4.2.1 Western diet-induced weight gain and steatosis

Our initial observation indicating fat-induced NFATc1 activation in hepatocytes prompted us to develop genetically modified mouse models with either ablation ($NFATc1^{-/-}$) or constitutive activation ($NFATc1^{+/-}$) of NFATc1 under control of albumin promoter (see section 3.1) to assure hepatocyte-specific expression of the factor.

To induce NAFLD, mice were treated with high-fat diet along with glucose and fructose in drinking water. Control animals were provided with normal diet and water [Fig 7A]. Animals gained weight already after 4 weeks of treatment, but reached maximum after 12 weeks, respectively [Fig 7B-7D].

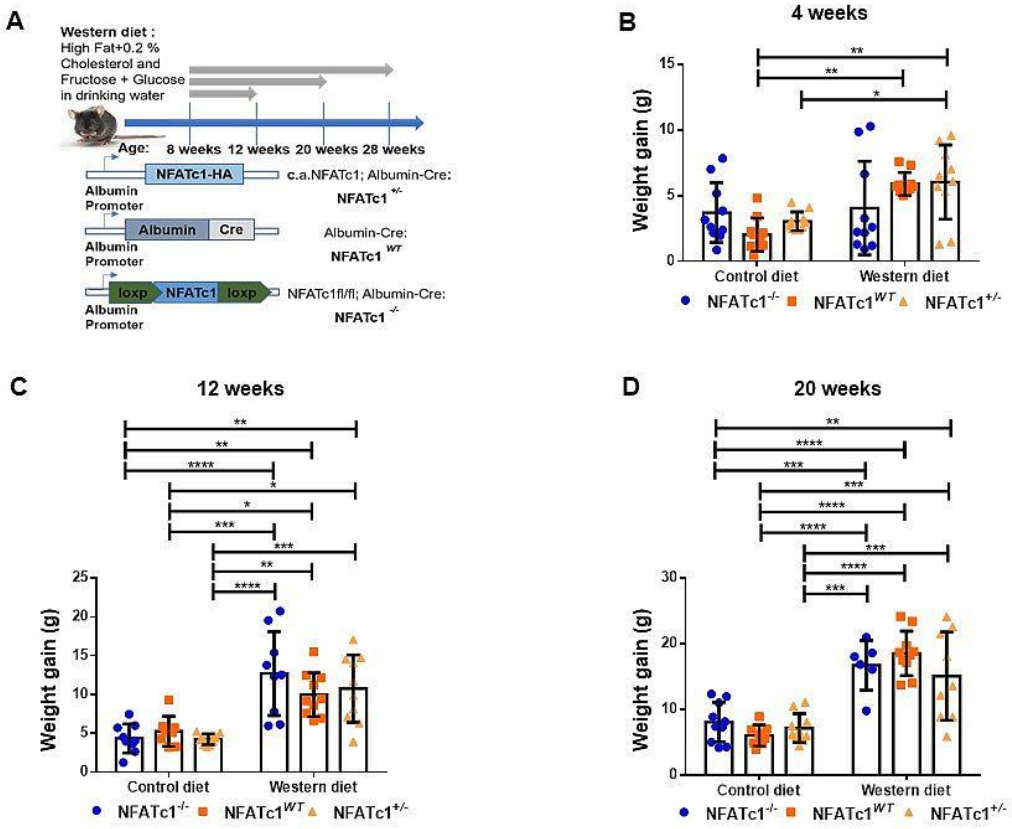

Figure 7: Western diet-induces progressive weight gain in mice

(A) Genetic mouse model and western diet treatment scheme. **(B-D)** Body weight after 4 weeks **(B),** 12 weeks **(C)** and 20 weeks **(D)** of control and western diet treatment, respectively (n=10)**.** Statistical analysis was performed by Tukey's multiple comparisons test using two-way ANOVA by comparing each cell mean with every other cell mean. (***** = $p < 0.05$, ****** = $p < 0.005$, ******* = $p < 0.0005$, ******** = $p < 0.0001$).

Next, we analyzed the effect of western diet on liver structure and physiology, and with respect to NFATc1 activation. Upon 4 weeks of treatment, we did not observe a significant amount of steatosis. However, following 12 weeks of western diet feeding, steatosis was detected in all genotypes and after 20 weeks all mice developed a severe form of fatty liver. In contrast, none of the normal diet treated animals exhibited any signs of steatosis.

We also studied the degree of inflammation upon the western diet. Figure 8 summarizes our findings and demonstrates the absence of significant immune cell infiltration in liver of NFATc1$^{-/-}$ mice with genetic depletion of the transcription factor. By contrast, NFATc1^{WT} and NFATc1$^{+/-}$ mice showed a remarkable degree of hepatic inflammation and this was particularly true for NFATc1$^{+/-}$ mice displaying progressive inflammation over time and even without administration of

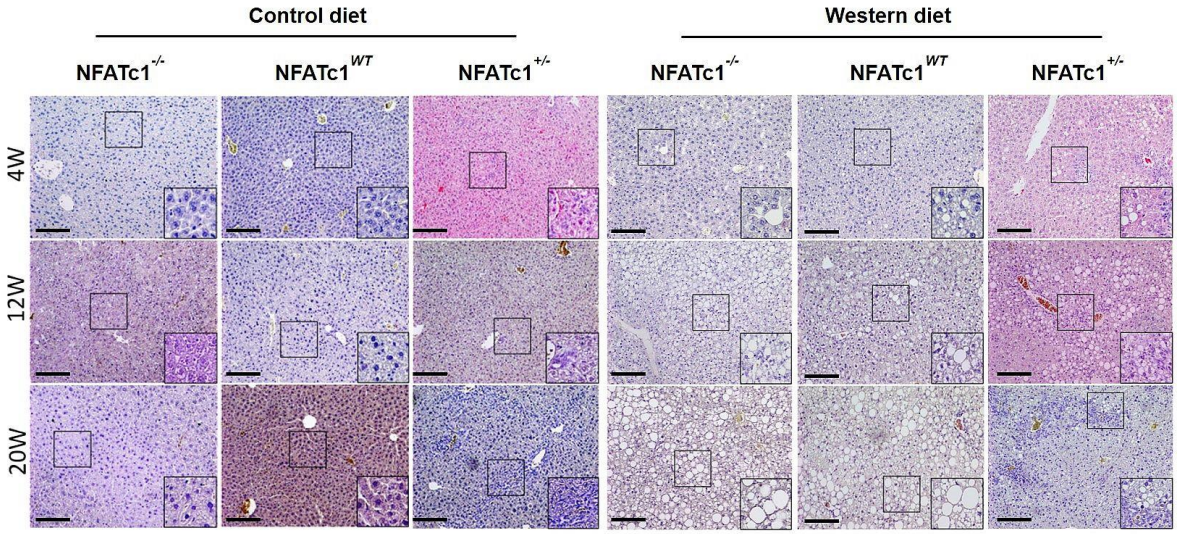

Figure 8: NAFLD following western diet treatment

Liver structure was analyzed by H&E staining of tissue sections harvested from 4, 12- and 20-weeks control and western diet treated mice, respectively (n= 5).

high-fat diet [Fig 8].

4.2.2 NFATc1-mediated steatohepatitis

Following 20 weeks of treatment, most of the mice developed a NAFLD phenotype along with an inflammatory niche, as validated by histological analysis. Therefore, we selected 20 weeks of treated mice for further characterization of NFATc1-mediated signaling in NAFLD-NASH progression.

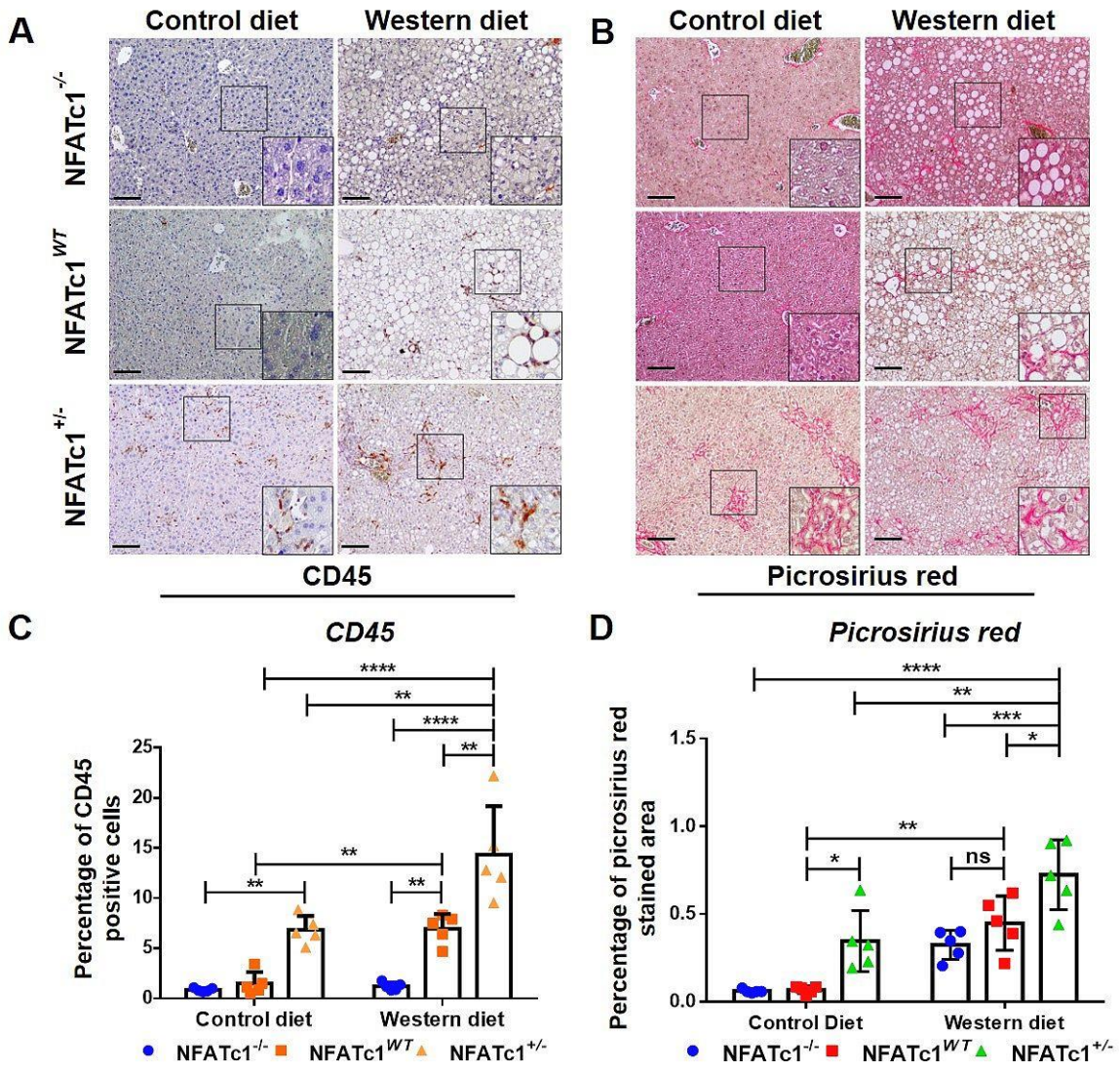

Figure 9: Western diet-induces NFATc1-dependent inflammation and fibrosis

Analysis of inflammation and fibrosis by CD45 IHC **(A)** and **(B)** picrosirius red staining in 20 weeks control and western diet treated mice (n=5). (**C-D)** Quantitative analysis of CD45 **(C)** and Picrosirius red staining **(D)**. 10 random images of each mouse per staining were quantified using image j. Statistical analysis was performed by two-way ANOVA as described before. Scale bar for sections **A and B**= 100µm. (*p < 0.05, **p < 0.005, ***p < 0.0005, ****p < 0.0001)**.**

CD45 and picrosirius red staining were performed to assess inflammation and fibrosis, respectively, in liver tissues of mice treated with normal or western diet [Fig 9A-9B]. Hepatocyte-specific NFATc1 activation ($NFATc1^{+/-}$) resulted in particular high levels of inflammation and fibrosis both upon normal and western diet treatment, whereas NFATc1 knock-out ($NFATc1^{-/-}$) protected mice from fat-

induced liver inflammation and fibrosis [Fig 9C-9D]. These findings suggested that NFATc1 induction in hepatocytes is required and sufficient to promote fat-induced liver inflammation and fibrosis, and thus to foster NAFLD progression towards NASH.

4.2.3 NFATc1 regulates thioacetamide-induced inflammation and fibrosis

We next sought to analyze whether NFATc1 induction also drives liver inflammation in models other than the western diet approach. For this purpose, we took advantage of another well-established model in mice, which exhibits inflammation following administration of thioacetamide (TAA). Importantly, TAA treatment led to a time-and dose-dependent induction and nuclear localization of NFATc1 in hepatic AML12 cells [Fig 10A-10B].

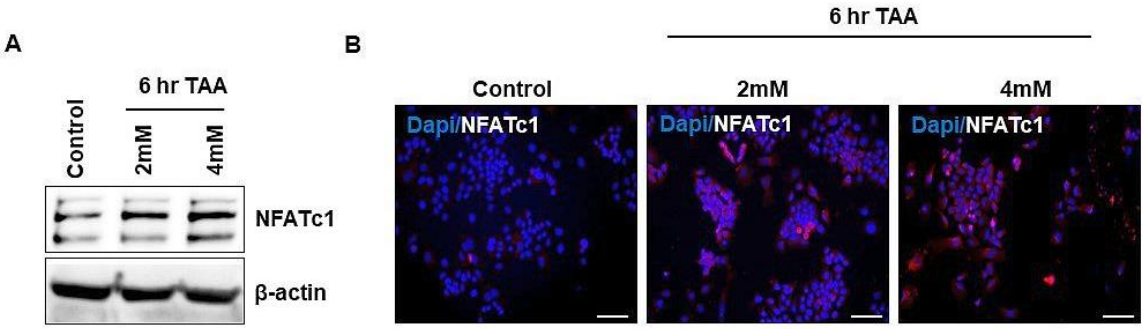

Figure 10: TAA exposure induces NFATc1 activation

(A-B) Western blot and IF **(B)** analysis of NFATc1 in AML12 cells treated with 2mM and 4mM TAA. Control was treated with vehicle (H_2O). Scale bar in section **B** = 100µm.

Moreover, i.p. TAA treatment at a concentration of 25mg/kg body weight, caused significant induction of liver inflammation and fibrosis, as demonstrated by CD45 and picrosirius red staining, in NFATc1 expressing NFATc1^{WT} and NFATc1$^{+/-}$ mice. Again, constitutive activation of NFATc1 in NFATc1$^{+/-}$ mice already resulted in significant recruitment of CD45 positive cells and deposition of collagen, and these effects were further increased upon treatment with TAA. Similar but less pronounced effects were found in the NFATc1^{WT} situation. By contrast, genetic deletion of NFATc1 resulted in remarkable protection of mice from TAA induced inflammation and fibrosis [Fig 11A-11C].

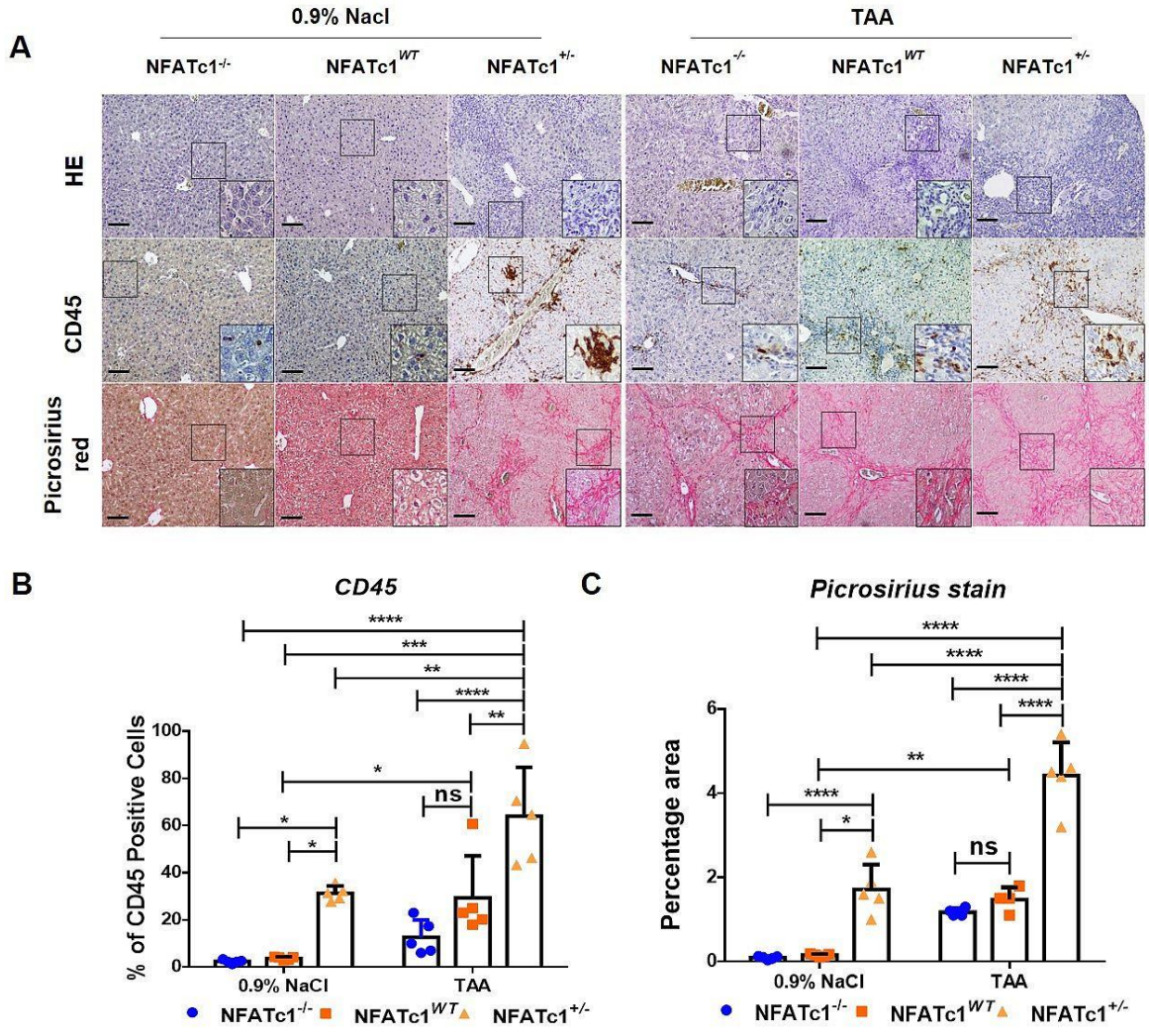

Figure 11: NFATc1 regulates TAA-induced inflammation and fibrosis

(A) Histological analysis of liver tissue section (n=5) from 20 weeks 0.9%NaCl/TAA treated mice for liver damage (HE is staining), inflammation (CD45) and fibrosis (picrosirius red staining). **(B-C)** Quantitative analysis of CD45 and picrosirius red staining. Cellular quantification area measurement was done using image j. Statistical analysis was performed by two-way ANOVA as described previously. (*p < 0.05, **p < 0.005, ***p < 0.0005, ****p < 0.0001)**.** Scale bar for section **A** = 100µm.

4.3 NFATc1 regulated gene signatures

Together, these data suggested that NFATc1 promotes liver inflammation and mediates NAFLD progression in mice. To explore the underlying mechanisms by which NFATc1, following its activation in hepatocytes, regulates inflammation, we studied NFATc1-dependent gene expression and performed whole transcriptome analysis in AML12 cells. For this purpose, we extracted RNA from AML12 cells that were either transfected with HA-tagged c.n.NFATc1 or control plasmid and conducted RNA-Seq analysis. For transfection control, we also isolated proteins and performed western blot analysis using anti-HA antibodies [Fig 12A]. Both qRT-PCR and western blot analysis confirmed NFATc1 over-expression at mRNA levels and protein levels, respectively [Fig 12B].

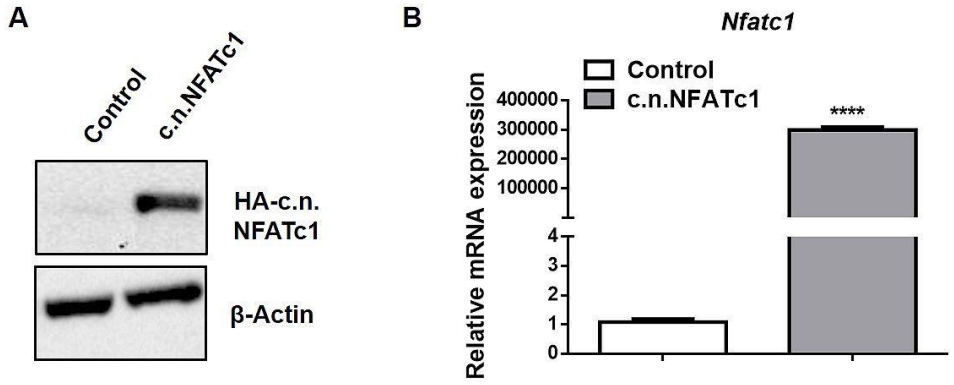

Figure 12: Treatment scheme for RNA-seq analysis

(A) Western blot analysis showing successful induction of HA-tagged c.n.NFATc1 in AML12 cells **(B)** Representative graph of *Nfatc1* mRNA expression following transfection with c.n.NFATc1, evaluated by qRT-PCR (n=3). Statistical analysis was performed by unpaired t-test. (******** = p < 0.0001)**.**

To compare expression profiles between control and NFATc1 overexpressing cells, principle component analysis (PCA) was performed. The primary PCA, accounting for the variability between replicates and groups, indicated that the transcriptome profiles of control and treated groups clustered separately. The replicates within each group clustered closely to each other [Fig 13].

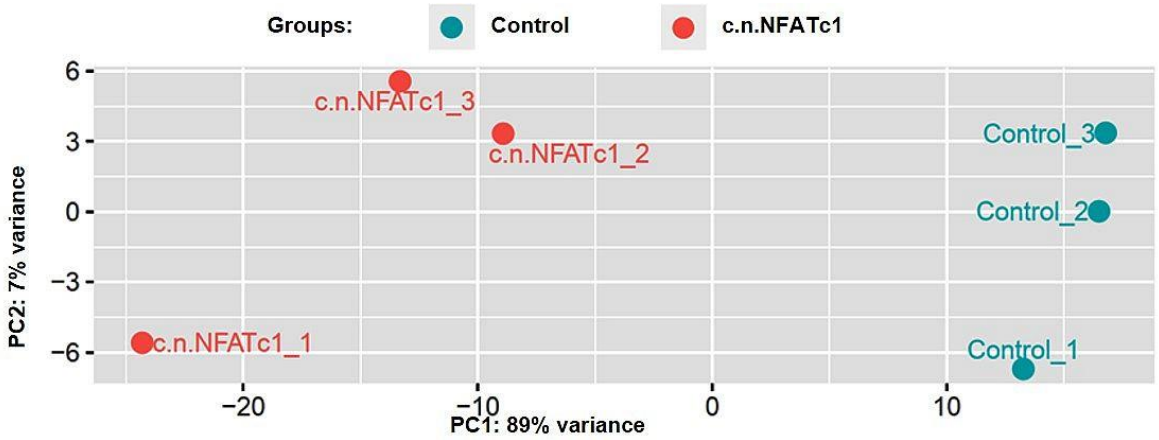

Figure 13: Principal component analysis

RNA sequences were subjected to Principal Component Analysis using usegalaxy.org, to assess the variance between replicates and samples (conditions) depending on NFATc1 expression. PCA plot demonstrates clustering of both conditions along with their replicates, expressing different levels of NFATc1.

At a statistical cut-off of “log2foldchange ≥ 0.5 or ≤ -0.5 and q < 0.05”, 636 genes were differentially expressed between the two groups. Specifically, 471 genes were upregulated, and 165 genes were downregulated in AML12 cells with constitutive activation of NFATc1. Pathway analysis using the Reactome pathway database can provide information about altered biological processes and disease-associated pathways. Consistent with the role of NFATc1 signaling in progression of NAFLD and inflammation, our REACTOME pathway analysis revealed activation of gene signatures involved in immune regulation and ER stress signaling.

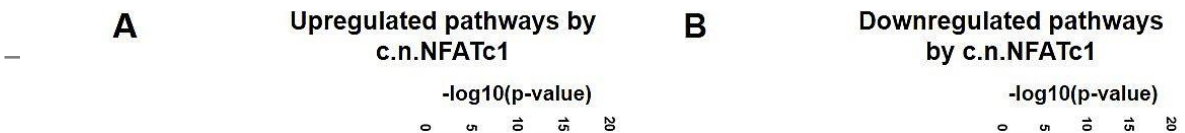

Specifically, we identified alteration in immune signaling involving remarkable upregulation of interferon and cytokine/chemokine signaling (i.e. cytokines *Il-1 receptor signaling, Il-10 and* chemokines *Cxcl2, Cxcl9 Cxcl10, Cxcl11),* pro-inflammatory (*Ccrl2, Ccl5, Stat1* and *Stat2*) and pro-apoptotic markers (*Bak1*, *Casp2*, *Casp7 and Tnfsf10*). In addition, induction of cellular stress responses

comprising activation of UPR component genes implicated in mediating ER stress (*Atf4* and PERK activated gene i.e. *Atf3, Chop, Cebpb and Ppp1r15a*) were also incorporated. Besides these, antiviral mechanisms i.e. TRAF6 mediated IRF7 activation and ISG15 antiviral mechanisms etc. were also identified among the top 25 upregulated pathways [Fig 14A-14B]. Further heat map analysis of candidate genes involved in these pathways showed z-score based differential expression patterns in replicates of control and NFATc1 overexpressing groups [Fig 14C-14D]. Importantly, it has been shown previously that cytokine/chemokine signaling and ER stress-mediated apoptosis and inflammasome activation are of utmost importance for various aspects in NAFLD progression to NASH. Figure 15 demonstrates NFATc1-dependent regulation of selected target genes with the implication in ER-stress, apoptosis and inflammatory responses, as revealed by qRT-PCR. Interestingly, we identified a robust and significant upregulation of several master ER stress sensors and inducers of pro-apoptotic and pro-inflammatory signaling pathways, e.g. (C/EBP) homologous protein (*Chop*), *Atf3*, *Cxcl10* and *Cxcl11* (Lebeaupin et al., 2016; Liu & Green, 2019; Willy et al., 2015)

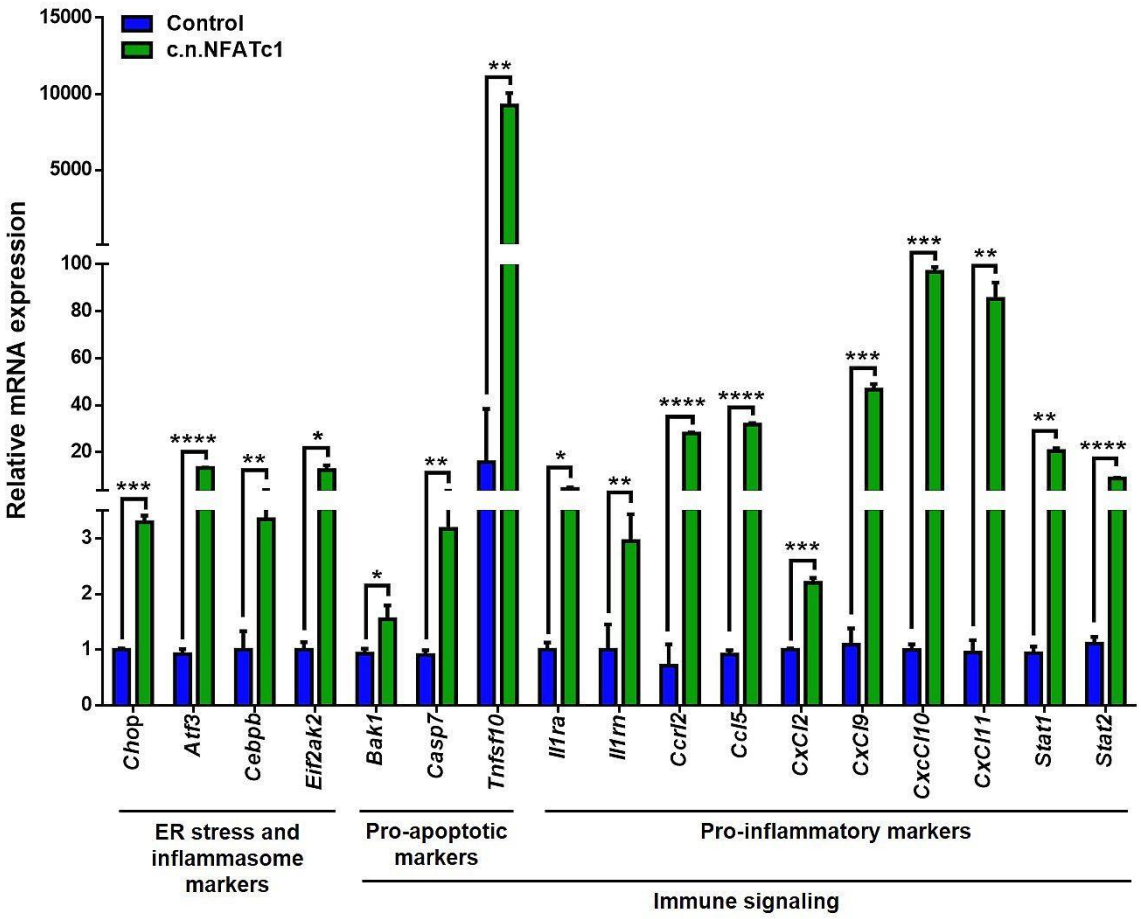

Figure 15: Validation of differentially expressed (DE) genes

Graph represents relative mRNA expression of differentially expressed genes validated through qRT-PCR analysis (n=3). Statistical analysis was performed using unpaired two-tailed t-test with Welch's correction. (***** = $p < 0.05$, ****** = $p < 0.005$, ******* = $p < 0.0005$, ******** = $p < 0.0001$)**.**

4.4 NFATc1 ablation prevents from induction of PERK signaling

Protein kinase RNA-like ER (PERK) kinase signaling has been described upregulated in fat accumulating hepatocytes following induction of chronic ER stress (Han et al., 2018; Liu & Green, 2019; Nakagawa et al., 2014). Accumulation of unfolded proteins in ER lumen results in activation of PERK upon its dissociation from Bip (GRP78) and subsequent autophosphorylation. Activated PERK phosphorylates eif2α and eventually promotes ATF4 translation to induce the pro-apoptotic and pro-inflammatory transcription factor (C/EBP)

homologous protein (CHOP). CHOP is a master regulator of ER stress-induced expression of pro-survival, pro-apoptotic and pro-inflammatory signaling genes (Lebeaupin et al., 2018; Romine & Wiseman, 2019) [Fig 16A]. Here we tested whether NFATc1 controls activation of the PERK- eif2α-CHOP pathway, as supported by our RNA-seq analysis, and carried out western blot analysis upon induction or silencing of the factor in AML12 cells. Figure 16 summarizes our findings and demonstrates increased eif2α phosphorylation and CHOP protein expression upon activation of NFATc1, whereas NFATc1 silencing prevented fat-induced eif2α phosphorylation and subsequent CHOP-induction both at mRNA and protein levels [Fig 16B-16C].

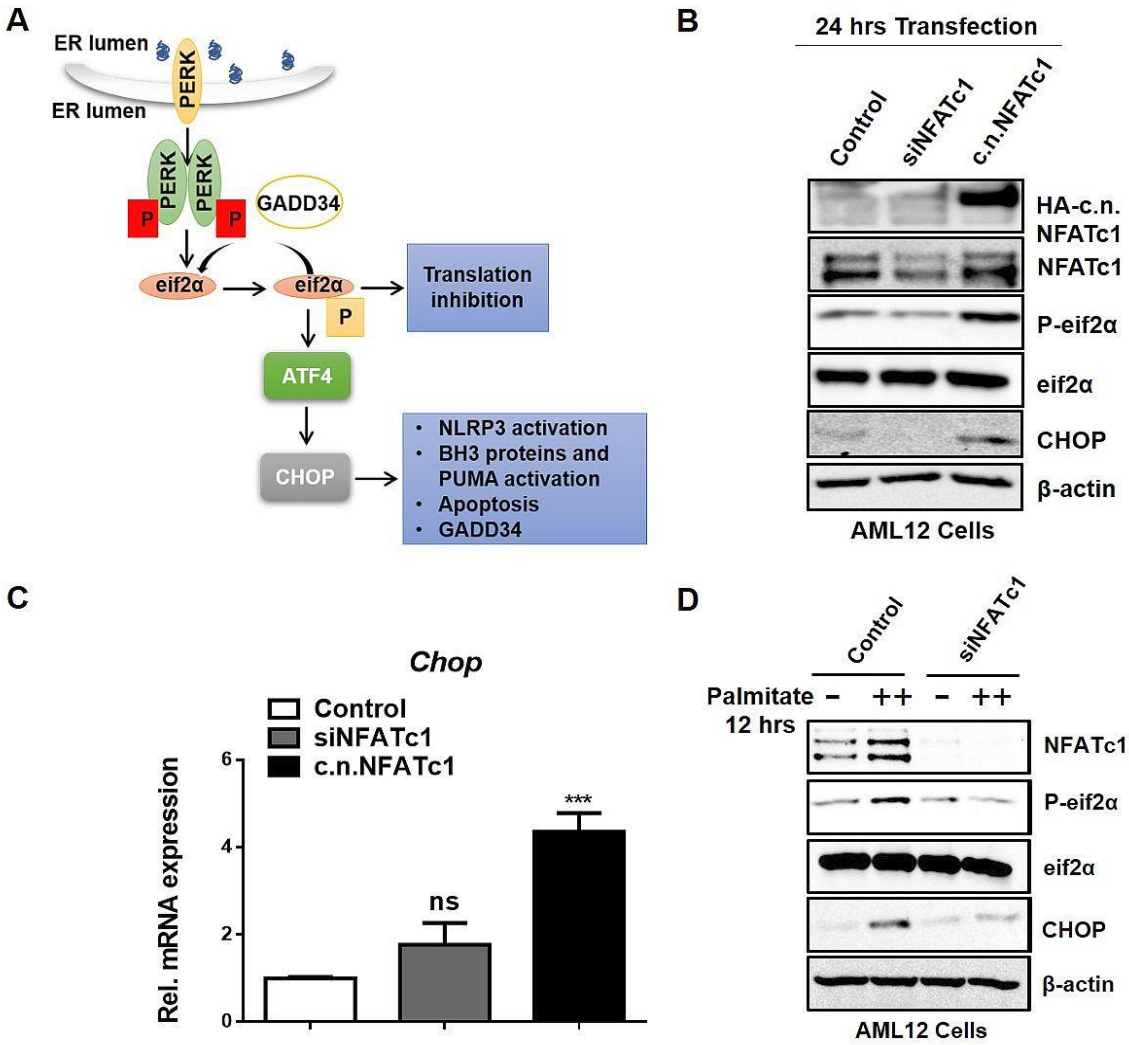

Figure 17: NFATc1-dependent regulation of the p-eif2α and CHOP pathway in primary hepatocytes

(A) Following activation, PERK phosphorylates eif2α, which in turn halts global translation and at the same time induces ATF4 translation, which leads to induction of CHOP. **(B)** Western blot analysis of eif2α phosphorylation and CHOP protein levels following NFATc1 siRNA-mediated knockdown and constitutive activation in AML12 cells. Data was analyzed with One-way ANOVA for comparing mean of each column with control using Brown-Forsythe test (***= p < 0.0001). **(C)** Densitometry for phosphorylated eif2α bands (+ = 100μM and ++ = 200μM). **(D)** Phosphorylated eif2α and CHOP levels were examined in AML12 control and siNFATc1 treated cells, respectively, following 12 hours exposure to palmitate (++ = 200μM).

Importantly and consistent with our studies in AML12 cells, we were also able to demonstrate NFATc1-dependent regulation of the eif2α-CHOP axis in primary hepatocytes isolated from genetically engineered mouse models with differential expression of NFATc1 [17A]. The strongest activation of the eif2α-CHOP pathway

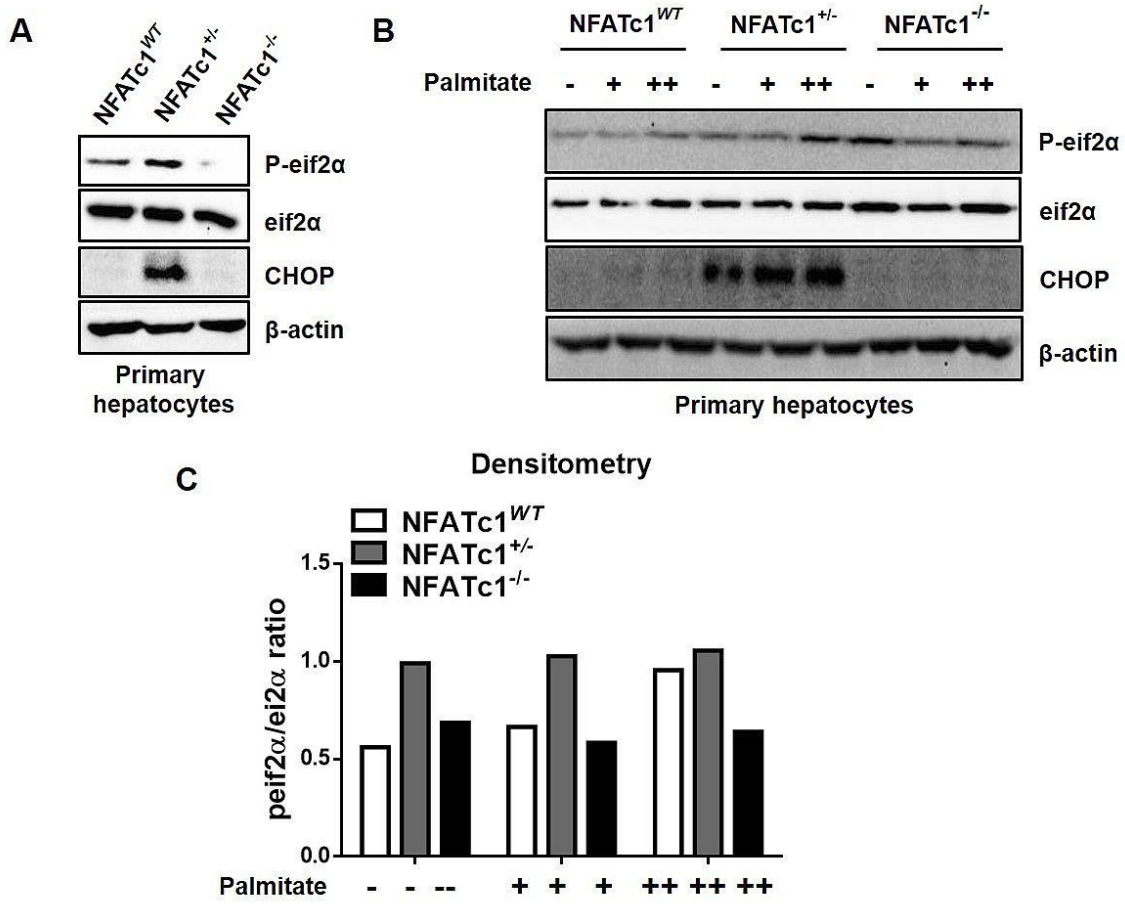

Figure 18: NFATc1-dependent regulation of the eif2α-CHOP pathway in genetically modified mouse models

Whole liver tissue lysates from mice treated with either western diet or control were investigated for p-eif2α-CHOP activation (n=3). **B)** Densitometry analysis. The graph represents quantitative levels of eif2α phosphorylation normalized to total eif2α levels, as evidenced by image j. Statistical analysis was performed using two-way ANOVA as described above. (** = p < 0.005 and **** = p < 0.0001)**.**

was found in hepatocytes with high levels of NFATc1 (NFATc1$^{+/-}$ mice) and following treatment with palmitate in NFATc1^{WT} hepatocytes [Fig 17B-17C].

Next, we analyzed whether NFATc1-dependent activation of the eif2α-CHOP pathway holds also true *in vivo* and NFATc1 transgenic mice treated with the high-fat western diet for up to 20 weeks. In line with our *in vitro* findings, these studies revealed a similar effect of NFATc1 activation on p-eif2α and CHOP, as shown in figure 18.

In detail, eif2α phosphorylation and CHOP expression were induced in

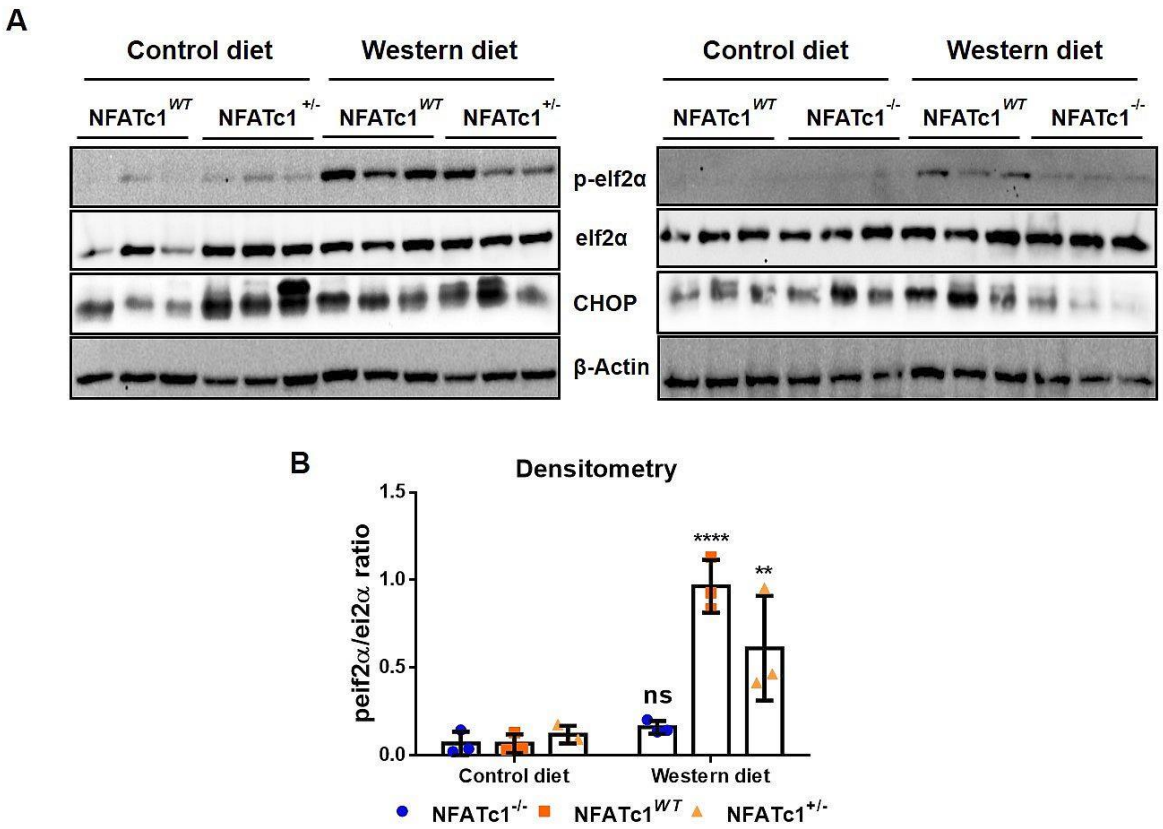

NFATc1^{WT} livers upon treatment with the western diet, and these effects were pronounced in NFATc1$^{+/-}$ mice with constitutive induction of NFATc1. By contrast, the peif2α-CHOP pathway remained unaffected in NFATc1$^{-/-}$ mice with

hepatocyte-specific loss of NFATc1, even upon treatment with the high-fat diet [Fig 18A-18B]. Together, these studies emphasized a role of NFATc1 in ER stress sensing and in the regulation of the eif2α-CHOP pathway.

4.5 Cell death and Inflammasome activation

When induced by chronic ER stress, CHOP controls transcription of multiple genes with the implication in cell death and inflammasome activation. For instance, CHOP induces the expression of caspase 1, which in turn activates the NLRP3 inflammasome and promotes apoptosis via caspase 3 activation. In addition, NLRP3 inflammasomes cooperate with caspase 1 in the secretion of pro-inflammatory cytokines and promote IL-1β cleavage (Lebeaupin et al., 2015) to foster inflammation and fibrosis (Lebeaupin et al., 2018). Of note, higher expression levels of NLRP3 inflammasome markers e.g. NLRP3, caspase 1, IL1β and IL18 have been found in liver biopsies from NASH patients (Csak et al., 2011; Wree et al., 2014). We, therefore, decided to further explore the interplay between NFATc1 signaling and activation of ER stress-induced inflammation by analyzing signaling components downstream of CHOP, both *in-vivo* and *in-vitro* models.

4.5.1 NLRP3 inflammasome activation

We first investigated activation of the inflammasome markers NLRP3, cleaved caspase -1 (Ccl1) and cleaved interleukin-1β (IL-1β) in primary mouse hepatocytes and dependent on NFATc1 activation. IL-1β is the ultimate measure of inflammasome activation. These studies revealed increased levels of the inflammasome in untreated hepatocytes with increased NFATc1 activity (received from c.a.NFATc1 mice), [Fig 19A]. Moreover, treatment with palmitate to induce ER stress significantly induced the expression of all tested inflammasome markers in NFATc1 expressing hepatocytes. By contrast, NFATc1 depletion reduced basal levels and inducibility of inflammasome markers in primary hepatocytes [Fig 19B]. Similar effects were observed in AML12 cells, in which siRNA mediated NFATc1 silencing blocked palmitate-induced activation of the inflammasomes [Fig 19C]. Finally, immunofluorescence

analysis confirmed NFATc1-dependent activation of NLRP3 in hepatocytes upon palmitate treatment [Fig 19D-19E]. Together these studies highly emphasized a critical role of NFATc1 in fat-induced ER stress and inflammasome activation.

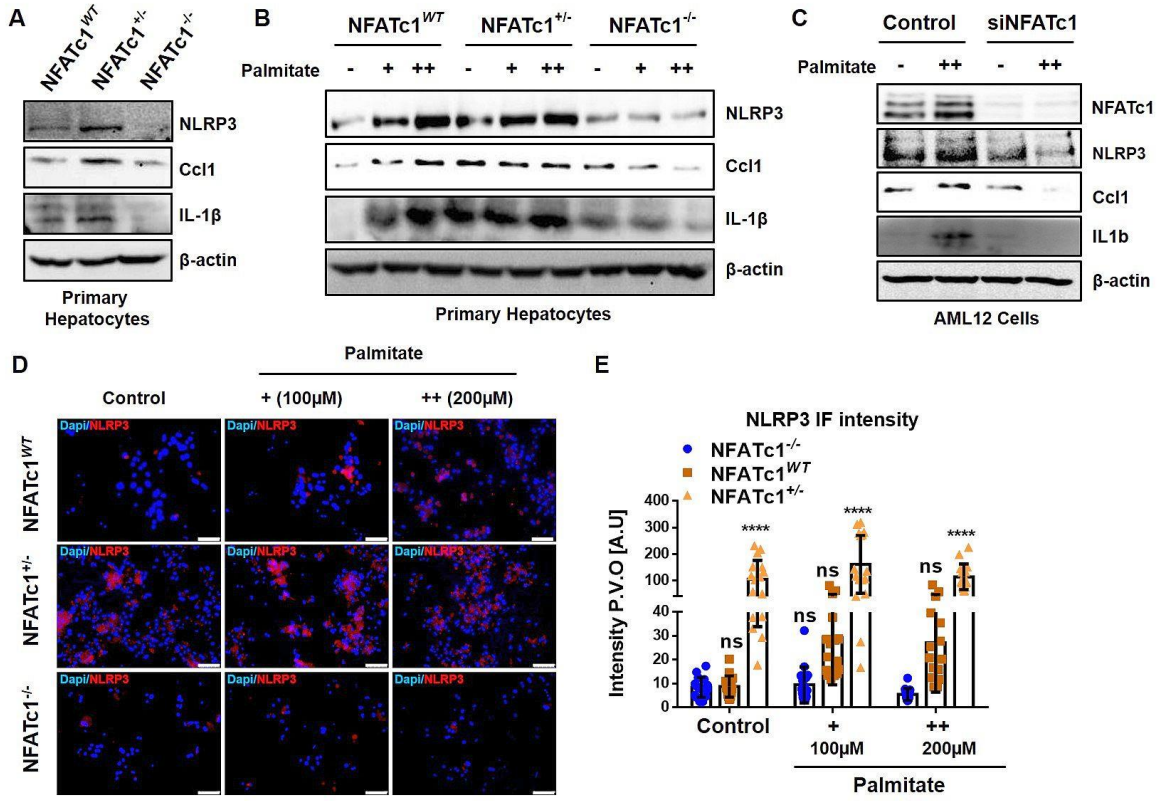

Figure 19: NFATc1-dependent NLRP3 inflammasome activation

(A-B) Untreated primary hepatocytes isolated from 8 weeks old NFATc1$^{-/-}$, NFATc1^{WT} and NFATc1$^{+/-}$ mouse and **(B)** following exposure to 100μM and 200μM palmitate for 12 hours were examined for inflammasome activation markers by western blot analysis. **(C)** NLRP3 inflammasome activation was analyzed in AML12 cells after exposure to 200μM palmitate for 12 hours following transfection with and without siRNA for NFATc1. **(D)** IF for NLRP3 was performed in primary hepatocytes isolated from genetically modified mouse models with different NFATc1 expression. **(E)** Graph represents quantitative analysis of NLRP3 IF. Data was analyzed by quantifying the fluorescence intensity in 15 images from each treatment using image j. Statistical analysis was performed using two-way ANOVA as previously. (******** = $p < 0.0001$)**.**

Next, we studied whether NFATc1 also controls inflammasome activation *in vivo*, and analyzed the level of NLRP3, Ccl1 and IL-1β in liver tissues from western diet treated mice and depending on NFATc1 expression. These studies, presented in Fig 20, confirmed our *in vitro* findings, and demonstrated induction

of the inflammasome markers upon treatment with western diet. Importantly, genetic depletion of NFATc1 diminished both basal and inducible activation of the inflammasome [Fig 20A-20B].

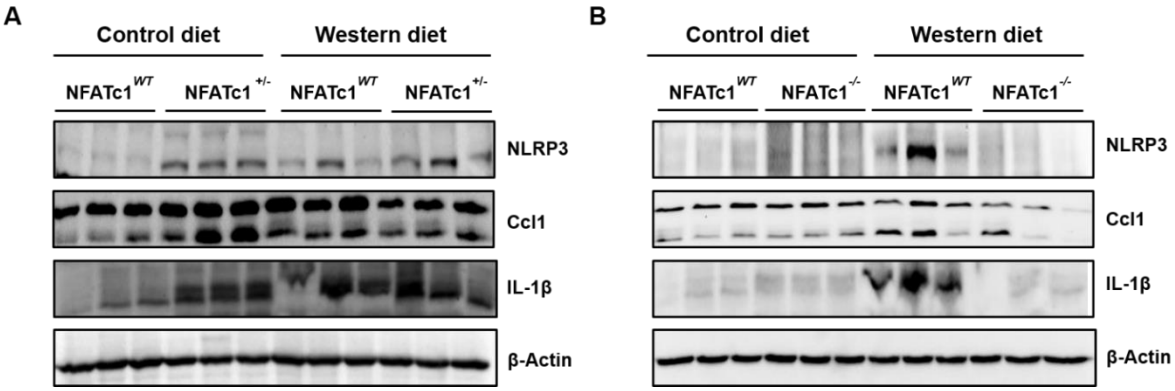

Figure 20: In vivo activation of the inflammasome

(A-B) Whole liver tissue lysates from 20 weeks treated mice were investigated for inflammasome markers via western blot (n=3), **(A)** represents immune blot comparison between NFATc1^{WT} and NFATc1$^{+/-}$ mice and **(B)** represents immune blot comparison between NFATc1^{WT} and NFATc1$^{-/-}$ mice, following control and western diet feeding, respectively.

4.5.2 NFATc1 induced cell death

Apart from the pro-inflammatory response, UPR signaling has been shown to induce cell death in a PERK-dependent manner. Here we analyzed whether NFATc1 is involved in this process and examined DNA damage and apoptosis markers in primary hepatocytes, AML12 cells and in western diet treated mouse models as well.

Figure 21 illustrates our findings in primary hepatocytes and shows a moderate basal and highly inducible expression of pP53-(s15) (DNA damage marker) and cleaved caspase 3 (Ccl3, apoptosis marker) in NFATc1 expressing hepatocytes from NFATc1^{WT} and NFATc1$^{+/-}$ mice. In contrast, NFATc1 depletion (NFATc1$^{-/-}$) prevented hepatocytes from ER stress-induced apoptosis and DNA damage, even upon administration of palmitate in high doses. Similar results were

obtained in human AML12 liver cells following either ectopic induction of NFATc1 or siRNA mediated silencing [Fig 21A-21D].

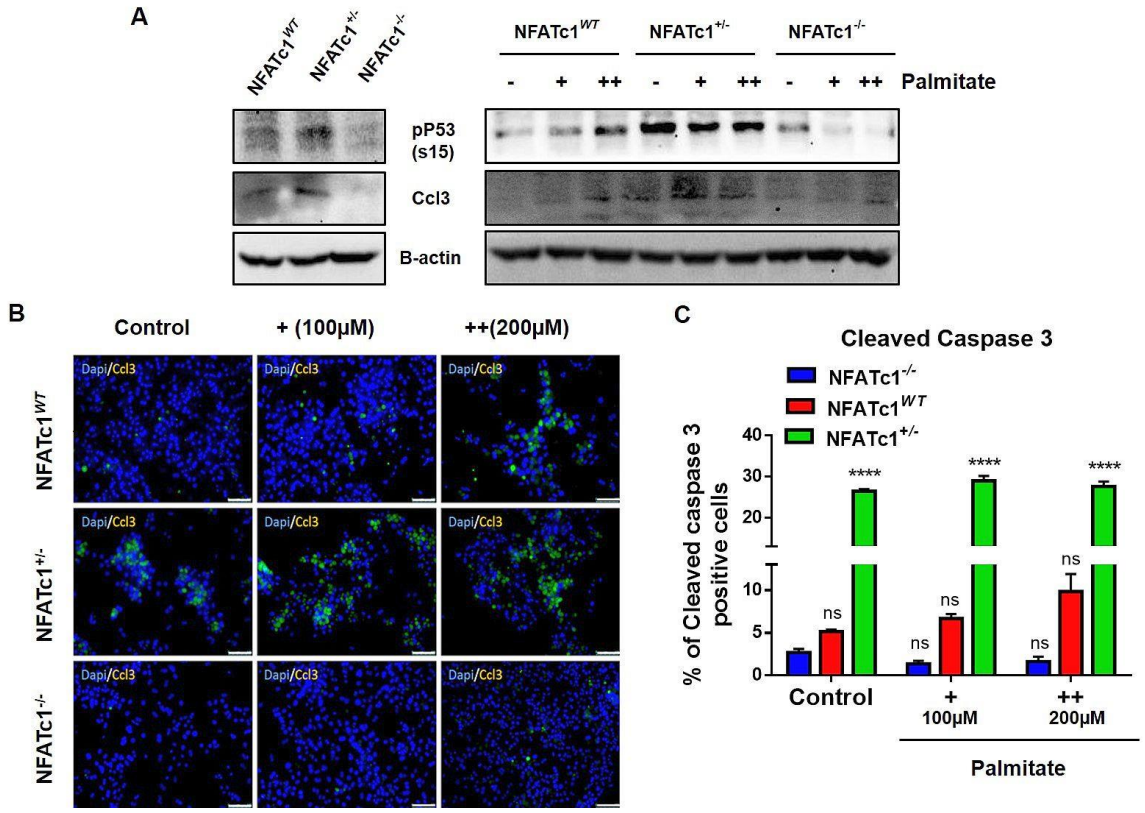

Figure 21: NFATc1-signaling is required for ER stress induced hepatocyte cell death

(**A)** Analysis of DNA damage and apoptotic markers in primary hepatocytes isolated from 8 weeks old NFATc1$^{-/-}$, NFATc1^{WT} and NFATc1$^{+/-}$ mice exposed to 100µM and 200µM palmitate for 12 hours (+ = 100µM and ++ = 200µM). **(B)** Cleaved caspase 3 (Ccl3) immunofluorescence analysis in primary hepatocytes after 12 hours treatment with 100µM and 200µM palmitate, respectively. **(C)** Quantitative analysis of Ccl3 positive cells from IF. Data was quantified using image j. Statistical analysis was performed using two-way ANOVA as described before (**** = $p < 0.0001$)**.**

Finally, we conducted TUNEL assays in AML12 cells and dependent on NFATc1 expression and activation levels. These studies, shown in Fig 22B-22C, confirmed a tremendous induction of DNA damage in cells with highly active NFATc1.

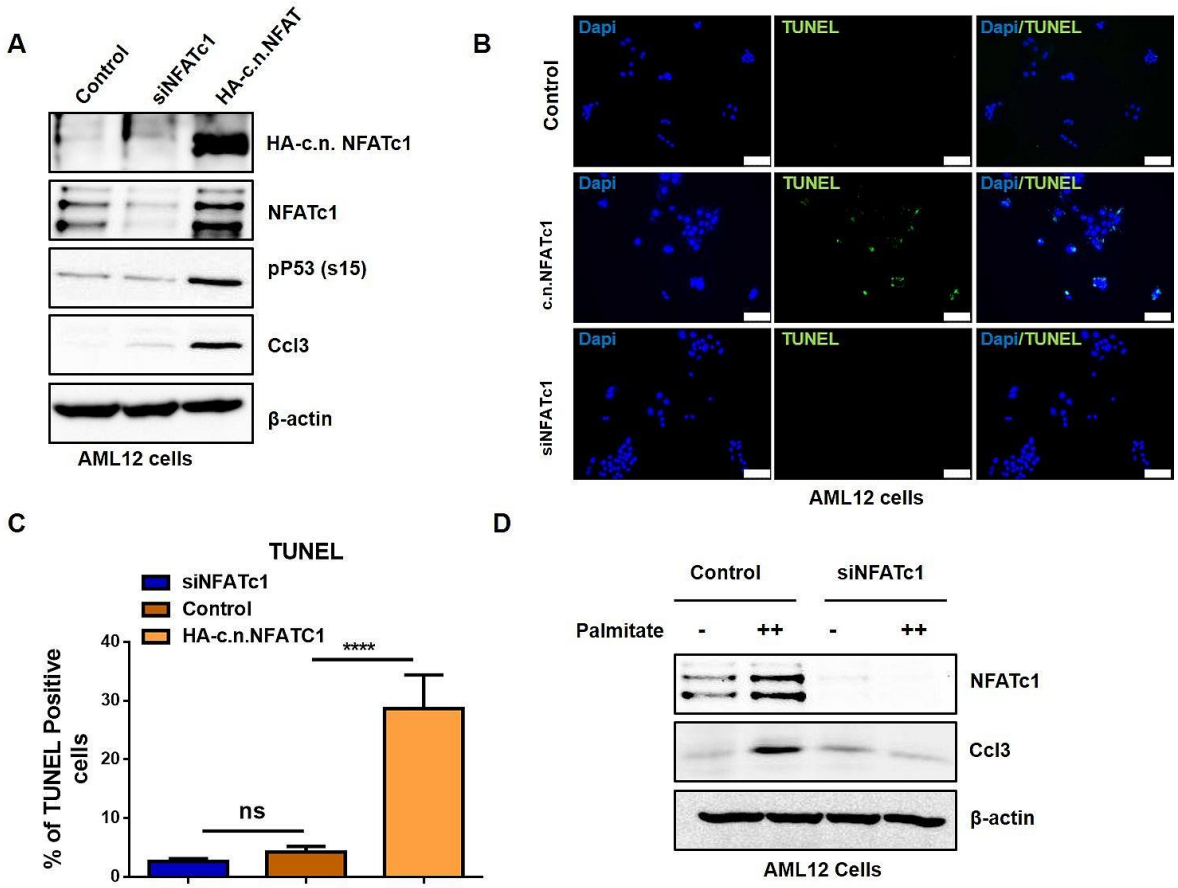

Figure 22: Induction of DNA damage and apoptosis in AML12 cells

(A) Western blot analysis of pP53-(s15) and Ccl3 in AML12 cells following transfection of either siRNA NFATc1 or a constitutively active NFATc1 construct. (**B-C)** TUNEL assay and quantification **(C)** for assessment of DNA damage in AML12 cells. Data was quantified in image j and statistical analysis was performed using one-way ANOVA as described before (******** = $p < 0.0001$)**. (D)** Expression of apoptosis marker was analyzed in AML12 cells following exposure to 200µM palmitate for 12 hours.

Consistent with our findings in cultured hepatocytes, we also observed the induction of apoptosis in murine liver tissues upon administration of the western diet. In fact, western diet feeding for 20 weeks led to a significant and reproducible increase of Ccl3 in hepatocytes from NFATc1^{WT} expressing mice. Moreover, similar levels of Ccl3 were detected in liver cells with highly active

NFATc1 (NFATc1$^{+/-}$), even without treatment, whereas loss of NFATc1 prevented from apoptosis despite long-term treatment with western diet [Fig 23A-23B].

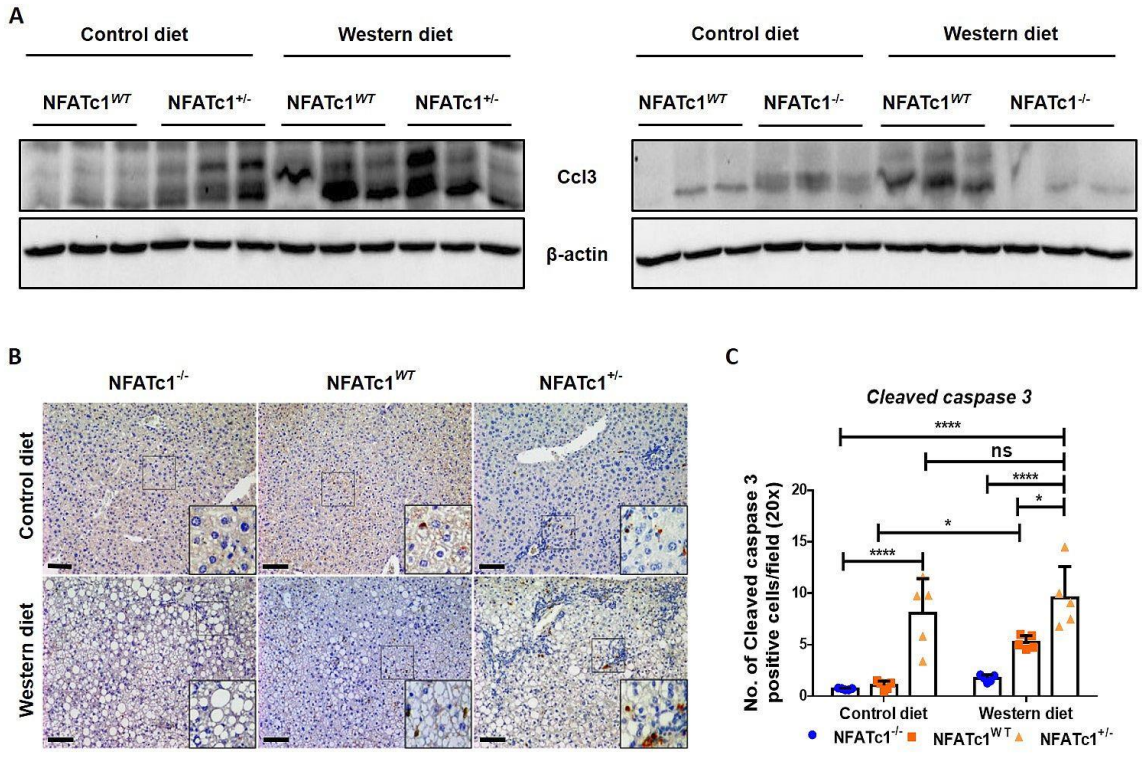

Figure 23: ER stress-induced expression of cleaved caspase 3

(A) Western blot analysis of Ccl3 in liver tissue lysates isolated from NFATc1^{WT}, NFATc1$^{+/-}$ and NFATc1$^{-/-}$ mice. **(B-C)** Ccl3 immunohistochemistry and **(C)** quantification in liver tissue sections from mice treated western diet or control. Quantification was performed using image j by quantifying number of Ccl3 positive cells in per field of view. Statistical analysis was performed using two-way ANOVA as before. **(*** = $p < 0.05$, **** = $p < 0.0005$, ***** = $p < 0.0001$)**.**

Together these studies revealed an essential role of NFATc1 in fat-induced liver injury. In particular, we propose from our combined *in vitro* and *in vivo* studies that NFATc1 promotes terminal UPR signaling and responses upon ER stress and hence, is required for sufficient inflammasome activation and induction of apoptosis.

4.6 Therapeutic potential of NFATc1 regulated signaling

Next, we examined the clinical impact of ER stress inhibition on NFATc1 driven NAFLD progression. For this purpose, we applied Tauroursodeoxycholic acid (TUDCA), a chemical chaperon of low molecular weight that has been shown to increase ER function and decrease the accumulation and aggregation of misfolded proteins in the ER lumen and, consequently, relieves ER stress. We first examined the potential of TUDCA treatment to overcome ER stress and terminal UPR signaling in liver cells. As expected, and in line with our studies shown in figure 24, palmitate treatment-induced NFATc1 expression and caused ER stress responses in liver cells, reflected by induction of eif2a phosphorylation and subsequent induction of CHOP. Induction of the terminal UPR pathway also resulted in the induction of the NLRP3 inflammasome and increased apoptosis, indicated by Ccl3 [Fig 24A]. Importantly, however, ER stress sensing and activation of terminal UPR signaling were fully prevented upon pretreatment of cells with TUDCA. According with a key role of NFATc1 in ER stress sensing and UPR signaling activation, ectopic expression of c.n.NFATc1 strongly induced CHOP, NLRP3 and Ccl3 in liver cells and even in the absence of palmitate. However, the application of TUDCA almost completely blocked NFATc1 driven UPR responses, without affecting the expression level of the transcription factor itself [Fig 24A-24B]. Together, these studies prompted us to validate the efficacy of TUDCA in the treatment of fat-induced liver injury and with respect to hepatocyte-specific NFATc1 expression.

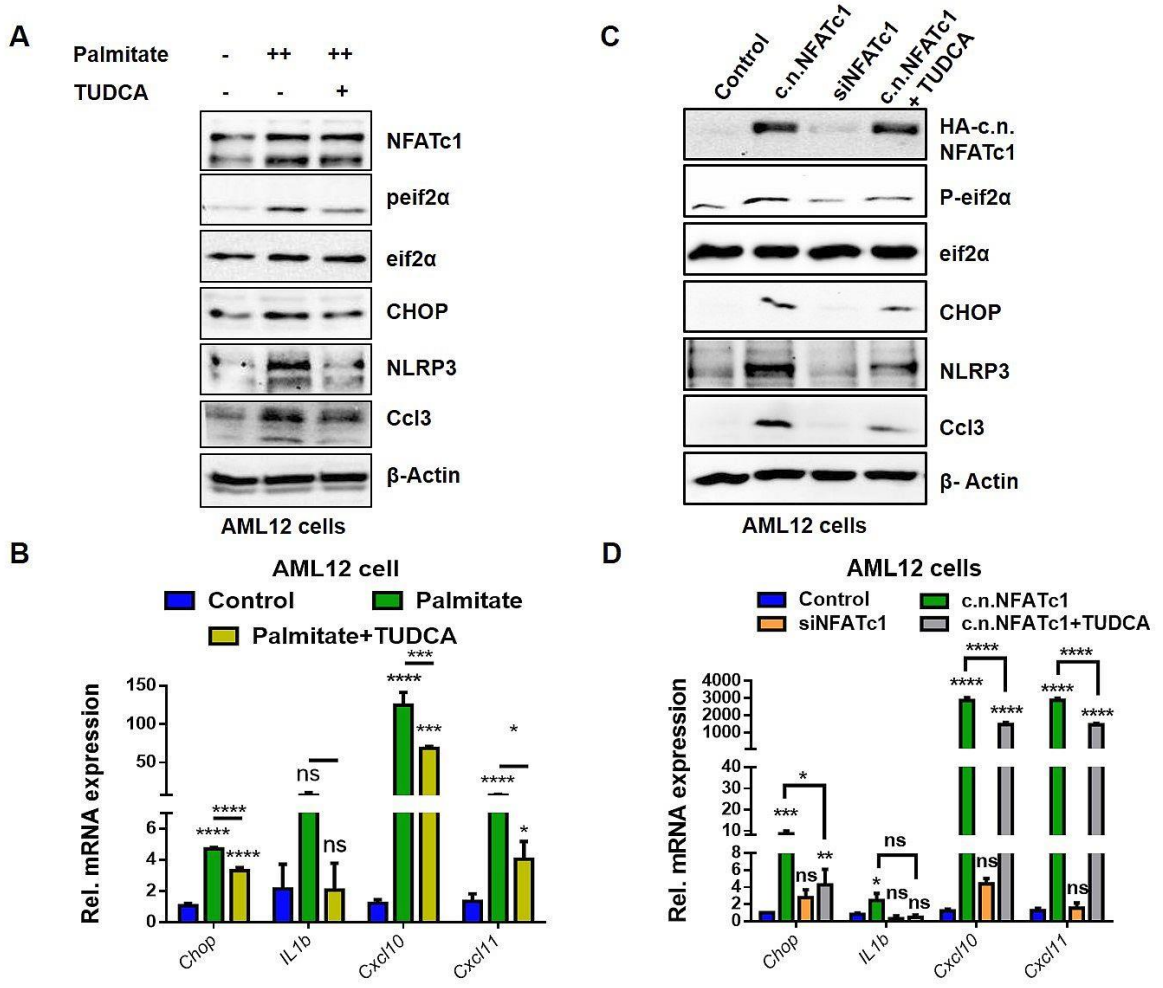

Figure 24: In-vitro inhibition of CHOP

(A) Western blot analysis of NFATc1, peif2α, eif2α, CHOP, NLRP3 and Ccl3 following exposure to palmitate (++ = 200µM) alone and palmitate in combination with TUDCA (++ = 200µM and + = 500µM). **(B)** Representative graph of qRT-PCR for mRNA analysis of *Chop*, *Il1b*, *Cxcll0* and *Cxcl11* in AMl12 cells (n=3). **(C)** Analysis of NFATc1 transfection (HA-c.n.NFATc1), silencing (NFATc1) and peif2α, eif2α, CHOP, NLRP3 and Ccl3 following transfection with/without TUDCA (500µM). ***(D)*** Representative graph of qRT-PCR for mRNA analysis of *Chop, Il-1b, Cxcll0* and *Cxcl11* in AMl12 cells (n=3). Statistical significance was calculated using one-way ANOVA as described before. (***** = $p < 0.05$, ****** = $p < 0.005$, ******* = $p < 0.0005$, ******** = $p < 0.0001$).

Subsequently, we fed NFATc1^{WT} and NFATc1$^{+/-}$ mice with western diet in combination with TUDCA (3x/week/i.p. injection) or PBS as a vehicle [Fig 25A]. Mice weight was monitored on a weekly basis. TUDCA administration significantly reduced weight gain in NFATc1^{WT} mice. A similar effect though not statistically significant was found in NFATc1$^{+/-}$ mice [Fig 25B].

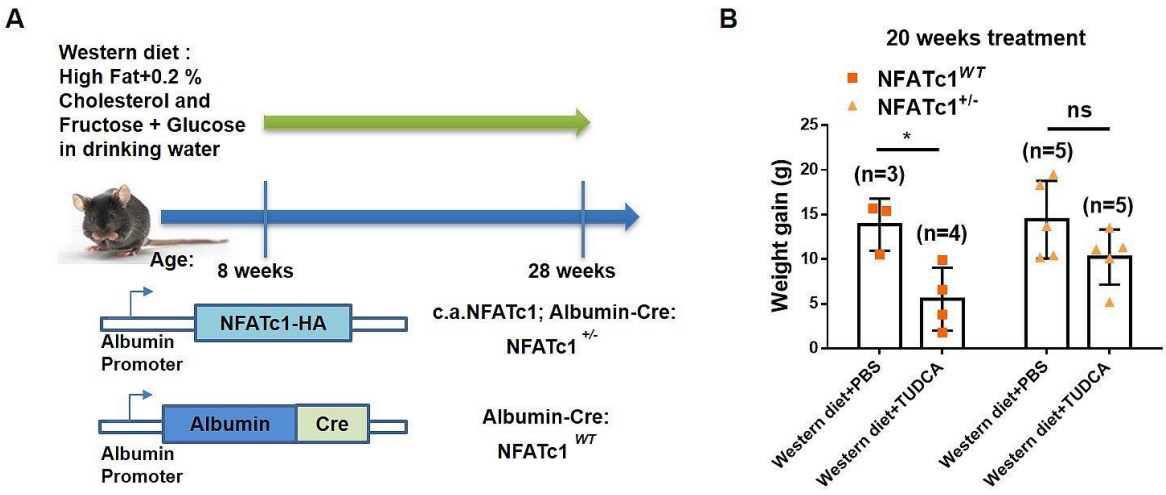

Figure 25: In-vitro administration of TUDCA reduces weight gain

(A) NFATc1^{WT} and NFATc1$^{+/-}$ mice were fed with western diet for 20 weeks along with 3x/week i.p. administration of either TUDCA (500mg/kg) or vehicle (PBS). **(B)** Mice weight was monitored on a weekly basis. Graph represents the gain of weight following treatment for 20 weeks. Statistical analysis was performed using two-way ANOVA as previously. (***** = $p < 0.05$).

We next analyzed activation of the UPR pathway and determined the expression levels of CHOP as well as markers of inflammasome and apoptosis in liver tissues from mice treated with either western diet alone or in combination with TUDCA. Again, western diet feeding induced NFATc1 and subsequent activation of the terminal UPR pathway, indicated by increased phosphorylation of eif2α and induction of CHOP, NLRP3 and Ccl3. Importantly, TUDCA application exerted a very strong effect on terminal UPR signaling and hence, blocked NFATc1 driven inflammasome activation and induction of apoptosis [Fig 26A]. Similar effects were observed in liver tissues from NFATc1$^{+/-}$ mice in which

terminal UPR responses, e.g. induction of NLRP3 and Ccl3 were abolished upon TUDCA treatment [Fig 26B].

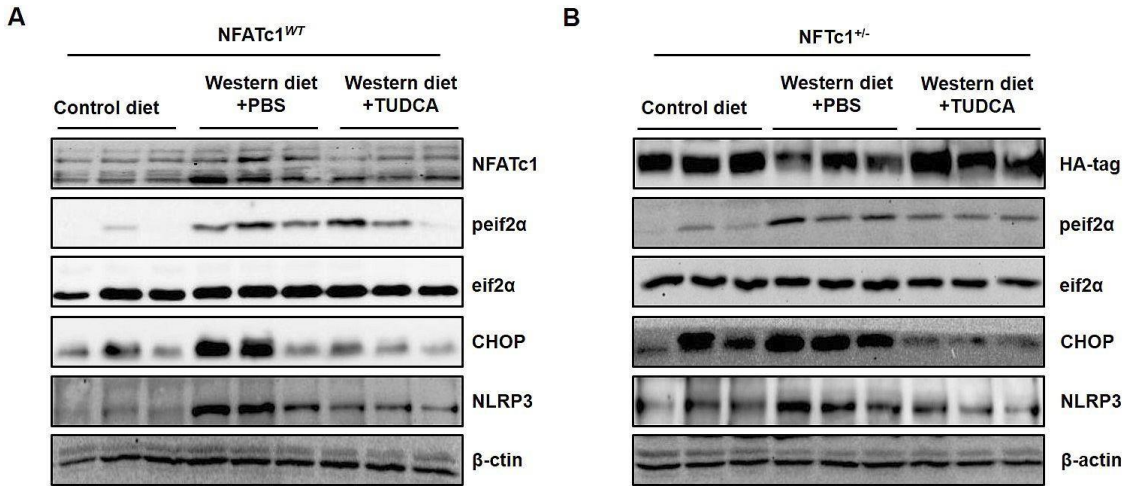

Figure 26: NLRP3 downregulation following CHOP inhibition

(A-B) Immunoblot analysis of liver lysates NFATc1^{WT} and **(B)** NFATc1$^{+/-}$ mice. Downregulation of peif2α, CHOP and NLRP3 following TUDCA administration has been shown.

Finally, the TUDCA treatment tremendously improved ER stress-induced NAFLD disease progression, even in the presence of highly active NFATc1. In fact, our histopathological analyses revealed significantly less inflammatory niches, reduced immune cell infiltration (CD45 staining) and a dramatic reduction of fibrosis (determined by picrosirius red staining) in all liver tissues when treated with TUDCA [Fig 27A-27D]. This is also true for NFATc1$^{+/-}$ mice, in which ER stress relief by TUDCA almost completely abolished fat-induced UPR responses and NAFLD progression, despite high levels of the transcription factor.

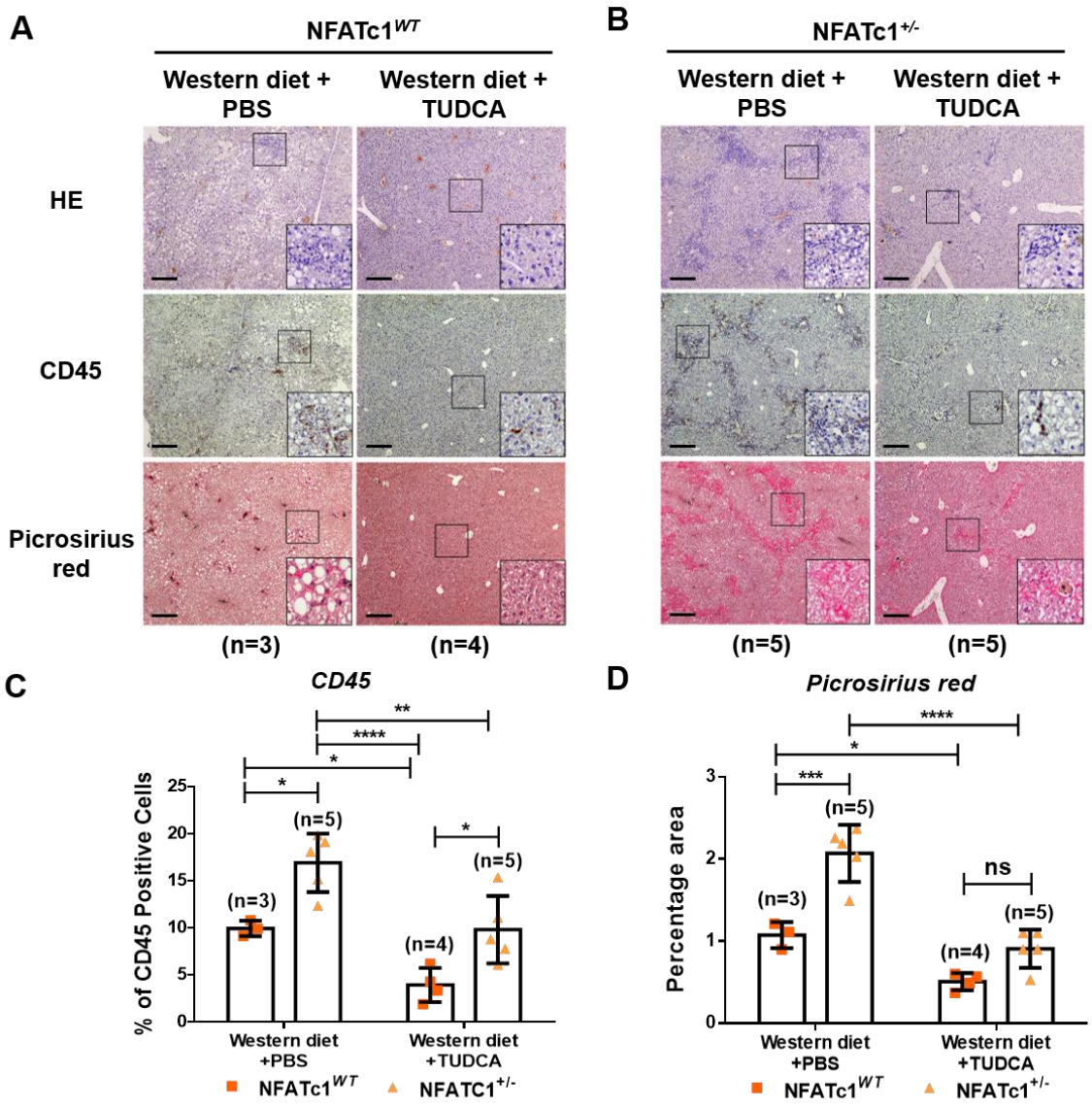

Figure 27: TUDCA alleviates murine Inflammation and fibrosis

(A and B) Analysis of inflammation and fibrosis by CD45 IHC **(A)** and **(B)** picrosirius red staining in 20 weeks western diet fed NFATc1^{WT} and NFATc1$^{+/-}$ mice co-treated with 3x/week i.p. injections of either PBS or TUDCA (500mg/kg). **(C-D)** Quantitative analysis of CD45 **(C)** and picrosirius red staining **(D)**. 10 random images of each mouse per staining were quantified using image j. Statistical analysis was performed by two-way ANOVA as previously. Scale bar for sections **A and B**= 100µm. (*p < 0.05, **p < 0.005, ***p < 0.0005, ****p < 0.0001)**.**

5.0 Discussion

NAFLD is characterized by increased deposition and accumulation of fat in hepatocytes. It is often associated with other metabolic- and obesity-associated diseases such as insulin resistance or diabetes mellitus. The prevalence of NAFLD has been steadily increasing worldwide over the last decades and is now becoming a major cause for liver transplantation. One major problem in NAFLD is the disease progression which is characterized by progressive inflammation and liver cirrhosis that in turn represents an increased risk for the development of hepatocellular carcinoma (Hirsova et al., 2016; Ibrahim et al., 2018; Wang et al., 2016). At the cellular level, the gradual progression of the disease is characterized by increased liver cell death, the release of inflammatory cytokines, activation and recruitment of immune cells as well as activation of connective tissue cells. Responsible for these remarkable cellular changes is a complex network of inflammatory signaling and transcription pathways that eventually control a multitude of gene signatures and functions in cell type-specific manners. One such important inflammatory signaling pathway is composed by the calcium-dependent transcription factor NFATc1, which controls the expression of a large number of genes in adaptation to extracellular and intracellular signals. Aberrant expression of NFATc1 has been reported in various inflammation-associated diseases including tumor development of the skin, colon and the pancreas (Baumgart et al., 2014; Chen et al., 2015; Singh et al., 2015). In addition, an increased expression of NFATc1 has been described in advanced NAFLD patients, although its precise role in liver inflammation and NAFLD/NASH development has not been characterized in detail.

Here, we have examined the expression, regulation, and function of NFATc1 signaling in the progression of NAFLD. By using a battery of in vitro and in vivo models to study fat-induced liver injury, we have conducted in-depth biochemical, cell biological and molecular biology approaches to define the underlying mechanisms of NFATc1-driven disease progression.

5.1 NFATc1 activation and steatosis

Consistent with previous studies we have described a strong and sustained induction of NFATc1 expression and nuclear localization in hepatocytes of NAFLD patients. The mechanism of NFATc1 activation and nuclear translocation is well studied and has been described in many studies. In brief, NFATc1 resides in the cytoplasm when present in a hyperphosphorylated and inactive form. Following stimulation of intracellular signaling, NFATc1 becomes activated by the calcium responsive calcineurin phosphatase that dephosphorylates the transcription factor thereby exposing its nuclear localization signal. Active NFATc1 then migrates into the nucleus to bind at specific DNA recognition sites of its target genes and regulates transcription in concert with other DNA binding factors, co-proteins and other cell-type-specific transcription factors (Fernandez-Zapico & Ellenrieder, 2010; Tripathi et al., 2014). We extended our analysis on NFATc1 regulation and observed a strong induction of NFATc1 mRNA and protein expression in AML12 cells and primary hepatocytes following treatment with palmitate, a saturated fatty acid, that causes fat accumulation in the liver (Ji et al., 2018; Pfaffenbach et al., 2010; Takahara et al., 2017). In addition, fat-induced NFATc1 expression and nuclear translocation was confirmed in vivo using a well-established high-caloric and fat-containing (called “western diet”; WD) NAFLD progression model that nicely recapitulates all key features of progressive human NAFLD (Garcia et al., 2019; Stephenson et al., 2018). Together, these studies supported the conclusion that induction and activation of NFATc1 might play a role in the development and progression of NAFLD.

5.2 Characterization of NAFLD/NASH in genetic mice

To get further insight into the role of NFATc1 in NAFLD development and progression, we generated different genetic mouse models with either hepatocytes-specific activation or deficiency of NFATc1 (referred to as NFATc1$^{+/-}$ and NFATc1$^{-/-}$, respectively). Mice were treated with WD and NAFLD development and progression was determined at different time points. We observed a time-dependent acceleration of liver steatosis and increases body weight. At the molecular level, liver steatosis is associated with altered cell metabolism and increased systemic inflammation, all key features of the obesity-

associated metabolic syndrome. Interestingly, the induction of NFATc1 expression is dispensable for fat-induced weight gain and development of progressive liver steatosis and therefore, onset and extent of fat accumulation in the liver remained unaffected by genetic depletion of the factor in our transgenic mouse model ($NFATc1^{-/-}$). Importantly, however, NFATc1 does play a crucial role in the progression of uncomplicated steatosis to steatohepatitis, and hence we observed a massive and time-dependent acceleration of the disease with the development of progressive inflammation and fibrosis in liver tissues with high levels of NFATc1 activity, induced by either WD treatment or genetic induction of constitutively active NFATc1. By contrast, genetic depletion of NFATc1 fully prevented the progression of NAFLD to steatohepatitis, thus confirming the central role of the transcription factor in disease progression. Together these studies supported the previously established **"two-hits hypothesis"** in which the first hit induces steatosis and the second hit promotes progression towards steatohepatitis. From our results, we further proposed that NFATc1 activation is not relevant for NAFLD development but required for subsequent progression of the disease, reflected by profound immune cell infiltration and collagen synthesis (fibrosis). In line with this assumption, accelerated immune cell infiltration and fibrosis were found in all experimental models with NFATc1 activation, but not in mice with NFATc1 deficiency, even upon long term feeding with the western diet.

5.3 Mechanisms of NFATc1 driven NAFLD progression

After establishing the imperative role of NFATc1 in NAFLD progression, we next scrutinized the underlying molecular mechanisms through which hepatocyte-specific NFATc1 activation might foster liver inflammation and fibrosis. To this end, we first carried out RNA-seq analysis in AML12 liver cells with ectopic expression of constitutively active NFATc1. These studies led to the identification of gene signatures involved in either immune cell regulation and inflammation (e.g. interferon signaling, cytokines and various inflammation-associated signaling and transcription pathways) or terminal ER stress responses (e.g. UPR, apoptosis and inflammasome mediators). We carried out validation experiments and confirmed NFATc1 mediated regulation of multiple candidate genes, specifically those with the implication in ER stress regulation and NAFLD

progression by RT-PCR analysis and western blot analysis. These studies were performed in AML12 cells and primary hepatocytes upon palmitate treatment and in liver tissues from WD treated mice with differential expression of NFATc1 (section 4.4). Together, our expression analysis strongly supported a role for NFATc1 in fat-induced regulation of ER stress responses. This key finding of our study is important, as it links for the first time NFATc1 signaling with ER stress and progression of liver steatosis. Functionally, the ER is responsible for the regulation of Ca^{2+} homeostasis, lipid biosynthesis and most important, for the synthesis, folding and maturation of secreted and transmembrane proteins. Defects in ER protein folding, on the other hand, can stem from multiple cellular defects (e.g. disturbed Ca^{2+} storage and signaling, changes in redox or ATP status and altered expression of ER chaperones), cause accumulation of misfolded proteins and eventually induces ER stress responses, also summarized as the “unfolded protein response” pathway (UPR). The primary goal of the UPR is to decrease the unfolded protein load and restore organelle homeostasis. For this purpose, the UPR decreases protein translation and induces transcription of components of the ER machinery involved in folding, *N*-glycosylation, ER-associated degradation (ERAD), quality control, redox and lipid biogenesis. The UPR response is an adaptive mechanism that is especially important in secretory cells, such as pancreatic β cells or hepatocytes. In fact, numerous previous studies have emphasized the role of ER stress activation and responses in liver diseases, and in particular in NAFLD progression (Lebeaupin et al., 2016; Nakagawa et al., 2014). On the molecular level, ER stress induction causes activation of three canonical ER stress transducers, namely PERK, IRE1 and ATF6 that are all bound to the GBP78 chaperone and localized at the ER membrane. However, ER stress induces binding of GBP78 (BiP) to lumenal misfolded proteins and its dissociation from the three master transducers, which in turn leads to their activation. Activation of the IRE1 and ATF6 stress sensor pathways are particularly important for cell adaptation and restoration of ER homeostasis, reflected by subsequent upregulation of chaperones and components of the ERAD machinery. Although some evidence from the literature proposed that activation of the IRE-Xbp-1 pathway and induction of ATF6 might be involved in ER stress responses in fat-induced liver diseases, we failed to demonstrate robust activation of other UPR pathway. Instead, we found a strong

activation of the apoptotic PERK UPR pathway in response to fat stimulation. PERK activation is particularly relevant in conditions of prolonged or severe ER stress (Lake et al., 2014; Lebeaupin et al., 2016; Lee et al., 2017). Induction of the pathway causes phosphorylation of the α subunit of eukaryotic translation initiation factor 2 (eIF2α) and this protein modification attenuates protein translation and relieves the ER workload. Importantly, we were able to show that palmitate-induced ER stress causes sustained activation of PERK signaling and subsequent eif2α phosphorylation. Consistent with previous studies, we also demonstrated the induction of the PERK downstream transcription factor CHOP in response to fat-mediated ER stress of AML12 cells. CHOP is a multifunctional transcription factor that simultaneously modulates liver cell survival, apoptosis and inflammation at least in part through activation of the inflammasome (NLRP3, Caspase-1, Caspase-11 and Il-1β) and inflammasome-associated apoptosis (Caspase-3 and BH3-only proteins). The important role of terminal PERK signaling activation in ER stress-induced NAFLD progression was recently emphasized by several studies showing that treatment with TUDCA, a well-established inhibitor of ER stress, protected from fat-induced NLRP3 inflammasome activation and apoptosis in mouse liver tissues. Similar effects were found in mice upon the silencing of PERK signaling components (i.e. CHOP). With this study, we extend the current mechanistic understanding of fat-induced ER stress responses in NAFLFD progression. In fact, the following findings emphasized a unique and previously unappreciated role of NFATc1 in ER stress responses: First, similar to palmitate treatment, overexpression of NFATc1 itself caused activation of the terminal PERK-eif2α-CHOP signaling pathway and ultimately led to inflammasome activation and induction of liver cell apoptosis (NLRP3, Cleaved caspase-1 (Ccl1), cleaved Il-1β (IL-1 β) and cleaved caspase 3 (Ccl3)). Second, palmitate-induced activation of the PERK-pathway and downstream consequences were abolished in NFATc1 deficient cells, both in vitro and in vivo. In detail, transient silencing of NFATc1 protected cells from fat-induced PERK-peif2α activation, reduced CHOP induction and prevented liver cells from inflammasome activation and apoptosis. Similar effects were seen in palmitate treated primary hepatocytes isolated from genetic mouse models and in liver tissue lysates from mice with differential expression of NFATc1.

Collectively, these findings led us to propose that NFATc1 activation drives NAFLD progression in response to ER stress and via regulation of the terminal PERK signaling pathway.

5.4 Inhibition of ER stress blocks NFATc1 driven NAFLD progression

Next, we investigated whether pharmacological inhibition of ER stress has therapeutic potential in NAFLD treatment and if so, whether this effect antagonizes disease-promoting impact of NFATc1. For this purpose, we applied tauroursodeoxycholic acid (TUDCA), an ambiphilic bile acid that has long been used to treat patients with cholestatic liver diseases and diseases of the central nervous system. Several studies have documented that TUDCA resolves ER stress and protects cells from PERK-mediated cell damage and inflammation (Lebeaupin et al., 2018; Sun et al., 2017). Here, we demonstrated that TUDCA blocks fat-induced PERK signaling activity and reduces inflammasome activation and apoptosis despite full activation of NFATc1 both in vitro and in vivo. For instance, the administration of TUDCA along with western diet feeding substantially resolved fat-induced inflammation and fibrosis in both NFAT expressing wild-type mice and in mice with constitutive activation of the proinflammatory transcription factor.

Together, this study demonstrated an important role of NFATc1 in the progression of NAFLD. Specifically, we have shown that NFATc1 promotes terminal ER stress and sustained induction of the PERK unfolded protein response pathway to stimulate inflammasome activation and apoptosis. We also provided evidence that interference with ER stress, for instance through the application of TUDCA, can inhibit the fatal impact of NFATc1 on NAFLD progression.

5.5 Limitations

Alongside these novel findings, this study has certain limitations. Firstly, large-scale analysis of NFATc1 activation and correlation of its downstream signaling (PERK-CHOP mediated NLRP3 inflammasome and apoptosis) is required in a huge number of human NAFLD patients. Secondly, these findings lack the

information regarding NFATc1-mediated transcriptional regulation of genes. In addition, the exact mechanism (direct or indirect) through which NFATc1 drives ER stress and terminal PERK signaling activation also need further investigations.

5.6 Conclusion

Results of this study successfully established the role of hepatocyte NFATc1 activation in NAFLD progression and demonstrated for the first time that hepatocyte-specific NFATc1 activation is required for fat-induced ER stress and subsequent activation promotion of inflammation and fibrosis in the liver.

Specifically, we conclude that

- NFATc1 activation is dispensable for the development of liver steatosis but required for the progression of the disease.
- Hepatocyte specific NFATc1 activation promotes NAFLD progression through terminal ER stress and subsequent activation of the PERK-CHOP unfolded protein response pathway.
- NFATc1-induced progression of NAFLD includes hepatocyte-specific inflammasome activation and apoptosis.
- Inhibition of ER stress by TUDCA blocks NFATc1 driven disease progression and thus has therapeutic potential in the treatment of NAFLD

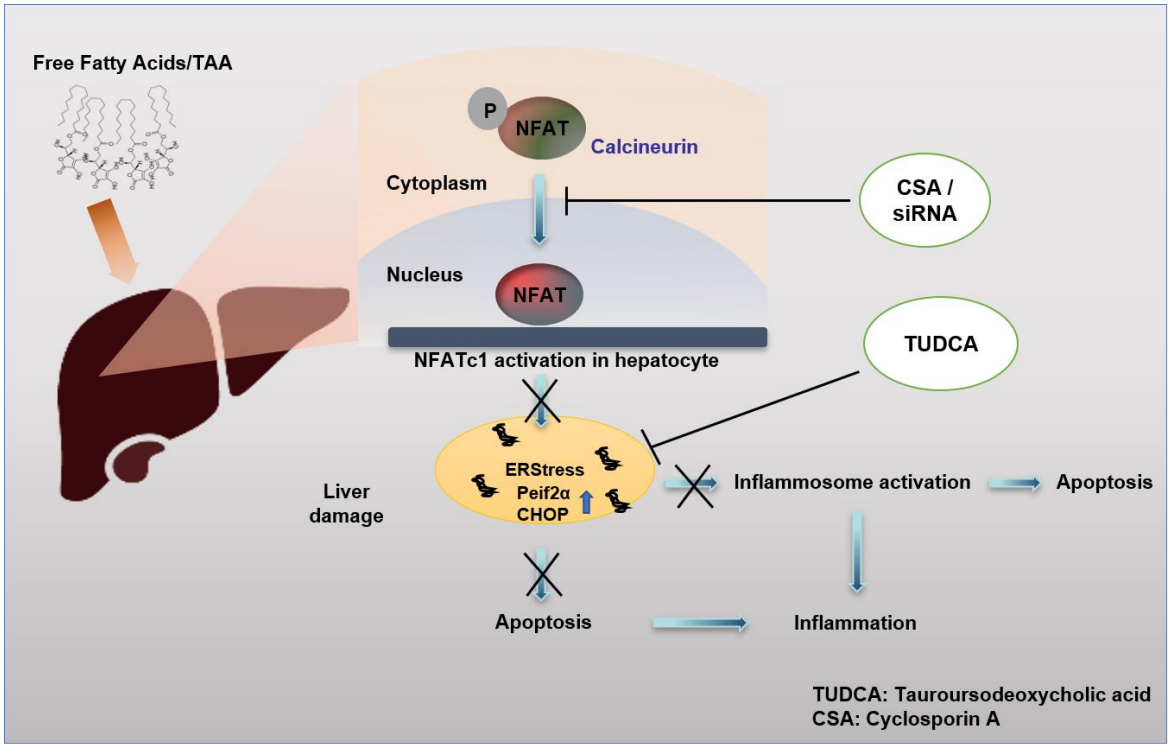

Figure 28: Schematic representation of NFATc1 activation and downstream signaling:

FFA's or TAA activates NFATc1 in hepatocyte followed by its nuclear translocation where it regulates expression of genes responsible for ER stress, inflammasome activation and apoptosis. CSA or siRNA mediated inhibition of NFATc1 activation blocks pro-apoptotic ER stress signaling and downstream apoptosis and inflammation. Downstream inhibition of CHOP by TUDCA also provides similar effects.

6.0 Bibliography

Adachi, Y., Yamamoto, K., Okada, T., Yoshida, H., Harada, A., & Mori, K. (2008). ATF6 is a transcription factor specializing in the regulation of quality control proteins in the endoplasmic reticulum. *Cell structure and function*, 0803130017-0803130017.

Adams, L. A., Lymp, J. F., Sauver, J. S., Sanderson, S. O., Lindor, K. D., Feldstein, A., et al. (2005). The natural history of nonalcoholic fatty liver disease: a population-based cohort study. *Gastroenterology, 129*(1), 113-121.

Afgan, E., Baker, D., Batut, B., Van Den Beek, M., Bouvier, D., Čech, M., et al. (2018). The Galaxy platform for accessible, reproducible and collaborative biomedical analyses: 2018 update. *Nucleic acids research, 46*(W1), W537-W544.

Aliprantis, A. O., Ueki, Y., Sulyanto, R., Park, A., Sigrist, K. S., Sharma, S. M., et al. (2008). NFATc1 in mice represses osteoprotegerin during osteoclastogenesis and dissociates systemic osteopenia from inflammation in cherubism. *The Journal of clinical investigation, 118*(11), 3775-3789.

Alkhouri, N., Carter-Kent, C., & Feldstein, A. E. (2011). Apoptosis in nonalcoholic fatty liver disease: diagnostic and therapeutic implications. *Expert review of gastroenterology & hepatology, 5*(2), 201-212.

Alrefai, H., Muhammad, K., Rudolf, R., Pham, D. A. T., Klein-Hessling, S., Patra, A. K., et al. (2016). NFATc1 supports imiquimod-induced skin inflammation by suppressing IL-10 synthesis in B cells. *Nature communications, 7*(1), 1-13.

Anders, S., Pyl, P. T., & Huber, W. (2015). HTSeq—a Python framework to work with high-throughput sequencing data. *Bioinformatics, 31*(2), 166-169.

Anstee, Q. M., Targher, G., & Day, C. P. (2013). Progression of NAFLD to diabetes mellitus, cardiovascular disease or cirrhosis. *Nature reviews Gastroenterology & hepatology, 10*(6), 330.

Arrese, M., Cabrera, D., Kalergis, A. M., & Feldstein, A. E. (2016). Innate immunity and inflammation in NAFLD/NASH. *Digestive diseases and sciences, 61*(5), 1294-1303.

Baumgart, S., Chen, N.-M., Siveke, J. T., König, A., Zhang, J.-S., Singh, S. K., et al. (2014). Inflammation-Induced NFATc1–STAT3 transcription complex promotes pancreatic cancer initiation by KrasG12D. *Cancer discovery, 4*(6), 688-701.

Berlanga, A., Guiu-Jurado, E., Porras, J. A., & Auguet, T. (2014). Molecular pathways in non-alcoholic fatty liver disease. *Clinical and experimental gastroenterology, 7*, 221.

Buchholz, M., Schatz, A., Wagner, M., Michl, P., Linhart, T., Adler, G., et al. (2006). Overexpression of c-myc in pancreatic cancer caused by ectopic activation of NFATc1 and the Ca2+/calcineurin signaling pathway. *The EMBO journal, 25*(15), 3714-3724.

Byrne, C. D., & Targher, G. (2015). NAFLD: a multisystem disease. *Journal of hepatology, 62*(1), S47-S64.

Capece, D., Fischietti, M., Verzella, D., Gaggiano, A., Cicciarelli, G., Tessitore, A., et al. (2013). The inflammatory microenvironment in hepatocellular carcinoma: a pivotal role for tumor-associated macrophages. *BioMed research international, 2013*.

Cha, J.-Y., Kim, D.-H., & Chun, K.-H. (2018). The role of hepatic macrophages in nonalcoholic fatty liver disease and nonalcoholic steatohepatitis. *Laboratory animal research, 34*(4), 133-139.

Chen, N.-M., Singh, G., Koenig, A., Liou, G.-Y., Storz, P., Zhang, J.-S., et al. (2015). NFATc1 links EGFR signaling to induction of Sox9 transcription and acinar–ductal transdifferentiation in the pancreas. *Gastroenterology, 148*(5), 1024-1034. e1029.

Chen, Y., Yousaf, M. N., & Mehal, W. Z. (2018). Role of sterile inflammation in fatty liver diseases. *Liver Research, 2*(1), 21-29.

Csak, T., Ganz, M., Pespisa, J., Kodys, K., Dolganiuc, A., & Szabo, G. (2011). Fatty acid and endotoxin activate inflammasomes in mouse hepatocytes that release danger signals to stimulate immune cells. *Hepatology, 54*(1), 133-144.

Daniel, C., Gerlach, K., Väth, M., Neurath, M. F., & Weigmann, B. (2014). Nuclear factor of activated T cells—A transcription factor family as critical regulator in lung and colon cancer. *International journal of cancer, 134*(8), 1767-1775.

de Freitas Carvalho, M. M., Lage, N. N., de Souza Paulino, A. H., Pereira, R. R., de Almeida, L. T., da Silva, T. F., et al. (2019). Effects of acai on oxidative stress, ER stress, and inflammation-related parameters in mice with high fat diet-fed induced NAFLD. *Scientific reports, 9*(1), 1-11.

Dowman, J. K., Tomlinson, J., & Newsome, P. (2010). Pathogenesis of non-alcoholic fatty liver disease. *QJM: An International Journal of Medicine, 103*(2), 71-83.

Elmore, S. (2007). Apoptosis: a review of programmed cell death. *Toxicologic pathology, 35*(4), 495-516.

Feldstein, A. E., Canbay, A., Angulo, P., Taniai, M., Burgart, L. J., Lindor, K. D., et al. (2003). Hepatocyte apoptosis and fas expression are prominent features of human nonalcoholic steatohepatitis. *Gastroenterology, 125*(2), 437-443.

Fernandez-Zapico, M. E., & Ellenrieder, V. (2010). NFAT transcription factors, the potion mediating" Dr. Jekyll-Mr. Hyde" transformation of the TGFβ pathway in cancer cells.

Garcia, D., Hellberg, K., Chaix, A., Wallace, M., Herzig, S., Badur, M. G., et al. (2019). Genetic liver-specific AMPK activation protects against diet-induced obesity and NAFLD. *Cell reports, 26*(1), 192-208. e196.

Giorgio, V., Prono, F., Graziano, F., & Nobili, V. (2013). Pediatric non alcoholic fatty liver disease: old and new concepts on development, progression, metabolic insight and potential treatment targets. *BMC pediatrics, 13*(1), 40.

Gkretsi, V., Apte, U., Mars, W. M., Bowen, W. C., Luo, J. H., Yang, Y., et al. (2008). Liver-specific ablation of integrin-linked kinase in mice results in abnormal histology, enhanced cell proliferation, and hepatomegaly. *Hepatology, 48*(6), 1932-1941.

Groenendyk, J., Peng, Z., Dudek, E., Fan, X., Mizianty, M. J., Dufey, E., et al. (2014). Interplay between the oxidoreductase PDIA6 and microRNA-322 controls the response to disrupted endoplasmic reticulum calcium homeostasis. *Sci. Signal., 7*(329), ra54-ra54.

Guo, H., Callaway, J. B., & Ting, J. P. (2015). Inflammasomes: mechanism of action, role in disease, and therapeutics. *Nature medicine, 21*(7), 677.

Han, C. Y., Rho, H. S., Kim, A., Kim, T. H., Jang, K., Jun, D. W., et al. (2018). FXR inhibits endoplasmic reticulum stress-induced NLRP3 inflammasome in hepatocytes and ameliorates liver injury. *Cell reports, 24*(11), 2985-2999.

Haukeland, J. W., Damås, J. K., Konopski, Z., Løberg, E. M., Haaland, T., Goverud, I., et al. (2006). Systemic inflammation in nonalcoholic fatty liver disease is characterized by elevated levels of CCL2. *Journal of hepatology, 44*(6), 1167-1174.

Hirsova, P., Ibrahim, S. H., Krishnan, A., Verma, V. K., Bronk, S. F., Werneburg, N. W., et al. (2016). Lipid-induced signaling causes release of inflammatory extracellular vesicles from hepatocytes. *Gastroenterology, 150*(4), 956-967.

Hollien, J., Lin, J. H., Li, H., Stevens, N., Walter, P., & Weissman, J. S. (2009). Regulated Ire1-dependent decay of messenger RNAs in mammalian cells. *Journal of Cell Biology, 186*(3), 323-331.

Hollien, J., & Weissman, J. S. (2006). Decay of endoplasmic reticulum-localized mRNAs during the unfolded protein response. *Science, 313*(5783), 104-107.

Hu, P., Han, Z., Couvillon, A. D., Kaufman, R. J., & Exton, J. H. (2006). Autocrine tumor necrosis factor alpha links endoplasmic reticulum stress to the membrane death receptor pathway through IRE1α-mediated NF-κB activation and down-regulation of TRAF2 expression. *Molecular and cellular biology, 26*(8), 3071-3084.

Ibrahim, S. H., Hirsova, P., & Gores, G. J. (2018). Non-alcoholic steatohepatitis pathogenesis: sublethal hepatocyte injury as a driver of liver inflammation. *Gut, 67*(5), 963-972.

Ji, C., Mehrian-Shai, R., Chan, C., Hsu, Y. H., & Kaplowitz, N. (2005). Role of CHOP in hepatic apoptosis in the murine model of intragastric ethanol feeding. *Alcoholism: Clinical and Experimental Research, 29*(8), 1496-1503.

Ji, J.-F., Jiao, W.-Z., Cheng, Y., Yan, H., Su, F., & Chi, L.-L. (2018). ShenFu Preparation Protects AML12 Cells Against Palmitic Acid-Induced Injury Through Inhibition of Both JNK/Nox4 and JNK/NFκB Pathways. *Cellular Physiology and Biochemistry, 45*(4), 1617-1630.

Jiang, S., Zhang, E., Zhang, R., & Li, X. (2016). Altered activity patterns of transcription factors induced by endoplasmic reticulum stress. *BMC biochemistry, 17*(1), 8.

Kamari, Y., Shaish, A., Vax, E., Shemesh, S., Kandel-Kfir, M., Arbel, Y., et al. (2011). Lack of interleukin-1α or interleukin-1β inhibits transformation of steatosis to steatohepatitis and liver fibrosis in hypercholesterolemic mice. *Journal of hepatology, 55*(5), 1086-1094.

Kanda, T., Matsuoka, S., Yamazaki, M., Shibata, T., Nirei, K., Takahashi, H., et al. (2018). Apoptosis and non-alcoholic fatty liver diseases. *World journal of gastroenterology, 24*(25), 2661.

Kim, D., Pertea, G., Trapnell, C., Pimentel, H., Kelley, R., & Salzberg, S. L. (2013). TopHat2: accurate alignment of transcriptomes in the presence of insertions, deletions and gene fusions. *Genome biology, 14*(4), R36.

Kim, J. Y., Garcia-Carbonell, R., Yamachika, S., Zhao, P., Dhar, D., Loomba, R., et al. (2018a). ER stress drives lipogenesis and steatohepatitis via caspase-2 activation of S1P. *Cell, 175*(1), 133-145. e115.

Kim, K. H., & Lee, M.-S. (2018b). Pathogenesis of nonalcoholic steatohepatitis and hormone-based therapeutic approaches. *Frontiers in endocrinology, 9*, 485.

Köenig, A., Linhart, T., Schlengemann, K., Reutlinger, K., Wegele, J., Adler, G., et al. (2010). NFAT-induced histone acetylation relay switch promotes c-Myc-dependent growth in pancreatic cancer cells. *Gastroenterology, 138*(3), 1189-1199. e1182.

Lake, A. D., Novak, P., Hardwick, R. N., Flores-Keown, B., Zhao, F., Klimecki, W. T., et al. (2014). The adaptive endoplasmic reticulum stress response to lipotoxicity in progressive human nonalcoholic fatty liver disease. *Toxicological sciences, 137*(1), 26-35.

Lebeaupin, C., Proics, E., De Bieville, C., Rousseau, D., Bonnafous, S., Patouraux, S., et al. (2015). ER stress induces NLRP3 inflammasome activation and hepatocyte death. *Cell death & disease, 6*(9), e1879.

Lebeaupin, C., Vallee, D., Gual, P., & Bailly-Maitre, B. (2016). Role of ER stress in inflammasome activation and non-alcoholic fatty liver disease progression. *Single Cell Biol, 5*, 140.

Lebeaupin, C., Vallée, D., Hazari, Y., Hetz, C., Chevet, E., & Bailly-Maitre, B. (2018). Endoplasmic reticulum stress signalling and the pathogenesis of non-alcoholic fatty liver disease. *Journal of hepatology, 69*(4), 927-947.

Lee, S., Kim, S., Hwang, S., Cherrington, N. J., & Ryu, D.-Y. (2017). Dysregulated expression of proteins associated with ER stress, autophagy and apoptosis in tissues from nonalcoholic fatty liver disease. *Oncotarget, 8*(38), 63370.

Lind, N. R., Qian, Q., & Yang, L. (2017). ER Stress and Autophagy in Obesity and Nonalcoholic Fatty Liver Disease. *Current Pathobiology Reports, 5*(3), 289-299.

Liu, X., & Green, R. M. (2019). Endoplasmic reticulum stress and liver diseases. *Liver Research*.

Liu, X., Henkel, A. S., LeCuyer, B. E., Schipma, M. J., Anderson, K. A., & Green, R. M. (2015). Hepatocyte X-box binding protein 1 deficiency increases liver injury in mice fed a high-fat/sugar diet. *American Journal of Physiology-Gastrointestinal and Liver Physiology, 309*(12), G965-G974.

Love, M. I., Huber, W., & Anders, S. (2014). Moderated estimation of fold change and dispersion for RNA-seq data with DESeq2. *Genome biology, 15*(12), 550.

Luedde, T., Kaplowitz, N., & Schwabe, R. F. (2014). Cell death and cell death responses in liver disease: mechanisms and clinical relevance. *Gastroenterology, 147*(4), 765-783. e764.

Machado, M. V., Michelotti, G. A., Xie, G., de Almeida, T. P., Boursier, J., Bohnic, B., et al. (2015). Mouse models of diet-induced nonalcoholic steatohepatitis reproduce the heterogeneity of the human disease. *PloS one, 10*(5).

Maiers, J. L., & Malhi, H. (2019). Endoplasmic reticulum stress in metabolic liver diseases and hepatic fibrosis. *Seminars in liver disease, 39*(02), 235-248.

Mancini, M., & Toker, A. (2009). NFAT proteins: emerging roles in cancer progression. *Nature Reviews Cancer, 9*(11), 810-820.

Nadanaka, S., Yoshida, H., Kano, F., Murata, M., & Mori, K. (2004). Activation of mammalian unfolded protein response is compatible with the quality control system operating in the endoplasmic reticulum. *Molecular biology of the cell, 15*(6), 2537-2548.

Nakagawa, H., Umemura, A., Taniguchi, K., Font-Burgada, J., Dhar, D., Ogata, H., et al. (2014). ER stress cooperates with hypernutrition to trigger TNF-dependent spontaneous HCC development. *Cancer cell, 26*(3), 331-343.

Negrin, K. A., Flach, R. J. R., DiStefano, M. T., Matevossian, A., Friedline, R. H., Jung, D., et al. (2014). IL-1 signaling in obesity-induced hepatic lipogenesis and steatosis. *PloS one, 9*(9).

Oikawa, D., Kimata, Y., Kohno, K., & Iwawaki, T. (2009). Activation of mammalian IRE1α upon ER stress depends on dissociation of BiP rather than on direct interaction with unfolded proteins. *Experimental cell research, 315*(15), 2496-2504.

Pan, M.-G., Xiong, Y., & Chen, F. (2013). NFAT gene family in inflammation and cancer. *Current molecular medicine, 13*(4), 543-554.

Pfaffenbach, K. T., Gentile, C. L., Nivala, A. M., Wang, D., Wei, Y., & Pagliassotti, M. J. (2010). Linking endoplasmic reticulum stress to cell death in hepatocytes: roles of C/EBP homologous protein and chemical chaperones in palmitate-mediated cell death. *American Journal of Physiology-Endocrinology and Metabolism, 298*(5), E1027-E1035.

Postic, C., & Girard, J. (2008). Contribution of de novo fatty acid synthesis to hepatic steatosis and insulin resistance: lessons from genetically engineered mice. *The Journal of clinical investigation, 118*(3), 829-838.

Romeo, S., Kozlitina, J., Xing, C., Pertsemlidis, A., Cox, D., Pennacchio, L. A., et al. (2008). Genetic variation in PNPLA3 confers susceptibility to nonalcoholic fatty liver disease. *Nature genetics, 40*(12), 1461-1465.

Romine, I. C., & Wiseman, R. L. (2019). PERK Signaling Regulates Extracellular Proteostasis of an Amyloidogenic Protein During Endoplasmic Reticulum Stress. *Scientific reports, 9*(1), 1-11.

Schuppan, D., & Schattenberg, J. M. (2013). Non-alcoholic steatohepatitis: pathogenesis and novel therapeutic approaches. *Journal of gastroenterology and hepatology, 28*, 68-76.

Seki, E., & Schwabe, R. F. (2015). Hepatic inflammation and fibrosis: functional links and key pathways. *Hepatology, 61*(3), 1066-1079.

Severgnini, M., Sherman, J., Sehgal, A., Jayaprakash, N. K., Aubin, J., Wang, G., et al. (2012). A rapid two-step method for isolation of functional primary

mouse hepatocytes: cell characterization and asialoglycoprotein receptor based assay development. *Cytotechnology, 64*(2), 187-195.

Shaw, J.-P., Utz, P. J., Durand, D. B., Toole, J. J., Emmel, E. A., & Crabtree, G. R. (1988). Identification of a putative regulator of early T cell activation genes. *Science, 241*(4862), 202-205.

Shen, J., Chen, X., Hendershot, L., & Prywes, R. (2002). ER stress regulation of ATF6 localization by dissociation of BiP/GRP78 binding and unmasking of Golgi localization signals. *Developmental cell, 3*(1), 99-111.

Singh, S. K., Chen, N. M., Hessmann, E., Siveke, J., Lahmann, M., Singh, G., et al. (2015). Antithetical NFATc1–Sox2 and p53–miR200 signaling networks govern pancreatic cancer cell plasticity. *The EMBO journal, 34*(4), 517-530.

Sircana, A., Paschetta, E., Saba, F., Molinaro, F., & Musso, G. (2019). Recent insight into the role of fibrosis in nonalcoholic steatohepatitis-related hepatocellular carcinoma. *International journal of molecular sciences, 20*(7), 1745.

Steneberg, P., Sykaras, A. G., Backlund, F., Straseviciene, J., Söderström, I., & Edlund, H. (2015). Hyperinsulinemia enhances hepatic expression of the fatty acid transporter Cd36 and provokes hepatosteatosis and hepatic insulin resistance. *Journal of Biological Chemistry, 290*(31), 19034-19043.

Stephenson, K., Kennedy, L., Hargrove, L., Demieville, J., Thomson, J., Alpini, G., et al. (2018). Updates on dietary models of nonalcoholic fatty liver disease: current studies and insights. *Gene Expression The Journal of Liver Research, 18*(1), 5-17.

Sun, D., Gu, G., Wang, J., Chai, Y., Fan, Y., Yang, M., et al. (2017). Administration of tauroursodeoxycholic acid attenuates early brain injury via Akt pathway activation. *Frontiers in cellular neuroscience, 11*, 193.

Syn, W.-K., Choi, S. S., & Diehl, A. M. (2009). Apoptosis and cytokines in non-alcoholic steatohepatitis. *Clinics in liver disease, 13*(4), 565-580.

Takahara, I., Akazawa, Y., Tabuchi, M., Matsuda, K., Miyaaki, H., Kido, Y., et al. (2017). Toyocamycin attenuates free fatty acid-induced hepatic steatosis and apoptosis in cultured hepatocytes and ameliorates nonalcoholic fatty liver disease in mice. *PloS one, 12*(3).

Tamaki, N., Hatano, E., Taura, K., Tada, M., Kodama, Y., Nitta, T., et al. (2008). CHOP deficiency attenuates cholestasis-induced liver fibrosis by reduction of hepatocyte injury. *American Journal of Physiology-Gastrointestinal and Liver Physiology, 294*(2), G498-G505.

Tirosh, B., Iwakoshi, N. N., Glimcher, L. H., & Ploegh, H. L. (2006). Rapid turnover of unspliced Xbp-1 as a factor that modulates the unfolded protein response. *Journal of Biological Chemistry, 281*(9), 5852-5860.

Trapnell, C., Williams, B. A., Pertea, G., Mortazavi, A., Kwan, G., Van Baren, M. J., et al. (2010). Transcript assembly and quantification by RNA-Seq reveals unannotated transcripts and isoform switching during cell differentiation. *Nature biotechnology, 28*(5), 511.

Tripathi, P., Wang, Y., Coussens, M., Manda, K. R., Casey, A. M., Lin, C., et al. (2014). Activation of NFAT signaling establishes a tumorigenic microenvironment through cell autonomous and non-cell autonomous mechanisms. *Oncogene, 33*(14), 1840-1849.

Urano, F., Wang, X., Bertolotti, A., Zhang, Y., Chung, P., Harding, H. P., et al. (2000). Coupling of stress in the ER to activation of JNK protein kinases by transmembrane protein kinase IRE1. *Science, 287*(5453), 664-666.

Van Herck, M. A., Weyler, J., Kwanten, W. J., Dirinck, E. L., De Winter, B. Y., Francque, S. M., et al. (2019). The differential roles of T cells in non-alcoholic fatty liver disease and obesity. *Frontiers in immunology, 10*.

Vonghia, L., Michielsen, P., & Francque, S. (2013). Immunological mechanisms in the pathophysiology of non-alcoholic steatohepatitis. *International journal of molecular sciences, 14*(10), 19867-19890.

Wang, L., Athinarayanan, S., Jiang, G., Chalasani, N., Zhang, M., & Liu, W. (2015). Fatty acid desaturase 1 gene polymorphisms control human hepatic lipid composition. *Hepatology, 61*(1), 119-128.

Wang, P., Li, J., Tao, J., & Sha, B. (2018). The luminal domain of the ER stress sensor protein PERK binds misfolded proteins and thereby triggers PERK oligomerization. *Journal of Biological Chemistry, 293*(11), 4110-4121.

Wang, S., Kang, X., Cao, S., Cheng, H., Wang, D., & Geng, J. (2012). Calcineurin/NFATc1 pathway contributes to cell proliferation in hepatocellular carcinoma. *Digestive diseases and sciences, 57*(12), 3184-3188.

Wang, X., Zheng, Z., Caviglia, J. M., Corey, K. E., Herfel, T. M., Cai, B., et al. (2016). Hepatocyte TAZ/WWTR1 promotes inflammation and fibrosis in nonalcoholic steatohepatitis. *Cell metabolism, 24*(6), 848-862.

Willy, J. A., Young, S. K., Stevens, J. L., Masuoka, H. C., & Wek, R. C. (2015). CHOP links endoplasmic reticulum stress to NF-κB activation in the pathogenesis of nonalcoholic steatohepatitis. *Molecular biology of the cell, 26*(12), 2190-2204.

Wong, R. J., Aguilar, M., Cheung, R., Perumpail, R. B., Harrison, S. A., Younossi, Z. M., et al. (2015). Nonalcoholic steatohepatitis is the second leading etiology of liver disease among adults awaiting liver transplantation in the United States. *Gastroenterology, 148*(3), 547-555.

Wree, A., McGeough, M. D., Peña, C. A., Schlattjan, M., Li, H., Inzaugarat, M. E., et al. (2014). NLRP3 inflammasome activation is required for fibrosis development in NAFLD. *Journal of molecular medicine, 92*(10), 1069-1082.

Wu, J., Rutkowski, D. T., Dubois, M., Swathirajan, J., Saunders, T., Wang, J., et al. (2007). ATF6α optimizes long-term endoplasmic reticulum function to protect cells from chronic stress. *Developmental cell, 13*(3), 351-364.

Yamamoto, K., Sato, T., Matsui, T., Sato, M., Okada, T., Yoshida, H., et al. (2007). Transcriptional induction of mammalian ER quality control proteins is mediated by single or combined action of ATF6α and XBP1. *Developmental cell, 13*(3), 365-376.

Younossi, Z., Anstee, Q. M., Marietti, M., Hardy, T., Henry, L., Eslam, M., et al. (2018). Global burden of NAFLD and NASH: trends, predictions, risk factors and prevention. *Nature reviews Gastroenterology & hepatology, 15*(1), 11.

Younossi, Z. M., Koenig, A. B., Abdelatif, D., Fazel, Y., Henry, L., & Wymer, M. (2016). Global epidemiology of nonalcoholic fatty liver disease—meta-analytic assessment of prevalence, incidence, and outcomes. *Hepatology, 64*(1), 73-84.

Younossi, Z. M., Otgonsuren, M., Henry, L., Venkatesan, C., Mishra, A., Erario, M., et al. (2015). Association of nonalcoholic fatty liver disease (NAFLD) with hepatocellular carcinoma (HCC) in the United States from 2004 to 2009. *Hepatology, 62*(6), 1723-1730.

Younossi, Z. M., Stepanova, M., Afendy, M., Fang, Y., Younossi, Y., Mir, H., et al. (2011). Changes in the prevalence of the most common causes of chronic liver diseases in the United States from 1988 to 2008. *Clinical Gastroenterology and Hepatology, 9*(6), 524-530. e521.

Zámbó, V., Simon-Szabó, L., Szelényi, P., Kereszturi, É., Bánhegyi, G., & Csala, M. (2013). Lipotoxicity in the liver. *World journal of hepatology, 5*(10), 550.

Zhang, X.-Q., Xu, C.-F., Yu, C.-H., Chen, W.-X., & Li, Y.-M. (2014). Role of endoplasmic reticulum stress in the pathogenesis of nonalcoholic fatty liver disease. *World journal of gastroenterology: WJG, 20*(7), 1768.

Zhu, R., Baker, S. S., Moylan, C. A., Abdelmalek, M. F., Guy, C. D., Zamboni, F., et al. (2016). Systematic transcriptome analysis reveals elevated expression of alcohol-metabolizing genes in NAFLD livers. *The Journal of pathology, 238*(4), 531-542.

Appendix

%	Percentage
α	Alpha
AFLD	Alcoholic fatty liver disease
ASK1	apoptosis-signal-regulating kinase 1
Alb	Albumin
AML12	Alpha mouse liver 12
ATF6	Activating transcription factor 6
ATF4	Activating transcription factor 4
ATF3	Activating transcription factor 3
β	Beta
Ccl2	C-C motif ligand 2
Ccl5	C-C motif ligand 5
CHOP	CCAAT enhancer-binding protein (C/EBP) homologous protein
C.casp3	Cleaved caspase 3
C.casp3	Cleaved caspase 1
ERAD	ER associated degradation
Eif2α	Eukaryotic initiation factor 2 alpha
p-eif2α	Phosphorylated eukaryotic initiation factor 2 alpha
ER	Endoplasmic reticulum
FFA’s	Free fatty acids
HSCs	hepatic stellate cells
HCC	Hepatocellular carcinoma
TG	Triglyceride
TGF-*β*	tumor growth factor-*β*
TAA	Thioacetamide

T2DM	Type 2 diabetes mellitus
NAFLD	Non-alcoholic fatty liver disease
NASH	Non-alcoholic steatohepatitis
NFAT	Nuclear factor of activated T cells
VLDL	Very low-density lipoprotein
UNOS/OPTN	United network for organ sharing and organ procurement transplantation network
SREBP1	sterol regulatory element binding transcription factor 1
ChREBP	Carbohydrate responsive element-binding protein
FADS	fatty acid desaturase
PNPLA3	patatin-like phospholipase domain-containing protein 3
NLRP3	NOD-, LRR- and pyrin domain-containing protein 3
IL1	Interleukin 1
IL6	Interleukin 6
Cxcl10	CXC motif chemokine 10
Cxcl11	CXC motif chemokine 11
DAMPs	Damage-endogenous-associated molecular patterns
RT-PCR	Real time Polymerase chain reaction
TNFα	Tumor necrosis factor alpha
TUDCA	Tauroursodeoxycholic Acid
TRAF2	tumor-necrosis factor receptor associated factor 2
PERK	Protein kinase RNA-like endoplasmic reticulum kinase
IRE1	inositol-requiring enzyme 1
UPR	Unfolded protein response
XBP1	X-box binding protein 1
JNK	c-Jun N-terminal kinase
PAMPs	pathogen-associated molecular patterns

WT	Wild type
WB	western blot
IHC	Immunohistochemistry
IF	Immunofluorescence